Alma Mater Studiorum – Università di Bologna

DOTTORATO DI RICERCA

IN INGEGNERIA CHIMICA, DELL'AMBIENTE E DELLA SICUREZZA

Ciclo XXI

Settore scientifico disciplinare ING-IND/24

Mass transport in polymers

Candidato:

Maria-Chiara Ferrari

Relatore:

Prof. Ing. Giulio Cesare Sarti

Correlatori:

Dott. Ing. Maria Grazia De Angelis
Dott. Ing. Marco Giacinti Baschetti

Coordinatore del corso di dottorato:

Prof. Ing. Giulio Cesare Sarti

Esame finale anno 2009

Table of contents

Introduction

The study of mass transport in polymeric membranes has grown in importance due to its potential application in many processes of industrial relevance such as separation of gases and vapors, packaging, controlled drug release. The diffusion of a low molecular weight species in a polymer is affected by many factors such as penetrant and polymer type, temperature, pressure, polymer formation procedure, history of the membrane. The transport is often accompanied by other phenomena like swelling, reactions, stresses, that have not been investigated in all their aspects yet. Furthermore, in the last ten years novel materials have been developed that include inorganic fillers, reactive functional groups or ions, that make the scenery even more complicated and require new tools to be properly represented.

This work was focused on some important and poorly investigated aspects of the mass transport processes in polymeric systems.

The first feature investigated was the effect of solvent-induced deformation in polymeric films during sorption processes. The exploration of this problem is very important because the dimension stability is crucial in most applications of polymers, and the sorption of an external phase has often a dramatic impact on the swelling of the material, leading to an improvement or drop of the membrane performances. The dilation, especially in constrained membranes, has to be taken into account also because it causes the development of stresses that can cause early failures of the device in which the material is employed.

A second fundamental aspect investigated in the present work is the effect of the addition of fillers on the transport properties of polymeric films. In the last decade, it has been seen that the addition of inorganic particles to polymers can be used to tune the gas transport properties to obtain the desired behavior. Mixed Matrix Membranes (MMM) formed by glassy polymers and inorganic fillers were developed, with the aim of increasing the separation ability of polymers through the incorporation of more rigid and thermally stable inorganic media. The mechanisms that control the gas transport in filled polymers is still object of discussion and these phenomena will be properly addressed in the present work.

Subsequently, a fundamental investigation was carried on polymers that contain reactive groups. In particular, the case was studied of oxygen scavenging components that are added to the polymer with the aim of increasing its oxygen barrier performance. The lack of oxygen barrier properties of common polymers has always ruled against their employment in sensitive applications but their processability and lightness makes their use appealing. A possible approach to improve the barrier properties is by scavenging or immobilizing the penetrant as it diffuses through the film coupling the physical diffusion to chemical reactions.

Finally, polymers containing ionic functional groups (perfluorosulphonic acid ionomers (PFSI)) were considered. This class of selective materials is capturing increasing attention due to a high thermal and chemical resistance coupled with very peculiar transport properties, that make them appropriate to be used in many demanding separation fields, such as in the chloro-alkali industry, and in electrochemical applications such as fuel cells. The strong interactions that these materials undertake with water determine their properties during operations and have to be studied in detail. The FTIR-ATR technique can provide a deeper insight into the process of water diffusion and absorption into PFSI membranes and into the understanding of the interactions between water and ionic groups of the membranes.

The dissertation is organized in four chapters, each one devoted to a different diffusion problem; in all cases the systems will be first characterized experimentally and then the data will be described with suitable models. First the coupling between the mass transport problem and the mechanical one will be examined considering the swelling and the stress induced by sorption in constrained films with the bending beam technique. The focus will be then moved to the incorporation of impermeable inorganic particles in a high free volume glassy matrix in order to increase the separation ability of the membrane. The last two chapters will then be dedicated to reacting systems. First, oxygen scavenging membranes for barrier applications such as food packaging will be studied; this part of the work was conducted at The University of Texas at Austin under the supervision of Dr. Don Paul and Dr. Benny Freeman and is part of a project funded by CLiPs (Center for Layered Polymeric System) which aim is to find the best structure for a multilayer material that optimize the barrier performance

against oxygen. In the end also the case of ionomeric materials that show strong interactions with water will be presented.

1 Stress induced by vapor sorption in glassy polymers: Bending Beam technique

The study of the transport properties of gases, vapors or liquids in polymeric materials and coatings has grown in interest and importance in many industrial fields. The diffusion of a penetrant in a polymeric matrix is often accompanied by the dilation of the matrix itself that, if hindered by an external constraint, can lead to delamination, ruptures, stress cracking and finally to the failure of the system [1]. The study of the dilation and of the stresses that can be induced in the polymer by the diffusion process is thus required for many different industrial applications.

The bending beam technique is a simple method that can be used to study the effect of mass transport on a polymeric coating and to measure the stress induced in the system by the diffusion process [2]; it is based on the measurement of the deflection of the free end of a cantilever, caused by the stress field induced by applying a temperature or a swelling gradient. Such an experimental technique was widely used to study metals and laminates under mechanical or thermal stresses [3], and it was also applied to polymeric coatings for microelectronic applications and several other fields [4-6]; the stress levels in polymer coatings [1,7-9], as well as the inception of delamination or cracking processes [1], have been studied with this technique, determining also several material properties as glass transition temperature, elastic modulus and thermal expansion coefficient of polymers [1,9-11].

In its application to mass transport studies, the typical experiment considers the system exposed to a penetrant at a given temperature and pressure or solvent activity to allow sorption to take place; the diffusion of the penetrant causes the swelling of the film that, being hindered by the substrate, induces a stress field in the system and a progressive deflection of the cantilever. Such a bending is obviously related to the stress and concentration profile in the polymeric film, as well as to the elastic and transport properties of the polymer and of the support; therefore, the method can be used to obtain relevant information on all these quantities, on the basis of a proper theoretical model for diffusion and for the simultaneous solvent induced stresses.

The usual experimental set up can be based on many different kinds of sensors to measure the cantilever bending, like capacitive or inductive devices, that can reach very high accuracy and precision; however such experimental systems usually do not allow to obtain useful information about the dilation of the polymer that, on the other hand, is extremely important when the relationship between the diffusion process and the stress profile in the system is considered. The volumetric behavior of the polymer as a function of penetrant concentration is required for a complete characterization of the system under investigation, while it is not often available experimentally; therefore, the dilation-concentration relationship must be obtained from independent measurements or reasonable correlations, or can be regressed from a consistent physical model.

In the present work the technique has been used to study the stress profile induced by penetrant diffusion in a polymeric coating. The apparatus is based on the bending beam technique and it is able to measure at the same time both the bending of the cantilever and the dilation of the polymer film during sorption/desorption processes. The system allows also to obtain more information on the film properties than other more common setups, and provides all the independent information required to solve the complete elastodiffusive problem without any assumption on the volumetric behavior of the polymer.

The system was applied to study the effects induced in polymeric films of bisphenol-A- polycarbonate (PC) by the sorption of acetonitrile, at 40°C and at different activities up to the value of 0.35. The results obtained were also compared with sorption and swelling results obtained with a gravimetric technique as well as with FTIR-ATR data, already presented in literature [12].

The experimental data were then simulated considering an elastic mechanical response of PC and Fickian diffusion, with a multi-layer system; the model predictions are then compared with the collected experimental data.

1.1 Theory

A sketch of the working principle of the bending beam techniques is shown in Fig. 1.1, where a cantilever coated with a thin polymeric film is exposed to a penetrant and bends during penetrant sorption because of polymer swelling. To obtain quantitative information on the stress distribution in the system, the complete elastodiffusive problem must be considered and solved to account for the combined effects of the diffusion process and of the elastic response of the cantilever. For the geometry under consideration many simplifications are possible and the deflection data can be easily modeled; in particular a simple multi-layer model that is adapted from the classical laminate theory (CLT) can be used [13].

A laminated plate consists in two or more layers of materials with different properties that, due to perfect adhesion, behave like a single composite layer. The basic assumptions of the model that allow to consider the system as a laminate are:

i) the thickness of the plate is small compared to the other dimensions,

ii) the bond between the layers is perfect (i.e. no delamination is allowed),

iii) straight lines normal to the undeformed middle surface remain straight, inextensible and normal to the deformed middle surface (Love-Kirchoff hypothesis [14]),

iv) the normal stresses in the direction transverse to the plate can be neglected.

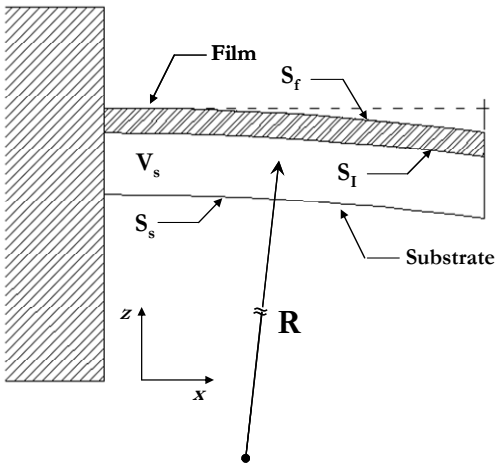

Fig. 1-1: Schematic of the bending-beam technique deflection measurements.

Consequently, the stress distribution is bi-dimensional with components in the $x-y$ plane only; on the other hand, due to the absence of constraints in the *z* direction, the strain in that direction has negligible effects on stress distribution, so that also the stress generating deformation becomes bi-dimensional.

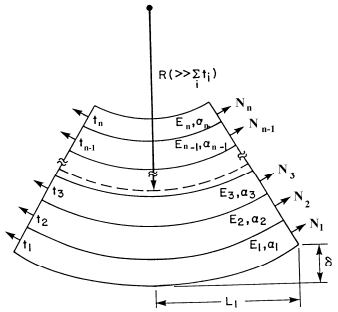

Fig. 1-2: Schematic of the polymer considered as a layer system.

The samples are formed by layers of two materials, polymer and metal support, the first of which develops a concentration profile of penetrant during the transient diffusion process. For numerical calculation purposes the polymer film can also be divided into several different parallel layers (Fig. 1-2), each one characterized by its own values of the relevant state properties which affect the mechanical response as temperature, penetrant concentration, strain and stress tensors; each layer then can be treated as a single lamella in a multi-laminate composite. The metal–polymer system of the cantilever is thus divided into $(n+1)$ layers: n for the coating, to describe the concentration profile in the polymer, and one for the metal substrate which has no penetrant but different mechanical properties with respect to the polymer. Considering isotropic materials and exploiting the superposition principle for small deformations and linear elasticity, the elastodiffusivity problem can be formulated in a relatively straightforward way, schematically summarized hereafter.

The strain distribution in the layers as well as the total deflection δ of the cantilever are related to the middle plane deformation vector, $\{\varepsilon_0\}$, and curvature vector, $\{k\}$, of the laminate as follows [13]:

$$\delta = \frac{1}{2} k_x L^2 \tag{1.1}$$

$$\begin{Bmatrix} \varepsilon_x \\ \varepsilon_y \\ \gamma_{xy} \end{Bmatrix} = \begin{Bmatrix} \varepsilon_x^0 \\ \varepsilon_y^0 \\ \gamma_{xy}^0 \end{Bmatrix} + z_{(i)} \begin{Bmatrix} k_x \\ k_y \\ k_{xy} \end{Bmatrix} \tag{1.2}$$

where L is the length of the cantilever in the x direction and $1 = 1, 2, ..., n+1$ labels the *i*-th layer of the multi-laminate film; the subscripts x and y indicate the direction to which the strain and curvature are referred to, while the xy subscript is related to the cross terms (shear deformation and related curvature) that, due to the initial CLT assumptions, are presently equal to 0. The isotropy condition states that strain and curvature components in the x and y directions are equal.

From equation (1.2), one concludes that it is not necessary to solve the problem in every single layer, but the constitutive equation of the whole plate can be used [13] in order to find $\{\varepsilon_0\}$ and $\{k\}$:

$$\begin{Bmatrix} N \\ M \end{Bmatrix} = \begin{bmatrix} A & B \\ B & D \end{bmatrix} \begin{Bmatrix} \varepsilon_0 \\ k \end{Bmatrix} \tag{1.3}$$

In equation (1.3) $\begin{Bmatrix} N \\ M \end{Bmatrix}$ is a 6x1 vector combining the vectors of the total external forces, $\{N\}$, and moments, $\{M\}$, acting on the cantilever, while $[A]$, $[B]$ and $[D]$ are, respectively, the in-plane, the in-plane/flexural coupling and the flexural sub-matrices of stiffness of the laminate, which are directly related to the properties of each single layer of the cantilever. In particular they can be written as:

$$\begin{aligned} [A] &= \int_{z_{\min}}^{z_{\max}} [Q] dz \\ [B] &= \int_{z_{\min}}^{z_{\max}} [Q] z dz \\ [D] &= \int_{z_{\min}}^{z_{\max}} [Q] z^2 dz \end{aligned} \tag{1.4}$$

where $[Q]$ is the matrix of stiffness of each single layer and can be expressed as a function of Young modulus E and Poisson ratio ν of the material. Under isotropic conditions one has:

$$[Q]=\begin{bmatrix} \dfrac{E}{1-\nu^2} & \dfrac{E}{1-\nu^2} & 0 \\ \dfrac{E}{1-\nu^2} & \dfrac{E}{1-\nu^2} & 0 \\ 0 & 0 & \dfrac{E}{2(1+\nu)} \end{bmatrix} \tag{1.5}$$

The isotropy condition reduces to 3 the number of independent components of the stiffness matrix of the layer, while the presence of zero components is due to the laminate assumption.

In the case experimentally considered, there are no external mechanical forces and moments acting on the cantilever, so that the terms in the left hand side of equation (1.3) are identically zero. On the other hand, the presence of solvent induces dilation in the polymer matrix, which is equivalent to applying fictitious external forces and moments, $\{N_C\}$ and $\{M_C\}$, respectively, which satisfy the following conditions:

$$\begin{Bmatrix} 0 \\ 0 \end{Bmatrix}=\begin{bmatrix} A & B \\ B & D \end{bmatrix}\begin{Bmatrix} \varepsilon_0 \\ k \end{Bmatrix}-\begin{Bmatrix} N_C \\ M_C \end{Bmatrix} \tag{1.6}$$

where the concentration dependent terms, $\{N_C\}$ and $\{M_C\}$, are related to the volume changes induced in the polymer by the penetrant sorption and can be calculated as:

$$\{N_C\}=\int_{z_{\min}}^{z_{\max}}[Q]\{\beta\}c\,dz \tag{1.7}$$

$$\{M_C\}=\int_{z_{\min}}^{z_{\max}}[Q]\{\beta\}c z\,dz \tag{1.8}$$

In equations (1.7) and (1.8), c is the penetrant concentration and $\{\beta\}$ is the dilation coefficient vector, relating the penetrant concentration to the sorption induced stress free deformation in each layer, as follows:

$$\begin{Bmatrix} \varepsilon_x \\ \varepsilon_y \\ \gamma_{xy} \end{Bmatrix}^{c}_{(i)} = c_{(i)}\begin{Bmatrix} \beta_x \\ \beta_y \\ \beta_{xy} \end{Bmatrix} \equiv c_{(i)}\begin{Bmatrix} \beta \\ \beta \\ 0 \end{Bmatrix} \tag{1.9}$$

Due to material isotropy we have considered $\beta_x = \beta_y$ and β_{xy}, which is associated to the $x-y$ components of the strain tensor, is zero because the swelling induced by sorption does not introduce any shear deformations.

The mechanical problem represented by equations (1.1-9) can be solved once the mechanical properties E and ν of the materials are known, together with the proper expression for the sorption induced swelling coefficient $\beta(c)$, and the concentration profile in the polymer $c(t,z)$ as a function of time and position.

The values of Young modulus and Poisson ratio can be found in data collections, while $\beta(c)$ can be obtained directly from experimental data of swelling measurements. In this regard, however, some words of caution are in order when a glassy polymer as PC is considered because the dilation-concentration relationship depends also on the history of the sample and particular care should be used before generalizing the experimental results.

The concentration profile, finally, can be obtained by modeling the diffusion process in the coating film through Fick's law and solving the resulting mass balance equation with the appropriate set of boundary conditions, as follows:

$$\begin{aligned} &\frac{\partial c}{\partial t} = \frac{\partial}{\partial z}\left(D\frac{\partial c}{\partial z}\right) \\ &c = c_{eq} \qquad \forall P(x,y,z) \in S_f, \quad \forall t \\ &\nabla c \cdot \{n\} = 0 \qquad \forall P(x,y,z) \in S_I, \quad \forall t \\ &c = 0 \qquad \forall P(x,y,z) \in V_f, \quad t = 0 \end{aligned} \tag{1.10}$$

In equation (1.10), D is the diffusion coefficient, V_f is the film volume, S_f the external surface of the polymeric film, S_I indicates the interface between the polymer and the cantilever substrate and $\{n\}$ is the unit vector perpendicular to the surface. Of course, the diffusion coefficient can be either a constant or a variable quantity depending on concentration or on local stress.

Once the concentration and deformation profiles are available, the cantilever curvature and deflection are obtained through equations (1.6) and (1.1), respectively; then the

stress profile in each layer of the polymer film can be calculated through the following relationship:

$$\begin{Bmatrix} \sigma_x \\ \sigma_y \\ \sigma_{xy} \end{Bmatrix}_{(i)} = [Q]_{(i)} \begin{Bmatrix} \varepsilon_x - \beta(c)c \\ \varepsilon_y - \beta(c)c \\ \gamma_{xy} \end{Bmatrix}_{(i)} \tag{1.11}$$

where the matrix $[Q]_i$ is given by equation (1.5). Clearly, the solution of equations (1.1 ÷ 11) can be obtained sequentially if the diffusion coefficient is stress independent and the elastic properties are independent of concentration, so that the mechanical and diffusion problems are decoupled; alternatively, the set of equations must be solved simultaneously if the stress profile influences the diffusion coefficient and/or the elastic properties are concentration dependent. Once the elastic properties and diffusivity are known, equations (1.1 ÷ 11) allow to calculate the stress profile in the polymer as a function of time. In the present work, it was sufficient to consider the mechanical and mass transport problems uncoupled, with a diffusion coefficient varying as a function of penetrant concentration in the polymer, and constant values of Young modulus and Poisson ratio, in view of the small changes in penetrant concentration. For the solution of the problem, a simple MatLab based code was built on purpose, based on the finite volume method for the numerical integration of equation (1.10).

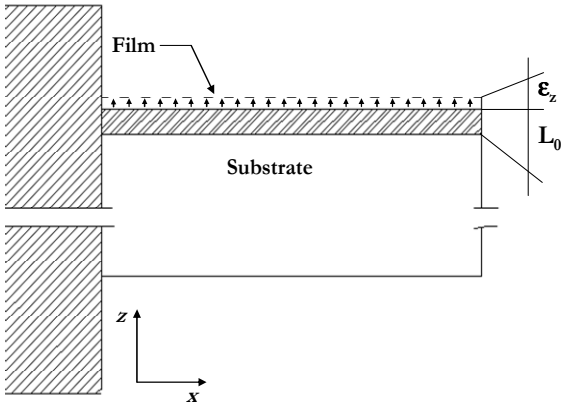

Fig. 1-3: Schematic of the swelling measurements.

In all cases, the swelling coefficient $\beta(c)$ plays an important role for the strain and stress profile and needs to be determined independently. It is worthwhile to notice that, when the substrate is completely rigid, as reported in Fig. 1-3, all the deformations in the plane of adhesion between polymer and support are hindered and the only dilation allowed is in the thickness direction, where no constraint and no stress component is present, so that $\varepsilon_z \equiv \varepsilon_z^{(c)}$. Monitoring the film thickness during time in such a system, therefore, allows a direct measurement of the sorption induced polymer swelling; that case applies to a cylindrical rigid rod coated by a polymer film and has been used in our experiments.

Proper comparisons among such measurements and typical literature data, usually taken in free standing samples, is not immediate, since the different stress and strain state in the polymer must be accounted for. In particular, it is well known that for an isotropic free sample the volume dilation is related to the deformation components in the following way:

$$\left.\frac{\Delta V_f}{V_f}\right|_{free} = \varepsilon_x + \varepsilon_y + \varepsilon_z = 3\beta(c)c \tag{1.12}$$

However such a relationship does not hold true when there are external constraints that hinder some components of the sample deformation, as it is the case of the polymer film on the cantilever. In this case, the boundary conditions are quite different and for a completely rigid plane substrate we have:

$$\sigma_x = \sigma_y = \frac{-E}{1-\nu}\beta(c)c \quad \sigma_z = 0 \tag{1.13}$$

$$\varepsilon_x = \varepsilon_y = 0 \quad \varepsilon_z = \left(\frac{1+\nu}{1-\nu}\right)\beta(c)c \tag{1.14}$$

so that the volume change is related to the penetrant induced dilation through the following relationship:

$$\left.\frac{\Delta V_f}{V_f}\right|_{planar\ coating} = \varepsilon_z = \left(\frac{1+\nu}{1-\nu}\right)\beta(c)c \tag{1.15}$$

which is clearly different from the case of isotropic dilation in free samples described by equation (1.12).

If the experimental determination of polymer swelling is performed in films cast over a cylindrical support, in order to avoid any bending and to increase the instrument sensitivity, the previous relationships have to be reworked in cylindrical coordinates, as follows:

$$\sigma_x = -E\beta(c)c \quad \sigma_r = \sigma_\vartheta = 0 \tag{1.16}$$

$$\varepsilon_x = 0 \quad \varepsilon_r = \varepsilon_\vartheta = (1+\nu)\beta(c)c \tag{1.17}$$

$$\left.\frac{\Delta V_f}{V_f}\right|_{cylinder} = \varepsilon_r + \varepsilon_\vartheta = 2(1+\nu)\beta(c)c \tag{1.18}$$

For rubbery polymers, whose Poisson ratio is close to the ideal value of 0.5, the two relationships of equations (1.15) and (1.18) are equivalent to one another. However, polycarbonate is glassy and its Poisson ratio is smaller (0.47) so that by using the relationship for a plane system the dilation value over the cylinder is underestimated.

1.2 Experimental

A schematic of the apparatus [15] is shown in Fig. 1-4, where the different parts of the experimental set up are shown. The system is composed of a special sample compartment, formed by a stainless steel cell endowed with two borosilicate glass windows in the opposite sides, to allow optical access for the measurements. The cell is connected to a reservoir containing the penetrant vapor and the pressure transducer, and to a second flask for the storage of liquid penetrant. A vacuum system, with a liquid nitrogen trap and a vacuum pump, is used to evacuate the apparatus before and after each experiment.

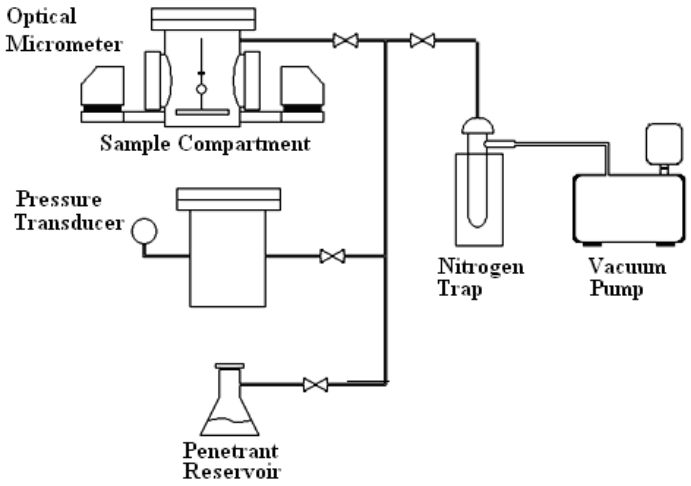

Fig. 1-4: Schematic of the bending beam apparatus used in the present work.

The sensing element is an optical micrometer (Keyence LS-7030-M) endowed with a high speed linear CCD sensor that ensures accuracy of 1 μm and reproducibility within 0.15 μm in the measurements. The measuring head features a gallium nitride (GaN) green LED whose light is converted into a parallel beam by a system of lenses, and it is directed on the cantilever through the borosilicate windows. The LED beam reaches then a telecentric optical system that uses only parallel light to form the image on the linear CCD sensor. The latter prevents fluctuations in lens magnification due to a change in target position and ensures an accurate measurement of the signal formed by bright and dark areas that correspond to the sample shade on the CCD. The measuring system is also provided with small CMOS image sensor for control purposes. The software used for signal elaboration is able to measure simultaneously two different distances between points characterized by a brightness difference higher than a chosen threshold, associated to a dark/bright transition. This feature permits to consider, at the same time, two separate measurements so that also the swelling progression of the polymer film can be registered, in addition to the deflection of the cantilever tip [16]. The dilation data are collected by monitoring the change in the thickness of a film supported on a rigid substrate that does not bend during the experiment.In Fig. 1-5 and Fig. 1-6, examples of the two experimental curves collected with the micrometer are shown.

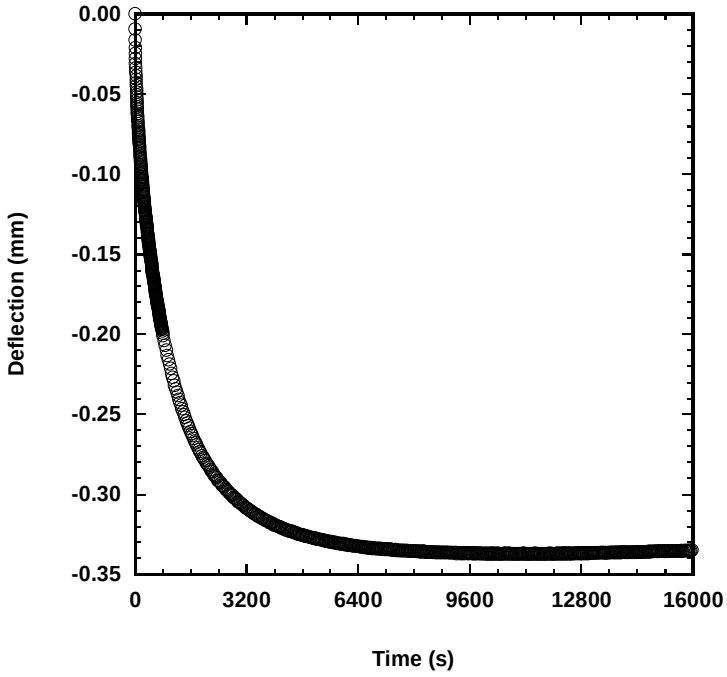

Fig. 1-5: Example of deflection experimental data.

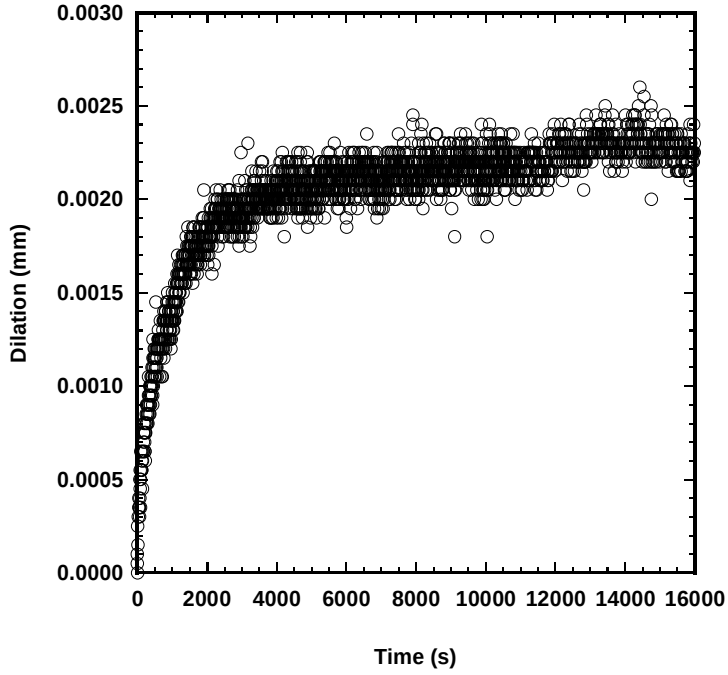

Fig. 1 6: Example of dilation experimental curve.

To avoid wrong positioning of the sample in the chamber, the micrometer is fixed on two manual roto-translational optical stages, one for the horizontal alignment of

transmitter and receiver with the sample, and one devoted to guarantee that the cantilever and the light beam are mutually orthogonal. The temperature is controlled in two stages: first the experimental cell is surrounded by two heating tapes that can reach temperatures up to 200°C, through which the temperature of the bending cantilever equipment is actually controlled; in addition, all the instrumentation is inserted in a thermostatic hood to eliminate the fluctuations of room temperature, due to the day/night cycles, that affect the response of the electronic devices. All the connections are made by stainless steel pipes and valves that are heated with a thermo resistance that can withstand 60°C. The system can operate under vacuum and up to a pressure of 8 bar that represents the working limit for the borosilicate windows of the sample cell.

Aluminum as well as stainless steel cantilevers (50.0x10.0x0.275 mm and 50.0x10.0x0.5 mm respectively) were used for the measurement of the deflection, while for the swelling data a stainless steel cylindrical support (about 15 mm in diameter) was used for more reliable measurements. Indeed such an axial-symmetric supports allowed to overcome the uncertainties that are associated to planar supports when the laser beam is not perfectly parallel to the surface of the cantilever, due to bending or not perfecting alignment.

The apparatus has been applied to polycarbonate-acetonitrile systems, for which a complete description of the transport properties as well as of the dilation can be found in literature [12], on the basis of different and more classical techniques such as FTIR-ATR spectroscopy and gravimetry. The experiments were conducted at 40°C through integral sorption runs, in which unpenetrated polymer films were exposed to different penetrant activities up to the value of 0.35.

Differential gravimetric tests were also performed in order to recover directly all the independent information needed for the simulation model, and to check also the applicability of the above mentioned literature data for the system under consideration. The apparatus used to that aim is a quartz spring balance [17], which was operated at the same temperatures and pressures used for the bending beam experiments, thus allowing the direct evaluation of solubility isotherm and diffusion coefficient of the polymer-penetrant pair considered.

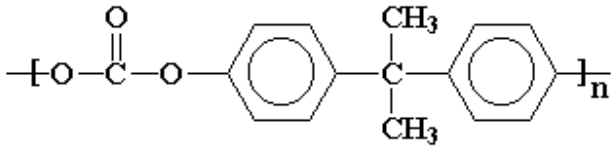

Fig. 1-7: Molecular structure of bisphenol-A- polycarbonate (PC)

The polycarbonate (Fig. 1-7) was provided by Sigma Aldrich and it was cast on the different cantilever supports using a 2% wt solution in dichloromethane. The casting on cylindrical rods was performed by rotating the support at controlled angular velocity while partially immersed in the solution. After casting, the samples were left to dry in a clean hood for few hours and then placed in a vacuum oven at 140°C overnight, in order to evaporate all the residual solvent and to relax the stress generated during deposition and drying. Such a procedure allowed to erase the effects of the past history of the glassy polymer, obtaining all samples in the same conditions at the beginning of the sorption tests. It is clear that the subsequent cooling stage induces a tensile stress in the PC coating over the cantilever, due to the differences in the thermal dilation coefficients of polymer and metal; therefore, the integral sorption step which follows produces an extra stress profile which adds to the one initially present in the samples.

After each experiment, the films were detached from the substrates and their thickness was measured obtaining values between 10 and 30 μm both in the case of planar cantilevers and cylindrical supports.

The solvent used for the experiments was purchased from Sigma Aldrich, 99,99% in purity, and was used without any further purification.

1.3 Results

The sorption experiments conducted with the gravimetric technique allowed the determination of both solubility and diffusion coefficient of acetonitrile in unconstrained films of PC. The sorption isotherm obtained is reported in Fig. 1-8 and shows the typical behavior encountered for glassy polymers with a concavity towards

the pressure axis at low penetrant pressures and an almost constant slope at the higher activities inspected. The data obtained are in very good agreement with those already presented in literature [12], in the common range of pressures.

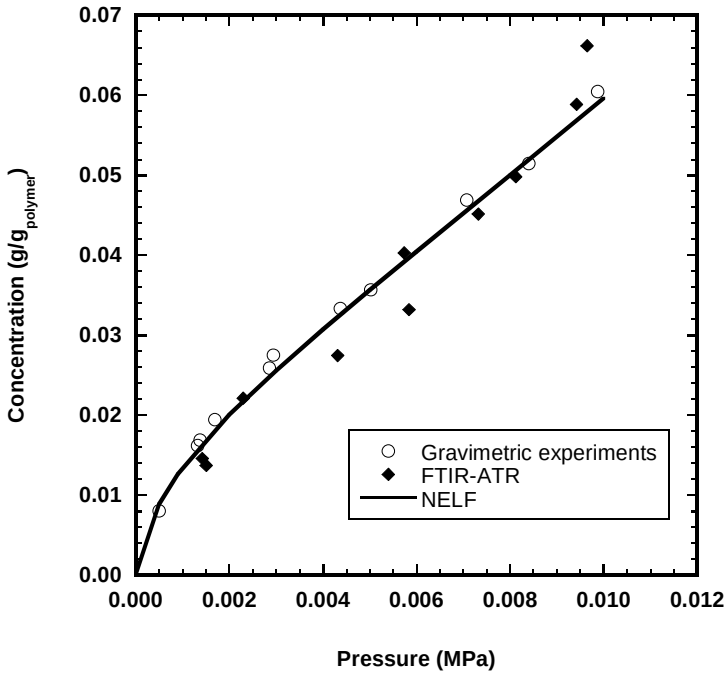

Fig. 1-8: Penetrant solubility for the system PC-CH_3CN, comparisons among literature and experimental data.

Together with experimental data, the solubility isotherm predicted by the non equilibrium lattice fluid model (NELF) [18-20] is also reported in the same figure. The NELF model is an extension of the Lattice Fluid equation of state [21, 22] for amorphous phases to the non equilibrium state that characterizes glassy polymers and allows the calculation of the sorption isotherm of one penetrant in a polymer known the parameters of the pure components. It is worth noting that the NELF model well represents the observed behavior by using the model parameters reported in ref. [12] and listed in Table 1-1; therefore, the NELF model will be used in the following to calculate the equilibrium penetrant concentration c_{eq} at the external polymer surface, to be used as the boundary condition in the mass transfer problem embodied by equation (1.10).

Film thickness	0.0155 mm
Young modulus -polymer -substrate	2400 MPa [23] 64000 MPa [24]
Poisson ratio -polymer -substrate	0.47 [23] 0.34 [24]
Diffusion kinetic	Fickian diffusion $D = 1\times10^{-9}e^{-7C}$
Concentration	Calculated from NELF model with following parameters [12]: CH_3CN: T^*= 505 K p^*= 910 MPa ρ^*= 0.885 g/cm^3 PC: T^*= 755 K p^*= 534 MPa ρ^*= 1.275 g/cm^3 k= 6.22 Mpa^{-1} ρ_0=1.200 g/cm^3 ψ=1.028
Linear swelling	Cubic Equation $\beta(c) = 0.056c + 3.11c^2 - 10.285c^3$ [12] Linear Equation $\beta(c) = 0.175c$

Table 1-1: Parameters used in the model

The typical transient sorption of CH_3CN in PC is presented in Fig. 1-9, where the data for differential sorption for an activity jump from 0.15 to 0.32 are reported. The mass uptake shows an initial Fickian behavior, followed by a relaxation process that takes place at the higher activities and over a longer time scale with respect to Fickian diffusion, and delays the attainment of the asymptotic equilibrium mass uptake. The relaxation stage is not always present but it is observed only for the integral sorptions ending at the higher activities.

Limiting the analysis to the Fickian part of the sorption process, the diffusion coefficient can be easily retrieved from the transient mass uptake data and equation (1.10), thus obtaining a slightly decreasing trend with concentration as it can be seen in Fig. 1-10. The values obtained are also in good agreement with literature data in a previous work and reported in the same figure for the sake of comparison.

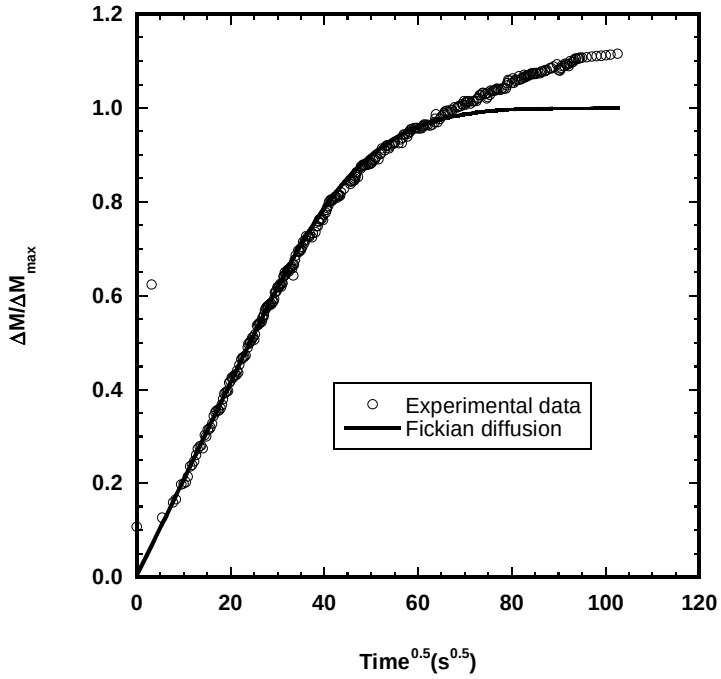

Fig. 1-9: Kinetics of the mass uptake by the polymer during a sorption experiment with an activity jump from 0.15 to 0.32. The line represents the results of the Fickian model.

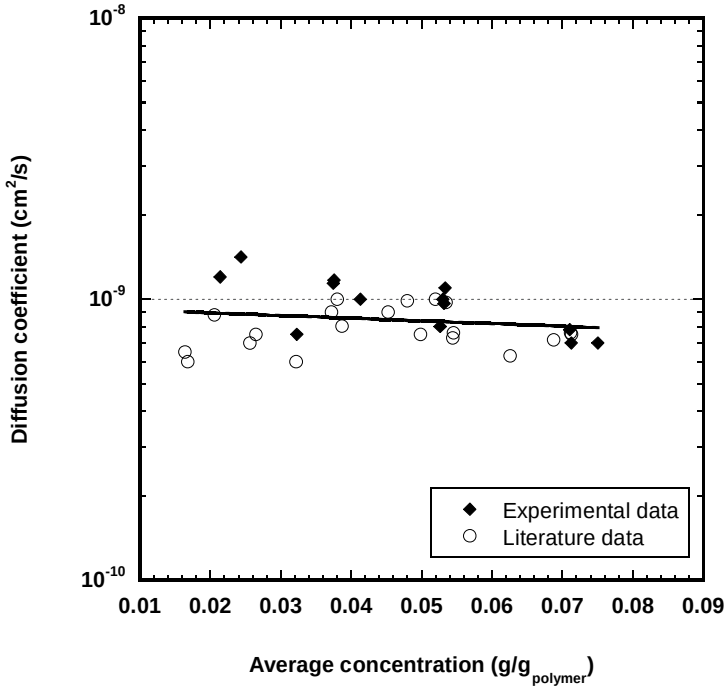

Fig. 1-10: Diffusion coefficient of CH_3CN in PC comparisons among literature data and data taken in the present work.

Consider now the swelling induced by the penetrant on the PC matrix, which represents important information for the elasto-diffusive problem. The swelling behavior in a film cast over a cylindrical support, obtained by using the experimental setup presented in this work, is reported in Fig. 1-11. The measured data were corrected by using equation (1.18) to convert the dilation in a constrained cylindrical geometry into the volume change of the corresponding unconstrained planar film. Clearly, in spite of some scatter in the data, a linear trend represents reasonably the dependence on penetrant concentration of the dilation behavior observed. The data obtained are in rather good agreement with the swelling behavior reported in literature [12] for unconstrained films and for the FTIR-ATR technique, in particular at the higher penetrant concentrations inspected, while at lower CH_3CN contents the dilation of the constrained film measured in this work are somewhat larger than the values obtained in ref. [12].

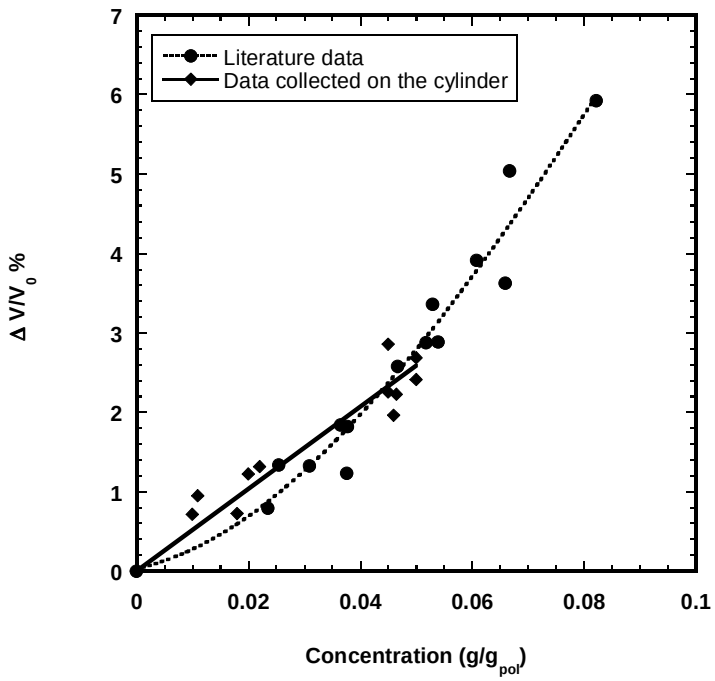

Fig. 1-11: Volume dilation of the polymer for integral sorption runs of acetonitrile in PC at 40°C; dotted line represents the cubic interpolation of data from ref. [12], solid line represents the linear behavior of the data obtained in this work.

From Fig. 1-11 one can also notice that over the broader concentration range inspected in ref. [12] the equilibrium dilation is a non linear function of penetrant concentration

and the best fitting of the dilation data is represented by a third order polynomial equation (also reported in Fig. 1-11) which, on the other hand, seems to underestimate at low activity the swelling data of the constrained films, for which a linear equation is more appropriate. It is useful to remember that previous studies conducted with the FTIR-ATR technique suggest that, during dynamic sorption the swelling process actually starts with some delay in time with respect to the concentration increase in the polymer [12], so that the partial molar volume of the penetrant increases as a function of penetrant concentration in the matrix.

It is also interesting to consider the evolution in time of the film swelling while penetrant sorption proceeds. In Fig. 1-12 the typical film thickness variation is reported versus the square root of time, considering the activity change from 0 to 0.35 for the constrained films inspected in this work. The experimental data clearly indicate a linear dependence of swelling with $t^{½}$, at least up to 70% of the maximum swelling, just as it is observed for the mass uptake. That appears an immediate consequence of the fact that volume dilation takes place simultaneously with the penetrant uptake. The observed behavior is also affected by the dilation coefficient β appearing in equation (1.9) and it is consistent with a constant value of β, namely with a linear dependence of dilation versus penetrant concentration, as it is actually observed for the swelling data obtained in the films constrained over the cantilever. The use of the cubic dilation relationship reported in literature, on the contrary, would not reproduce the trend experimentally observed. This is clearly demonstrated in Fig. 1-12 where it is also reported the sample thickness calculated versus time by using the concentration profile derived from equation (1.10) and the film thickness obtained by using equation (1.2). Solution of equation (1.10) was numerically obtained by using the concentration dependence of the diffusion coefficient reported in Table 1-1, while the equilibrium boundary condition, c_{eq}, was calculated by using the NELF model with the values of polymer and penetrant parameters reported in Table 1-1.

It is worth pointing out that no delay seems to exist between mass sorption and overall sample dilation, contrary to what was found through FTIR-ATR technique [12]. The volumetric data presented here do not show significant relaxation phenomena at longer times.

The deflection of the bending cantilever was monitored versus time during the integral sorption tests performed. A typical example of deflection curve as a function of time for the system under investigation is shown in Fig. 1 13, reporting the behavior of a film of about 16 μm, subject to an activity jump from 0 to 0.30 at 40 °C. Clearly also the deflection shows an initial linear behavior with the square root of time, as it is otherwise usual for processes driven by Fickian diffusion, with deviations from linearity starting approximately at 70% of the final deflection, before reaching the plateau corresponding to the asymptotic equilibrium deflection. In this case, relaxation phenomena may be visible if longer times are considered, with a very slow drift of the deflection that increases at longer times, likely because also the polymer mass uptake increases in the same time range.

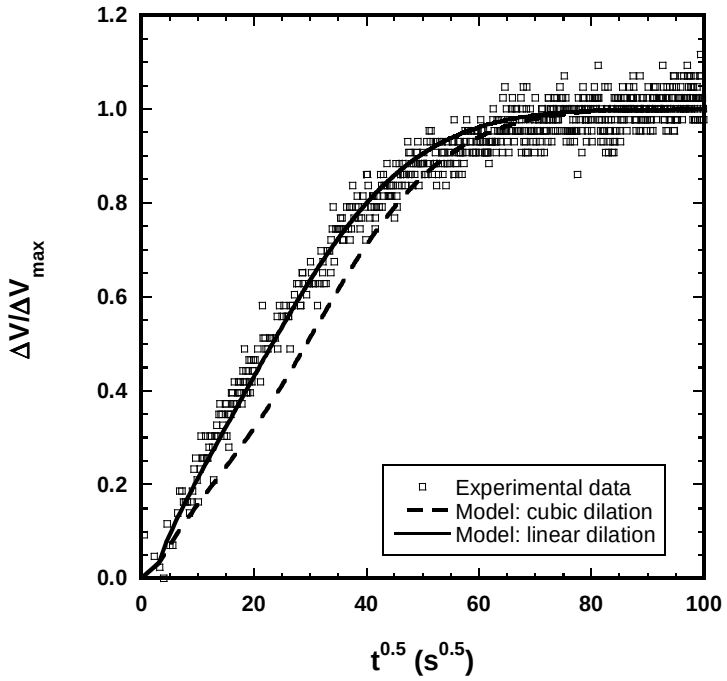

Fig. 1-12: Kinetics of polymer dilation for the system acetonitrile–PC at 40°C experimental data and comparisons with different models.

The behavior experimentally observed was also simulated by using the mathematical model represented by equations (1.1-11), by using the concentration dependence of diffusivity experimentally determined and reported in Table 1-1, as well as the values of the Young modulus and Poisson ratio obtained from refs. [23] and [24], reported in

the same table. The penetrant concentration at the polymer/vapor interface was calculated by using the NELF model [18-20] in a predictive way, as already mentioned above. The simulations were performed using both the linear relationship between volume dilation and penetrant concentration, measured for the constrained films, as well as the cubic relationship which results from FTIR-ATR technique in a broader concentration range. By using the values of the material properties listed in Table 1-1 the simulation does not contain any adjustable parameters and it is entirely predictive. The model outputs are the time dependences of the concentration profile, deformation and stress distributions in the polymer film and in the cantilever support, as well as the film thickness increase and the deflection of the cantilever tip.

It is remarkable to notice that the final value of cantilever deflection is dependent only on the equilibrium values of concentration, dilation and elastic properties of the system and is very well predicted by the model, as it is shown in Fig. 1-13. Different concentration dependences of dilation affect the evolution in time of the cantilever deflection, while they converge to the same final deflection experimentally observed at the end of sorption. This offers a strong support to the reliability and consistency of the model considered.

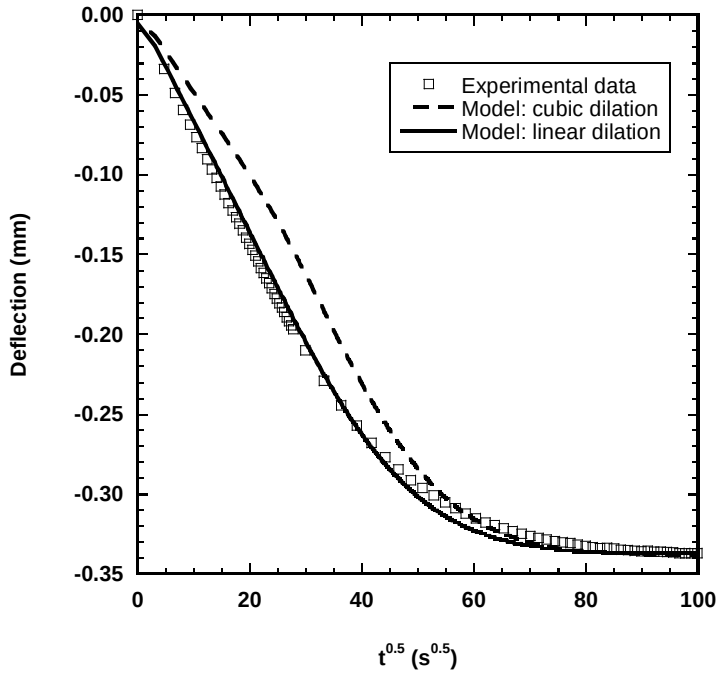

Fig. 1-13: Kinetics of deflection of an aluminum cantilever for an integral sorption run of acetonitrile in PC for an activity jump from 0 to 0.3 at 40°C, sample thickness 16 μm.

The analysis of the kinetics of the cantilever deflection needs to be considered with some attention due to the two different behaviors that can be used for the dilation of the polymer, with either a linear trend or a cubic dependence on concentration. The two different functions of $\beta = \beta(c)$ may be related to the different activity ranges in which the data are obtained in the different cases. However, it is not simply facing the case of approximating with a straight line a trend which is of higher order in a broader concentration range, since the use of a cubic dilation actually underestimates the polymer dilation observed for the constrained films, and its use in the simulation model to calculate the thickness of the polymer film (through equation (1.18), with the concentration profile given from the solution of equation (1.10)) leads to predictions which poorly represent the experimental data obtained (Fig. 1-12). On the contrary, the experimental data are indeed very well captured by the model using a constant value of β which corresponds to a linear relationship between swelling and concentration.

Such a discrepancy is reflected also on the simulations of the time evolution of deflection; the predictions obtained on the bases of the cubic concentration dependence of dilation, resulting from literature and FTIR-ATR data [12], clearly underestimate the deflection value measured with bending beam, while instead the observed behavior is well described by a simple linear equation as it can be seen in Fig. 1-13.

It is likely that differences in the dynamics of dilation are related to the different experimental techniques used to study the system. FTIR-ATR spectroscopy is actually a surface technique which samples only the interface between the sample and the ATR crystal, where the concentration is nearly homogeneous (for the so called “thick film approximation” [25]) and changes slowly with time with respect to what happens in the rest of the sample that, on the contrary, experiences great concentration gradients in a limited amount of time, especially in the early stages of diffusion. On the other hand, the optical technique applied monitors the overall sample in which the influence of the interfaces is usually small and its effects on the entire thickness are negligible. It is interesting to notice that the mentioned differences are limited to integral sorptions in the dry polymer since in subsequent differential sorption steps, as well as during desorptions, both FTIR-ATR spectrometry and the present technique show a constant

$\beta(c)$ value, namely a linear relationship between swelling and penetrant content in the matrix.

The validity of the simulation model was thus confirmed by the comparison with the time evolution of the sample thickness and of the cantilever deflection for all the runs performed. The model was then applied to calculate the time evolution of the stress profile inside the polymer film, during integral sorption steps, obtaining the typical behavior presented in Fig. 1-14, reporting the case of a film with about 18 μm of thickness during the sorption for an activity jump from 0 to 0.20; the values reported represent the stress change during penetrant sorption, whose profile is calculated through the model given by equations (1.1 ÷ 11) above. Indeed, at the beginning of the sorption tests the polymer films are not stress free since the sample preparation procedure, involving a thermal treatment at 140 °C, leaves a tensile stress in the polymer films at the test temperature of 40 °C; that is due to the different thermal expansion coefficients between PC and the metal support. By considering that the polymer film at 140 °C is stress free, and assuming an elastic behavior below T_g, the residual tensile stress after sample preparation can be estimated in a straightforward way and is in the order of 20 MPa. That initial value should be added to the compressive stress induced by swelling and reported in Fig. 1-14, to obtain the absolute stress in the sample.

During sorption in the films constrained over the cantilever the extra stress due to swelling is always compressive because the polymer dilation is prevented by the support; at any time the largest compressive stress is on the external surface of the sample, where the penetrant concentration has its higher value, and both penetrant concentration and stress decrease going from the external surface towards the more internal layers, closer to the interface between polymer and substrate. Noteworthy, the stress at the external surface of the films experiences a stepwise change, as it is the case for penetrant concentration, and remains practically constant during the diffusion process while the overall strain increases due to the progressive deformation of the inner layers of the polymer.

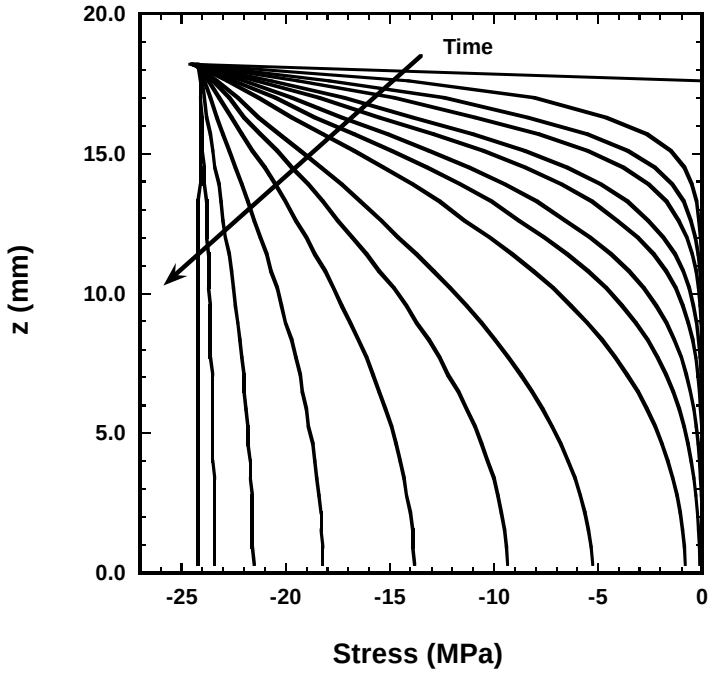

Fig. 1-14: Time evolution of the stress profile inside a PC film of δ=18 μm, during an integral sorption run of acetonitrile up to an activity of 0.20 at 40°C.

The value of the extra stress in excess to the initial stress distribution present in the polymer film ranges from zero to about -20÷-40 MPa, depending on the thickness of the polymer films, on the activity jump and on the material used as substrate; in view of the initial stress inside the film, after sorption has been completed the maximum stress in the polymer is thus around –10 MPa, which is rather low and well below the tensile strength of PC (62 MPa) [23], consistently with the fact that our model considers a completely elastic mechanical response for PC, with constant mechanical properties. Indeed, the polymer during the experiments remains well below its T_g and does not present any appreciable viscoelastic behavior. The relaxation phenomena some times visible at the later sorption times are essentially related to the presence of solvent which allows volume relaxation to take place, thus leading to the further increase of penetrant content in the polymer, without any detectable stress relaxation phenomena in the film, over the time scale inspected. The latter process would cause a decrease of the cantilever deflection rather than the slow increase visible in some experimental data, which confirms the ongoing dilation of the polymer.

The stress induced by penetrant sorption was in some cases sufficient to cause the detachment of the polymer film from the cantilever substrate, particularly during desorption, even if the extra stress calculated is rather limited in absolute value; this was also the main reason to switch to aluminum cantilevers from the stainless steel ones used in the first part of the study. In the cases in which loss of adhesion was observed, the stress value was not always the same and varied casually, suggesting the influence of various combined effects on the adhesion force, due to the sample roughness and random surface defects originated during sample preparation.

Conclusions

The bending beam technique was used to test the mass transport properties of acetonitrile in PC at 40°C and to evaluate the dilation and the stress induced in the polymer by penetrant diffusion.

Experiments were performed in integral sorption steps in which unpenetrated films cast over a metallic cantilever were exposed to different CH_3CN activities, up to 0.35. The experimental data collected include the evolution in time of cantilever deflection as well as the dilation of the film during sorption.

The experimental results were processed considering the solution of a simulation model which accounts for the calculation of the deformation and stress profiles due to swelling and calculates the cantilever deflection versus time. The model considers Fickian diffusion with a concentration dependent diffusivity, and a linear elastic mechanical response. The numerical values of Young modulus and Poisson ratio are taken from data collections, while the diffusion coefficient used in the simulation was obtained through independent measures of transient mass uptake in free films. The concentration dependence of the volume dilation was taken from direct experimental data. The solubility isotherm obtained for a free film matches very well the data in literature and are well described by the NELF model used in predictive way with the model parameters reported in ref. [12]. The dilation data obtained for the films constrained over the cantilever support indicate that a linear dependence on penetrant

concentration is more suitable than the cubic relationship reported over a broader concentration range, using both free films as well as FTIR-ATR technique. By accounting for the proper expression of volume dilation to compare the behavior of free and constrained films, the dilation data obtained match well with the data presented in ref. [12] in the higher concentration range, while somewhat larger swellings are observed at lower concentrations.

By using the material properties obtained from independent measurements, the simulation model becomes entirely predictive and its results were compared with the experimental data of cantilever deflection and overall film thickness versus time, during the integral sorption experiments. By using the linear concentration dependence of volume swelling the comparison between model predictions and experimental data is very good at all times, while the use of the cubic relationship obtained under different experimental conditions, allows only to calculate the correct value of the final asymptotic deflection and not the correct evolution in time observed for the cantilever bending which is initially linear with $t^{½}$. The time evolution of the stress profile induced by penetrant sorption in the polymer layer was also calculated and its maximum value for the films under study is in the order of -10 MPa, considering also the initial residual stress in the membrane due to the formation procedure.

References

1. Tong, H.M., Hu, C.K., Feger, C. and Ho, P., *Stress Development in Supported Polymer Films During Thermal Cycling.* Polym. Eng. Sci, 1986. **26**(1213).
2. Ferrari, M.C., Piccinini, E., Giacinti Baschetti, M., Doghieri, F. and Sarti, G.C., *Solvent-Induced Stresses during Sorption in Glassy Polycarbonate: Experimental Analysis and Model Simulation for a Novel Bending Cantilever Apparatus.* Industrial & Engineering Chemistry Research, 2008. **47**(4): p. 1071-1080.
3. Campbell, D.S., *Mechanical Properties of Thin Films*, in *Handbook of Thin Film Technology*, L.I. Maissel and R. Glang, Editors. 1969, McGraw-Hill: New York.
4. Hoffman, R.W., *Mechanical Properties of Non-metallic Thin Films*, in *Physics of Nonmetallic Thin films,* C.H.S. Dupuy and A. Cachard, Editors. 1976, Plenum: New York.
5. Tong, H.M. and Saenger, K.L., *Bending-Beam Characterization of Thin Polymer Films*, in *New Characterization Techniques for Thin Polymer Films*, H.M. Tong and L.T. Nguyen, Editors. 1990, Wiley Interscience: New York.
6. Wilcox, J.D. and Campbell, D.S., *A Sensitive Bending-Beam Apparatus for Measuring the Stress in Evaporated Thin Films.* Thin solid films, 1969. **3**: p. 3.
7. Berry, B.S. and Pritchet, W.C., *Elastic and Viscoelastic Behavior of a Magnetic Recording Tape.* IBM J. Res. Develop., 1988. **32**: p. 682.
8. Han, B., Tong, H.M., Saenger, K.L. and Gryte, C.C., *Mechanical Property Determination for Supported Polymer Films Using Double Bending-Beams.* Mat. Res. Soc. Symp. Proc., 1987. **76**: p. 123.
9. Jou, J.H., Hwang, J. and Hofer, D.C., *In Situ Measurement of Temperature Dependance of Internal Residual Stress in Polymide Films Coated on Silicon Substrate.* IBM Research Report, 1987. **RJ 5984**.
10. Astarita, G. and Sarti, G.C., *Class of Mathematical Models for Sorption of Swelling Solvents in Glassy Polymers.* Polym. Eng. Sci., 1978. **18**: p. 388.
11. Chen, S.T., Yang, C.H., Faupel, F. and Ho, P., *Stress Relaxation During Thermal Cycling in Metal/Polymide Layered Films.* J. Appl. Phys., 1988. **64**: p. 6690.

12. Giacinti Baschetti, M., Piccini, E., Barbari, T.A. and Sarti, G.C., *Quantitative Analysis of Polymer Dilation during Sorption Using FTIR-ATR Spectroscopy.* Macromolecules, 2003. **36**: p. 9574.
13. Dietz, A.G.H., *Composite engineering laminates*. 1969, Cambridge, MA: MIT Press.
14. Love, A.E.H., *On the Small Free Vibrations and Deformations of the Elastic Shells.* Phil. Trans. of the Royal Soc. A, 1888. **17**: p. 491.
15. Piccinini, E., *Studio delle Proprietà Volumetriche di Membrane Polimeriche nel Trasporto di Materia*, Ph.D Thesis, 2004, *DICMA*, Alma Mater Studiorum - Università di Bologna: Bologna.
16. Ferrari, M.C., *Analisi della dilatazione e dello stress indotti in film polimerici da processi di assorbimento/desorbimento: messa a punto di una tecnica di indagine sperimentale*, Thesis, 2004, *DICMA*, Alma Mater Studiorum - Università di Bologna: Bologna.
17. Piccinini, E., Giacinti Baschetti, M. and Sarti, G.C., *Use of an automated spring balance for the simultaneous measurement of sorption and swelling in polymeric films.* J. of Memb. Sci., 2004. **234**: p. 95.
18. Doghieri, F. and Sarti, G.C., *Nonequilibrium lattice fluids: A predictive model for the solubility in glassy polymers.* Macromolecules, 1996. **26**: p. 7885.
19. Giacinti Baschetti, M., Doghieri, F. and Sarti, G.C., *Solubility in glassy polymers: Correlations through the nonequilibrium lattice fluid model.* Ind. & Eng. Chem. Res., 2001. **40**: p. 3027.
20. Sarti, G.C. and Doghieri, F., *Predictions of the solubility of gases in glassy polymers based on the NELF model.* Chem. Eng. Sci., 1998. **53**: p. 3435.
21. Lacombe, R.H. and Sanchez, I.C., *Statistical thermodynamics of fluid mixtures.* J. Phys. Chem., 1976. **80**: p. 2568.
22. Sanchez, I.C. and Lacombe, R.H., *An elementary molecular theory of classical fluids. Pure Fluids.* J. Phys. Chem., 1976. **80**: p. 2352.
23. McCrum, N.G., Buckley, C.P. and Bucknall, C.B., *Principles of Polymer Engineering*. 1997, New York: Oxford University Press.
24. Tweeddale, J.G., *The mechanical properties of metals*. 1964, New York: Elsevier.
25. Elabd, Y.A., Diffusion in Polymers: Penetrant-Polymer and Penetrant-Penetrant Interactions. , Ph.D Thesis, 2000, Johns Hopkins Univ.: Baltimore, MD.

2 Mixed Matrix Membranes based on amorphous Teflon® and Fumed Silica

In gas separation, the performance of a membrane is evaluated through the selectivity with respect to the component *i* of a mixture formed by penetrants *i* and *j* that is defined as:

$$\alpha_{i,j} = \frac{P_i}{P_j} = \alpha_D \alpha_S = \frac{D_i}{D_j}\frac{S_i}{S_j} \tag{2.1}$$

where P_i is the permeability of the *i* penetrant and can be calculated as the product of diffusivity D and solubility coefficient S, provided that the solution-diffusion model holds true and the Fick's law can represent the diffusive mass flux.

Polymers are currently the dominant materials for gas separation membranes because of their processability that allows the economic production of modules for large scale separation. Their separation ability, however, is still low compared to more rigid and thermally stable inorganic molecular sieving media and this fact limits their employment. An upper limit for the performance of polymeric membranes in gas separation was estimated by Robeson [1] in early 1990s, based on experimental permeability and selectivity data for some gas pairs. Such limit was recently updated considering also the latest experimental data [2]. These plots indicate that, for polymeric materials there is a trade-off between permeability and selectivity with the upper bound limit shown in Fig. 2-1, while inorganic materials properties lie beyond this limit in the desired performance area.

The immediate application of inorganic membranes is, on the other hand, still hindered by the difficulties in forming defect-free membranes and by the extremely high costs of production. A significant development can be achieved taking advantage of the peculiar characteristic of both polymeric and inorganic materials, by dispersing an inorganic phase in a polymeric one, as shown schematically in Fig. 2-2 [3]. This class of composites is usually referred to as Mixed Matrix Membranes (MMM) and its investigation for gas separation was first reported in 1970s by Paul and Kemp [4] that

noticed that the time lag for gas diffusion was increased after adding zeolite to a rubbery polymer.

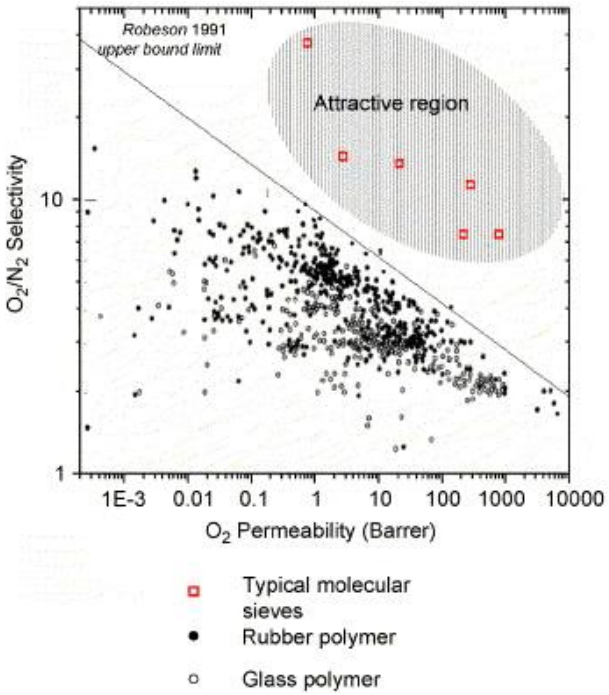

Fig. 2-1: Relationship between O_2/N_2 selectivity and O_2 permeability for polymeric and inorganic membranes. [1,3]

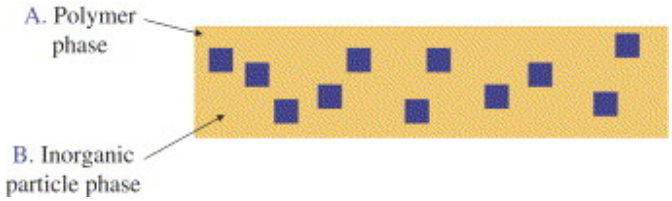

Fig. 2-2: Schematic of a mixed matrix membrane (MMM) [3].

Conventional MMMs [3,5-11] are obtained by addition of porous inorganic fillers like zeolites to polymeric matrices with similar selective behavior, that can result in a significant increase of the separation efficiency as predicted by the Maxwell model [12]. The model was originally derived for the dielectric properties of composite materials with spherical particles but it is a simple and effective tool even for this kind of MMMs.

The polymeric membranes employed show good selective properties in their pure form as polyimides or polysulfone.

An alternative concept has been introduced in the development of mixed matrix membranes in 2002 and implies the addition of non-porous nano-sized particles to high free volume glassy polymeric matrices [3,13-15]. Although the filler does not contribute to transport directly, because it is considered impermeable, it can modify the molecular packing of the polymer chains, in many cases resulting in an enhancement of the separation properties of glassy polymeric membranes. Among the polymers considered as matrices for such composite membranes, poly(4-methyl-2-pentyne) (PMP) is the one that shows the best performance, in combination with fumed silica. PMP is a reverse-selective glassy polymer that is more permeable to condensable vapors than to small, non-condensable ones, due to its high free volume that lowers the diffusivity selectivity, favorable to small penetrants, and enhances the solubility selectivity, favorable to condensable penetrants. The addition of non-porous hydrophobic fumed silica further increases the fractional free volume of the polymer and therefore increases the permeability to n-butane as shown in Fig. 2-3 [14].

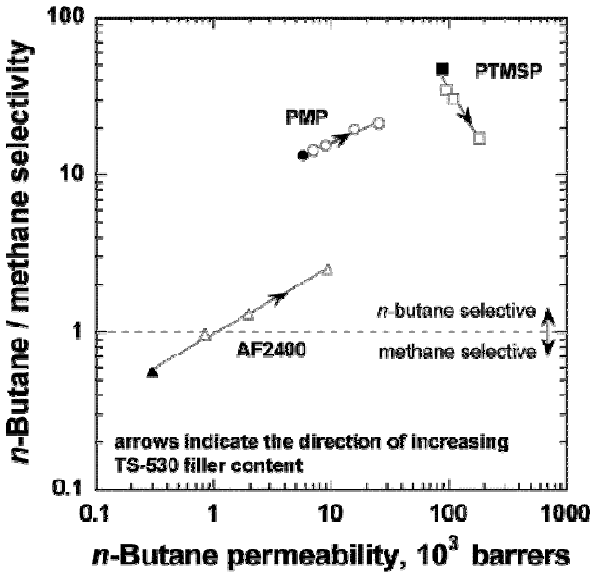

Fig. 2-3: Mixed gas n-butane/methane selectivity vs. n-butane permeability for different polymers [14].

Moreover, in the case of PMP the addition of silica leads to increased selectivity for the gas pair n-butane/methane. In Fig. 2-3 data for poly(1-trimethylsilyl-1-propyne) (PTMSP) and amorphous Teflon® are also reported. The effect of the addition of silica

particles clearly depends on the matrix: for PTMSP there is a decrease in selectivity while the permeability to n-butane increases with the introduction of inorganic phase. Such behavior can be related to the highly microporous structure [3] of this material that is further increased by the inorganic phase; the leading transport mechanism for gases therefore becomes the Knudsen diffusion which results in a selectivity inversely proportional to the diffusant molecular weight and compromises the initial n-butane selectivity. The case of Teflon® AF 2400 is rather peculiar: the pure polymer exhibits selectivity for the smaller penetrant (methane) but after the addition of particles, the composite materials becomes progressively n-butane selective. The sorption isotherm of this material is only slightly affected by the inorganic filler, while the diffusion coefficient is significantly increased by the addition of particles determining the increase in permeability. Fumed silica is a nonporous material and therefore a penetrant is adsorbed only on its surface; to explain the observed sorption behavior it can be supposed that the filler modifies the packing structure of the polymeric matrix increasing it sorption capacity that can compensate for the lower sorption in the particles. It can be assumed that the introduction of inorganic particles in an organic material creates additional free volume at the interface between the two phases and this leads to a slight variation of the sorption behavior but to an higher diffusivity even if there are more obstacles on the penetrant molecules path. This assumption is in agreement with PALS measurements that found two different populations of holes in the MMM, and that the ones characterized by the smaller size is increased after the addition of FS [13,15,16]. This could also explain the higher increase for the permeability of small gases compared to the one of larger penetrants in the composite.
For MMMs formed with high free volume polymers, the simple Maxwell model cannot certainly be applied and therefore there is need for a model that can predict the selective properties of these promising materials. Recently a method [17], based on the NELF model for solubility, was proposed to predict the enhancement in diffusivity due to the addition of fumed silica particles to high free volume matrices as PTMSP and Teflon® AF 2400 accounting for the contribution to permeability of diffusivity and solubility separately.

In this work mixed matrices based on amorphous Teflon® AF2400 and AF1600 have been tested extensively in order to obtain experimental values for all the transport properties; moreover the method based on the NELF model has been applied to describe the experimental data and predict gas separation performances of the membranes.

2.1 Theory

The addition of particles to a polymeric matrix follows the idea of combining qualities of the two materials and therefore it would be useful to predict the behavior of composite materials from the properties of the pure components. In literature there are no models that can predict correctly the behavior of the materials under investigation. Only models for permeability are available and they predict a decrease in permeability as rigid particles are added to the matrix due to the increase in the tortuosity of the path that the penetrant molecules have to follow in the diffusion through the membrane. One of the most commonly used is the Maxwell model [12], initially derived for the permittivity of a dielectric and for spherical particles, that relates the permeability in the composite material to the permeability in the pure matrix:

$$P_i = P_{i,P}\left(\frac{1-\Phi_F}{1+\Phi_F/2}\right) \qquad (2.2)$$

where Φ_F is the volume fraction of particles. Even if suitable for some MMM with non porous fillers, this model is certainly not applicable to the case of amorphous Teflon® and Fumed Silica. A new method [17] based on the NELF model was thus developed that can predict the behavior not only of permeability but also of solubility and diffusivity separately.

2.1.1 NELF model

The NELF model [18-20] is an extension of the Lattice Fluid equation of state [21-23] for amorphous phases to the non equilibrium state that characterizes glassy polymers. Starting from the Sanchez and Lacombe theory, the model uses the same characteristic parameters $\left(p^*, \rho^*, T^*\right)$ to evaluate the properties of pure components and the same mixing rules to estimate the mixture properties.

The characteristic lattice parameters ρ^* and p^* represent the mass density and cohesive energy density at close packed conditions, while T^* is associated with the average interaction energy between the chain segments contained in nearby lattice cells. These parameters can be calculated fitting the LF equation of state to PVT data above T_G for the polymer and to either PVT or VL data for the penetrant.

The number of lattice sites occupied by a molecule in its pure phase is given by:

$$r_i^0 = \frac{p_i^* M_i}{RT_i^* \rho_i^*} = \frac{M_i}{\rho_i^* v_i^*} \tag{2.3}$$

where M_i is the molecular weight of component i and v_i^* is the volume occupied by a mole of lattice sites of pure substance; the parameter r_i^0 is usually set to infinity for the polymer species. To calculate the mixture characteristic parameters the following mixing rules can be considered starting from the pure components values:

$$\frac{1}{\rho^*} = \frac{\omega_1}{\rho_1^*} + \frac{\omega_2}{\rho_2^*} \tag{2.4}$$

$$p^* v^* = RT^* \tag{2.5}$$

$$p^* = \phi_1^2 p_1^* + \phi_2^2 p_2^* + 2\phi_1\phi_2 p_{12}^* \tag{2.6}$$

where ϕ_i is the volume fraction of species i, defined in terms of the mass fraction ω_i as:

$$\phi_i = \frac{\omega_i / \rho_i^*}{\omega_1 / \rho_1^* + \omega_2 / \rho_2^*} \tag{2.7}$$

The binary characteristic pressure p_{12}^*, that represents the energetic interactions per unit volume between gas and polymer molecules, is constant with respect to composition and temperature and can be represented as:

$$p_{12}^* = \Psi\sqrt{p_{11}^* p_{22}^*} \tag{2.8}$$

where Ψ is the only adjustable parameter present in the model that can be determined through experimental miscibility data.. A first order approximation can be obtained using $\Psi = 1$ when no specific data for the mixture are available.

Using the Non Equilibrium thermodynamic for Glassy Polymers (NET-GP) approach [24], the model can be extended to non equilibrium states typical for glassy polymers. In this view, the state of the mixture is described by the usual state variables (temperature, pressure and composition) plus the polymer density ρ_2 that accounts for the departure from equilibrium. The density is assumed to be an internal state variable so that the usual thermodynamic relations for systems with an internal state variable holds true [25].

The phase equilibrium requires the equation of the chemical potential of the penetrant in the external gas phase and in the mixture with the polymer:

$$\mu_1^{NE(s)}\left(T, p, \Omega_1^{PE}, \rho_2^{PE}\right) = \mu_1^{Eq(g)}\left(T, p\right) \tag{2.9}$$

In order to evaluate solubility the characteristic parameters of the pure components are necessary together with the density of the glassy polymer in the experimental conditions. If the characteristic parameters for the pure components can be found in specific collections, the density depends also on the history of the samples and should be determined from the dilation during sorption experiments.

For non-swelling penetrants the density can be considered a constant and only the initial value has to be known but for swelling agents the density variation cannot be neglected. However, in most cases there is a linear dependence of the polymer density on the partial pressure of the vapor and a swelling coefficient k_{sw} can be introduced to account for its variation:

$$\rho_2\left(p\right) = \rho_2^0\left(1 - k_{sw}p\right) \tag{2.10}$$

Since specific dilation data are not usually available in literature, the parameter k_{sw} can be adjusted on one solubility datum at high pressure providing also an estimate of the swelling behavior of the matrix, while the binary parameter Ψ should be adjusted on the first section of the isotherm, i.e. at low pressure, where the swelling is not relevant yet even for high swelling penetrants.

The introduction of equation (2.10) in equation (2.9), leads to the new phase equilibrium condition that allows the calculation of the sorption isotherm for the mixture:

$$\mu_1^{NE(s)}\left(T, p, \Omega_1^{PE}, \rho_2^0, k_{sw}\right) = \mu_1^{Eq(g)}\left(T, p\right) \qquad (2.11)$$

The NELF model has been successfully used to predict gas sorption isotherms in pure glassy polymers and in polymer blends in the glassy state, both in the case of non-swelling or swelling penetrants [18, 26].

2.1.2 Free Volume estimation

A common way to evaluate factional free volume is based on the evaluation of the "occupied volume" V_0 that is related to the van der Waals volume of the molecule (V_W) by the approximate relationship: V_0=1.3 V_W:

$$FFV = \frac{V_2 - 1.3V_W}{V_2} = \frac{\rho_2^W - 1.3\rho_2^0}{\rho_2^W} \qquad (2.12)$$

the Van der Waals volume of the repeating unit of the polymer can be calculated with the group contribution method and its value is available in literature for the matrices of interest in this study [27].

The NELF model can be applied to calculate sorption isotherm of composite matrices [17] if the contributions of the two phases are considered separately. Gas solubility in a composite matrix is usually represented through a simple additive rule that considers the sorption capacity of the polymer and of the filler unaffected by the presence of the other component. This is not the case for mixed matrices of high free volume glassy

polymers and impermeable fillers where the addition of the inorganic rigid phase affects the actual free volume of the polymer and its swelling behavior. The different FFV is associated to defects at the polymer/filler interface and can be accounted for in the density of the polymeric phase in the composite. It can be assumed that the presence of filler affects only the organic phase, adding free volume elements at the interface with the inorganic particles and therefore increasing the mass uptake of the polymer, while the sorption capacity of the filler can be considered unchanged in the view of the fact that the adsorption occurs only on the surface and is rather small compared to the total solubility.

The total solubility can be written as a sum of two contributions, one due to the polymeric phase and one due to the filler:

$$C_{i,M} = \frac{n_{i,F} + n_{i,P}}{V} = \Phi_F C_{i,F} + \left(1 - \Phi_F\right) C_{i,P} \qquad (2.13)$$

where Φ_F is the volume fraction of the filler, $C_{i,M}$ is the gas solubility per unit volume of mixed matrix, $C_{i,F}$ and $C_{i,P}$ are the gas solubilities in the filler and in the polymer, per unit volume of filler and per unit volume of polymer, respectively. Using the simple additive rule would lead to consider $C_{i,P} = C^0_{i,P}$ and $C_{i,F} = C^0_{i,F}$ and hence:

$$C_{i,M} = \Phi_F C^0_{i,F} + \left(1 - \Phi_F\right) C^0_{i,P} \qquad (2.14)$$

As it will be shown in the results section, equation (2.14) cannot represent the data for MMMs with non porous fillers in high free volume polymers.

If one assumes, instead, that only the filler mass uptake is unchanged in mixed matrix conditions, $C_{i,F} = C^0_{i,F}$, equation (2.13) becomes:

$$C_{i,M} = \Phi_F C^0_{i,F} + \left(1 - \Phi_F\right) C_{i,P} \qquad (2.15)$$

If the experimental solubility for a given penetrant in the mixed matrix and in the pure filler is available, the solubility isotherm for the polymeric phase in composite condition can now be determined. The NELF model can be consequently applied to the polymer contribution in order to derive the two parameters ρ_2^0 and k_{sw}, through a best fitting procedure. The binary parameter Ψ is reasonably considered the same in the

pure polymer and in the polymeric fraction of the composite sample, while the value of ρ_2^0 representing the pure polymer density in the mixed matrix conditions will vary with the content of filler but not with the penetrant. The value of k_{sw} accounts for the swelling effects of the specific penetrant on the polymer and thus has a different value for every couple polymer-gas.

2.1.3 Estimation of diffusivity and permeability in mixed matrix membranes

The influence of the penetrant concentration on the diffusion coefficient in composite membranes can be well represented with an exponential law:

$$D_C = D_C(0)\exp(\beta C) \tag{2.16}$$

where $D_C(0)$ is the infinite dilution apparent diffusion coefficient in the mixed matrix, C the average concentration and β is a constant that is characteristic of the polymer-gas couple and depends on temperature. If only the infinite dilution diffusivity $D_C(0)$ is considered, the swelling effects can be neglected.

A semi empirical law, based on the free volume theory [28,29], is usually considered to hold between the infinite dilution diffusion coefficient in the polymer and the FFV in the same phase:

$$\ln\left(D_P(0)\right) = A - \frac{B}{FFV} \tag{2.17}$$

where A and B are parameters that depends on temperature and are specific to each system polymer-gas.

The diffusion coefficient of the mixed matrix is influenced not only by the diffusivity in the polymeric phase but also by the presence of the filler: the particles are impermeable and act as an obstacle on the path of the gas molecules through the membrane. $D_C(0)$ is then an apparent diffusion coefficient that can be related to $D_P(0)$ using a tortuosity factor τ:

$$D_C(0) = \frac{1}{\tau} D_P(0) \tag{2.18}$$

τ can be evaluated from the Maxwell model [12] derived for spherical particles:

$$\tau = 1 + \frac{\Phi_F}{2} \tag{2.19}$$

Combining equations (2.17) and (2.18), a relation between the apparent infinite dilution diffusion coefficient in the mixed matrix and the FFV of the polymeric fraction is obtained:

$$D_C(0) = \frac{1}{\tau} \exp\left(A - \frac{B}{FFV} \right) \tag{2.20}$$

Considering experimental diffusivity data for at least two values of FFV, that can be calculated from the sorption isotherm of a reference vapor in two different mixed matrix formulations, the parameters A and B can be determined and used to predict $D_C(0)$ for any other value of filler loading. Moreover, the ratio between the diffusivity in the composite and the diffusivity in the pure polymer can be determined with only one adjustable parameter B:

$$\frac{D_C(0)}{D_P^0(0)} = \frac{1}{\tau} \exp\left[B\left(\frac{1}{FFV_P^o} - \frac{1}{FFV} \right) \right] \tag{2.21}$$

where FFV_P^0 is the fractional free volume of the unloaded pure polymer. To calculate the ratio between the infinite dilution diffusion coefficients at any filler loading only one experimental point is needed.

In the end also the permeability ratio can be evaluated:

$$\frac{P_C(0)}{P_P^0(0)} = \frac{D_C(0)}{D_P^0(0)} \frac{S_C(0)}{S_P^0(0)} \tag{2.22}$$

where the ratio between diffusivities can be calculated from equation (2.21) and solubility ratio comes from the calculation with the NELF model. Finally, the NELF model can also be used to evaluate the swelling of the matrix induced by the sorption process, which can be compared to experimental swelling data to evaluate the reliability of the procedure.

The proposed method is summarized as in the scheme of Fig. 2-4.

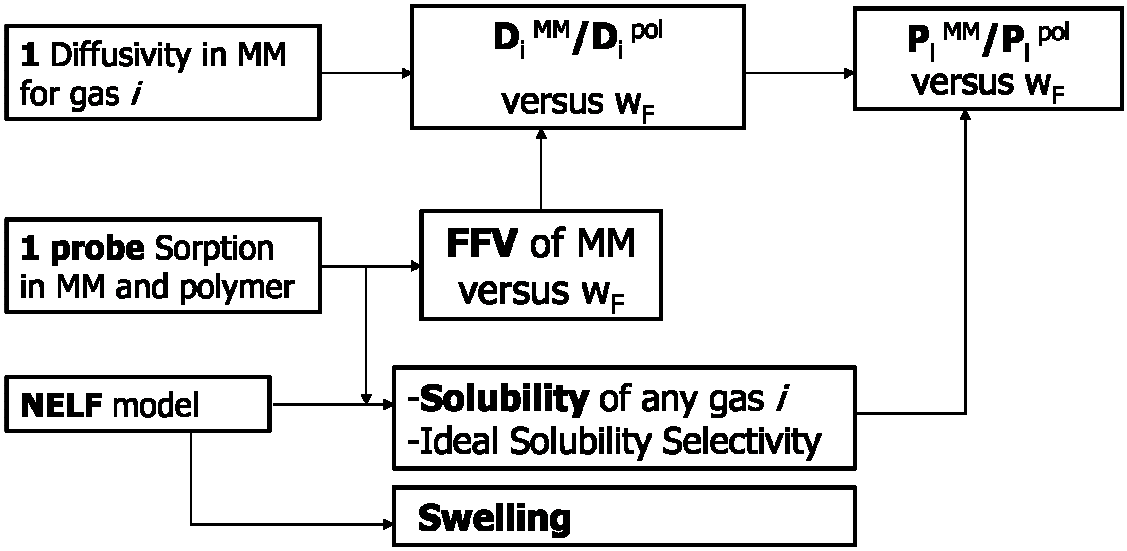

Fig. 2-4: scheme of the approach used to evaluate the transport properties of mixed matrix membranes.

2.2 Experimental

2.2.1 Materials

Teflon® AF2400 is a glassy perfluorinated copolymer obtained by random copolymerization of 2,2-bis(trifluoromethyl)-4,5-difluoro-1,3-dioxole (BDD) and tetrafluoroethylene (TFE) (Fig. 2-5) at mole fractions of 87% and 13% respectively. Its glass transition temperature is 240°C and its density is equal to 1.74 g/cm^3; the polymer has an excellent chemical resistance and high gas permeability. Teflon® AF1600 is obtained by copolymerization of the same monomers with different mole fractions: 65% of BDD and 35% of TFE and its density is 1.85 g/cm^3.

The filler used (nonporous Fumed Silica TS-530, *Cabot Corporation*) (Fig. 2-6). has been chemically treated with hexamethyldisilazane, in order to replace hydroxyl surface groups with hydrophobic trimethylsilyl groups. The particles have an average diameter of 12 nm and a density of 2.2 g/cm^3.

Pure and composite films were obtained by solution casting: the polymer was dissolved in a perfluorinated solvent (perfluoro-N-methyl-morfoline, PF5060, supplied

by 3M) to obtain a 1% wt solution. The appropriate amount of filler was added to the solution and the resulting mixture stirred at 15000 rpm for 2-3 min in a Waring two-speed laboratory blender: the mixture was then casted into a Petri dish and covered with an aluminum foil, allowing the solvent evaporation. The films were completely dried within about 48h and they did not undergo any treatment before sorption experiments.

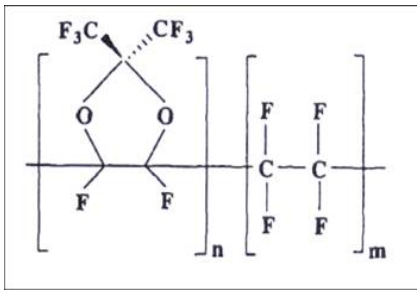

Fig. 2-5: Molecular structure of Teflon® AF.

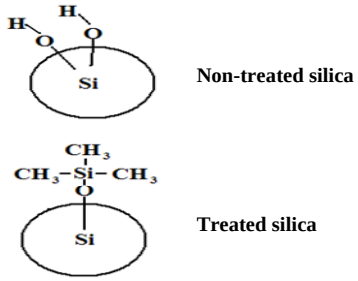

Fig. 2-6: Non porous fumed silica before and after treatment to have a hydrophobic surface.

It seems that the solvent evaporation is the critical step to obtain good films, while the stirring time has no influence on the resulting membranes. Mixed matrices with different loading of filler were prepared: 10 and 25% wt for AF1600 and 25 and 40% wt for AF2400 and the final thickness of all the films was about 90 μm.

The penetrants used in all the experiments, n-butane and n-pentane, were supplied by Sigma-Aldrich and used without any further purification.

2.2.2 Density

The initial density of the membrane is a key parameter in the modeling approach proposed and therefore conspicuous efforts were made to measure its value for all the

mixed matrices. Different techniques were used to this aim, but the results were not always satisfying.

The simplest method used requires a determination of the film volume and weight: such method is expected to be not the most accurate but reliable for a first estimate. A sample of regular shape was weighted with a balance of accuracy $\pm 10^{-5}$g ; the film thickness was measured with a micrometer of accuracy $\pm$ 1 μm and the area with a calipers of accuracy $\pm$ 0.05 mm. The density measured in this way for AF2400 matrices gave the results that are listed in Table 2-1. In the table we also reported the value of the density of the polymeric phase, considering the filler density to be equal to its pure value, as well as the FFV value calculated through eq. (2.12). It can be seen that the density of the polymeric phase does not vary monotonically with filler content, as it was expected, and the data obtained with this method were not used for modeling purposes.

The second method used was an hydrostatic weighing method that employed a precision balance Sartorius and a density determination kit provided by the same company. The measurement consists in weighing the sample in air and then in deionized water at fixed temperature; the density of the sample can then be calculated after evaluating the buoyancy force. The results of this set of measurements were extremely scattered and several different methods were attempted to reduce the scattering, such as sonication of the water bath to remove air bubbles, but none of these could reduce the dispersion to an acceptable level.

Finally, another method that is based on the evaluation of the buoyancy force was used, using a Rubotherm magnetic suspension balance (MSB). In this case the sample is first weighed in vacuum and than in a nitrogen atmosphere. Particular attention has to be paid since nitrogen is absorbed in the polymer: to account for this phenomenon, that alters the weight of the sample an iterative procedure was used. First the film density was calculated from the MSB experiment and the value obtained was used to calculate the mass uptake value with the NELF model (parameters for the system are already available in literature [30]); then the sorption contribution was subtracted from the weight of the sample to calculate the new density value. If the result was considerably far away from the first attempt, the procedure was repeated. The results

obtained (Table 2-1), follow the trend expected with a decrease of the density of the polymeric phase as the filler content increases, coherent with the idea of additional free volume inserted in the polymer by the presence of inorganic particles

	ρ_{solid} (g/cm^3)	$\rho_{polymer}$ (g/cm^3)	*FFV*	Measurement
AF2400	1.75	1.75	0.315	Volume
AF2400 + 25% FS	1.69	1.57	0.383	Volume
AF2400 + 40% FS	1.84	1.66	0.349	Volume
AF1600	1.844	1.844	0.302	MSB
AF1600 + 10% FS	1.871	1.841	0.303	MSB
AF1600 + 25% FS	1.886	1.801	0.319	MSB

Table 2-1: Density values for all the samples studied, measured with different techniques.

2.2.3 Membrane characterization

TEM and DSC analysis were performed for pure and nanocomposite membranes based on Teflon® AF1600 (Fig. 2-7 and Fig. 2-8). From the TEM picture one can see that the inorganic particles, represented by the dark colour, are well dispersed into the matrix. A similar behavior was observed for the AF2400 nanocomposites produced by Merkel et al. [15, 16].

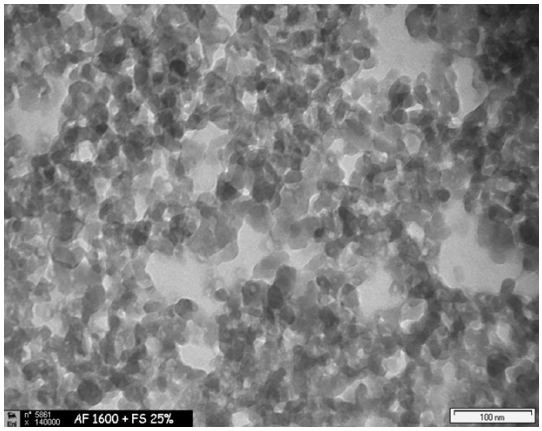

Fig. 2-7: TEM image of a mixed matrix of AF1600 + 25% wt of FS.

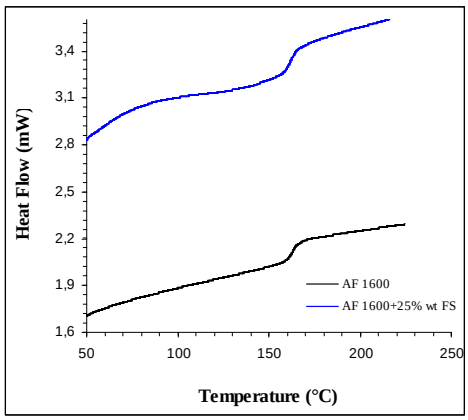

Fig. 2-8: Comparison of DSC characterization for pure AF1600 and a mixed matrix with 25% wt of FS.

DSC runs were performed in a nitrogen atmosphere with a heating rate of 20 °C/min, from room temperature to 230 °C: it results that for pure Teflon® AF1600 the glass transition temperature is 163 °C, whereas for AF1600 containing 25% of FS it is 162.2 °C. The differences between pure and filled polymer are rather negligible, this meaning that the filler addition does not influence the long-range chains motion, which impact directly the glass transition processes: in other words, the filler plays a very important role on chain packing and not on long-range chain segmental dynamic.

2.2.4 Vapor sorption

A pressure decay apparatus was used to determine solubility isotherms of n-butane and n-pentane in pure Teflon® and in mixed matrices at 25°C, as well as adsorption on the pure inorganic filler. The measurement is manometric and the decrease in the partial pressure of the penetrant in a known volume over time is converted into moles of penetrant entered the sample through the ideal gas law.

Solubility isotherms for AF2400 and AF1600 for both penetrants, n-butane and n-pentane, are shown in Fig 2-9. Together with the values for the pure polymer and for the mixed matrices, reported as grams of penetrants per grams of total solid, even the adsorption in the pure filler is reported in Fig 2-9(a) and Fig 2-9(b) and it is significantly less than in the other samples.

The addition of filler in AF2400 does not affect the solubility of n-C_4 (Fig 2-9(a)) and influences the values for n-C_5 (Fig 2-9(b)) only at high activity where the plasticization effect of the penetrant is already present, as it can be seen from the positive concavity of the isotherm. In the Fig 2-9(a) the simple additive model expressed by equation (2.14) is also reported for the mixed matrix with 40% of fumed silica: the model underestimates the sorption capacity of the composite and cannot be used with this class of materials. The effect of silica is more clearly present in the case of AF1600 because the value of adsorption on the FS particles is closer to that in the pure polymer. In Fig 2-9(c) and Fig 2-9(d), it is shown that the addition of the inorganic phase increases the mass uptake of the composite.

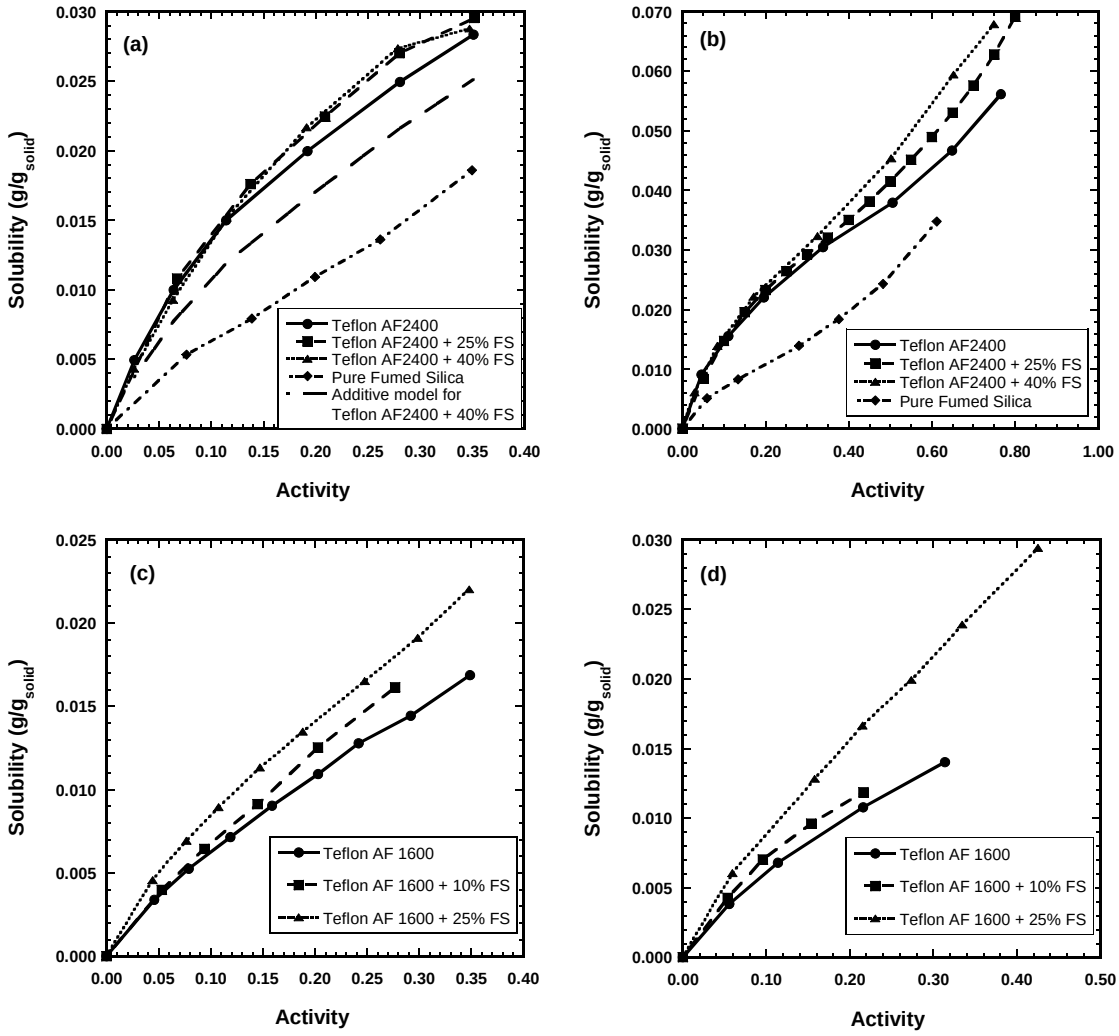

Fig. 2-9: experimental solubility isotherms at 25°C reported as grams of penetrant per grams of total solid: (a) n-C_4 in Teflon® AF2400, AF2400+25%wt FS and AF2400+40%wt FS and adsorption onto pure silica; (b) n-C_5 in Teflon® AF2400, AF2400+25%wt FS and AF2400+40%wt FS and adsorption onto pure silica; (c) n-C_4 in Teflon® AF1600, AF1600+10%wt FS and AF1600+25%wt FS and (d) n-C_5 in Teflon® AF1600, AF1600+10%wt FS and AF1600+25%wt FS. Data for AF1600 courtesy of Michele Galizia.

2.2.5 Diffusivity

The diffusion coefficient was calculated in every sorption step in the pressure decay experiments by fitting the exact solution of the local mass balance with the appropriate boundary conditions to the transient data of mass uptake. Fick's law is used to describe

the diffusive flux inside the membrane, with an average diffusion coefficient in every step.

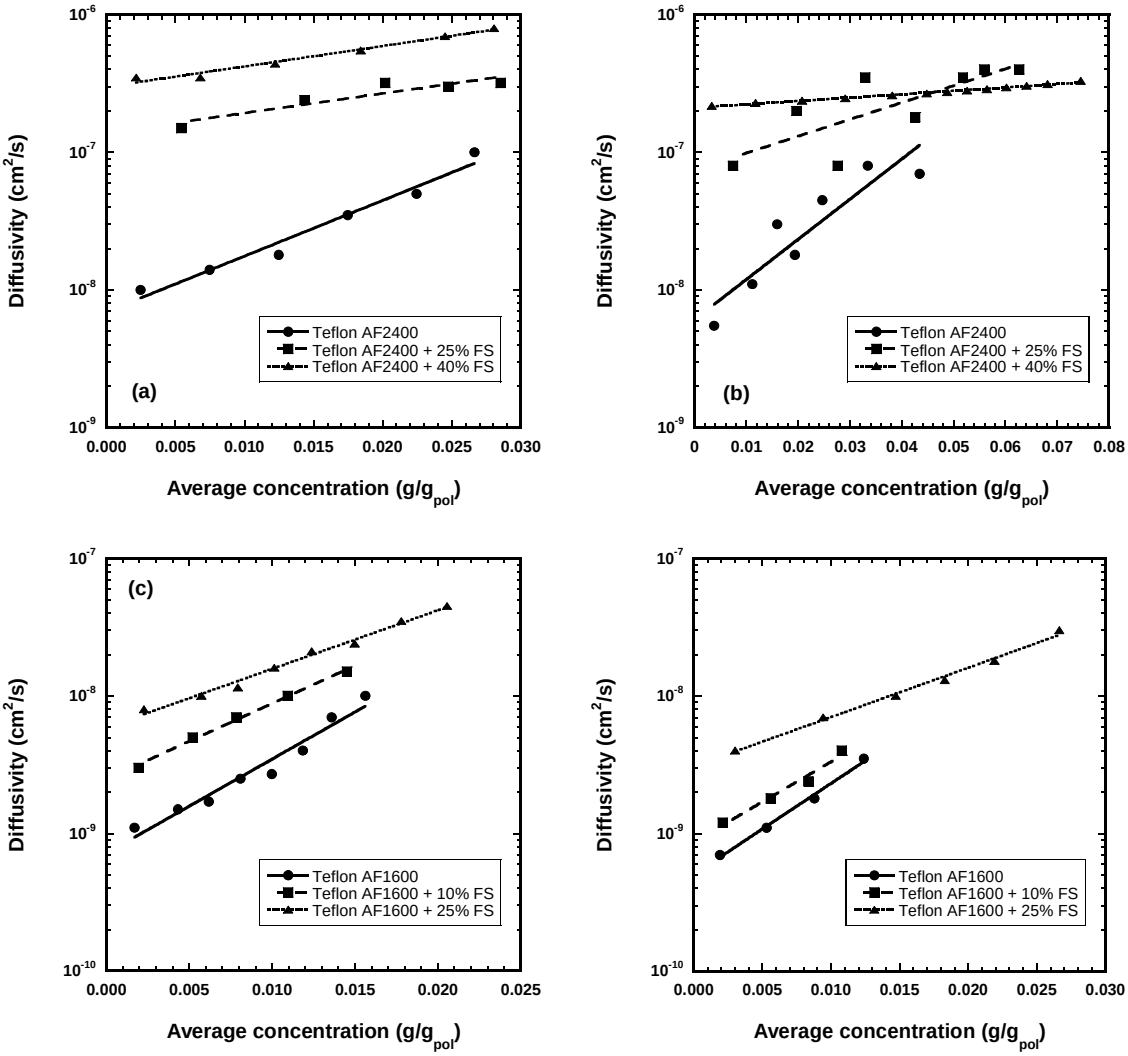

Fig. 2-10: diffusivity data at 25°C versus average penetrant concentration: (a) n-C_4 in mixed matrices of Teflon® AF2400; (b) n-C_5 in mixed matrices of Teflon® AF2400; (c) n-C_4 in mixed matrices of Teflon® AF1600 and (d) n-C_5 in mixed matrices of Teflon® AF1600. Data for AF1600 courtesy of Michele Galizia.

2.2.6 Dilation

Swelling experiments were performed in a dedicated optical apparatus equipped with a CCD camera: the free samples were hung and the relative position of two points on the main dimension of the film was measured during sorption.

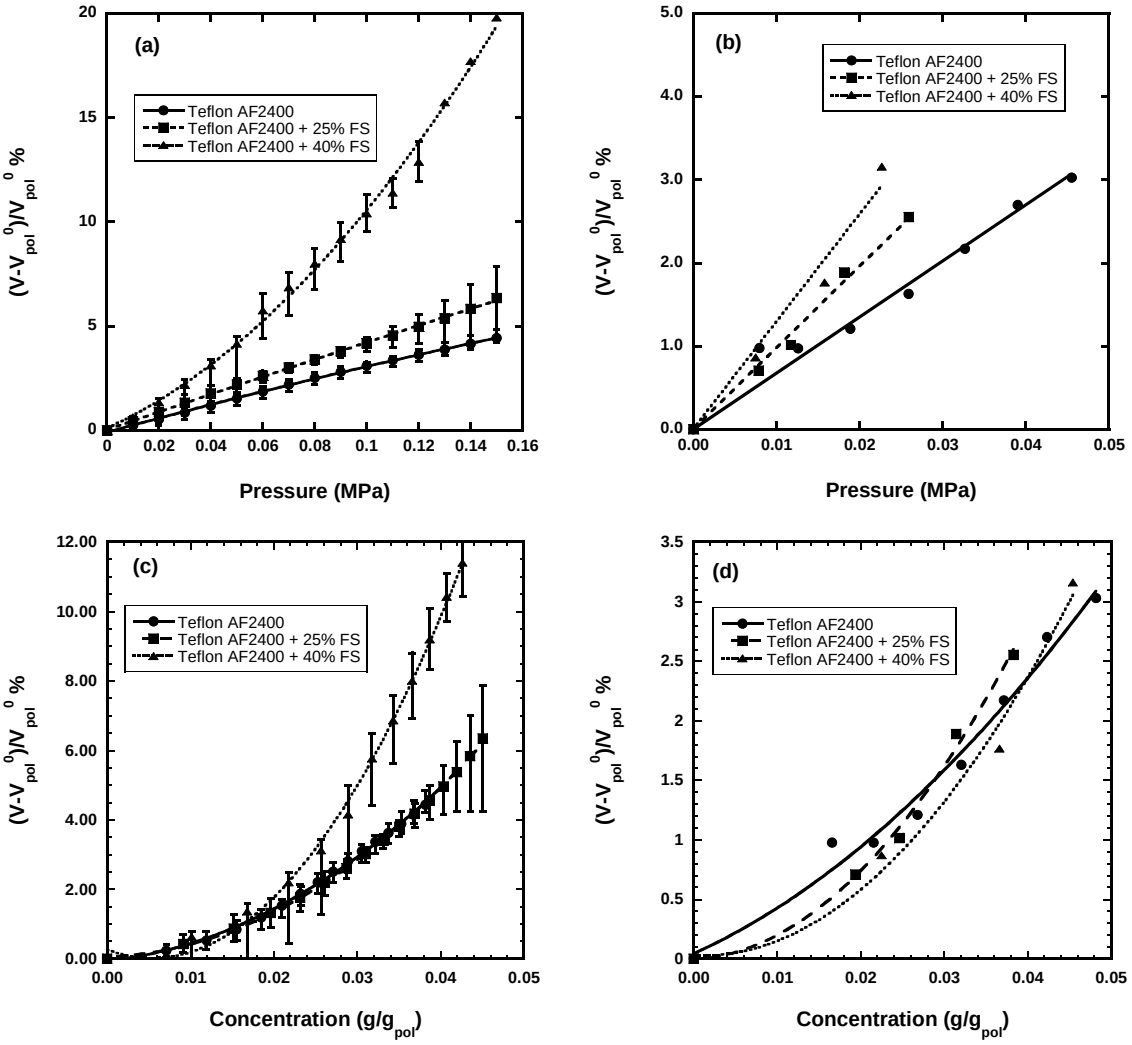

Fig 2-11: experimental dilation data at 25°C: (a) n-C_4 in mixed matrices of Teflon® AF2400 versus pressure; (b) n-C_5 in mixed matrices of Teflon® AF2400 versus pressure; (c) n-C_4 in mixed matrices of Teflon® AF2400 versus penetrant concentration and (d) n-C_5 in mixed matrices of Teflon® AF2400 at versus penetrant concentration.

The dilation experiments were performed only in one direction, and the data were converted to volumetric swelling values considering the material isotropic; the results are shown in Fig 2-11(a) and Fig 2-11(b) for AF2400 as a function of the partial pressure of the penetrant at equilibrium. In most cases there is a linear dependence of dilation on partial pressure from which the swelling coefficient, i.e. the slope of the curve, can be calculated. For the case of butane in the mixed matrix AF2400 + 40% FS, the dependence of dilation on partial pressure is quadratic, therefore only the data where the curve can be approximated with a straight line, were considered in the

calculation of the swelling coefficient. If the dilation is reported as a function of the concentration in the sample (Fig 2-11(c) and Fig 2-11(d)), all the curves tend to overlap, indicating that the swelling is slightly affected by the introduction of particles. This is not true for the case of n-butane in AF2400 + 40% FS where the deviation from the data for the pure polymer is relevant especially at high concentration of vapor.

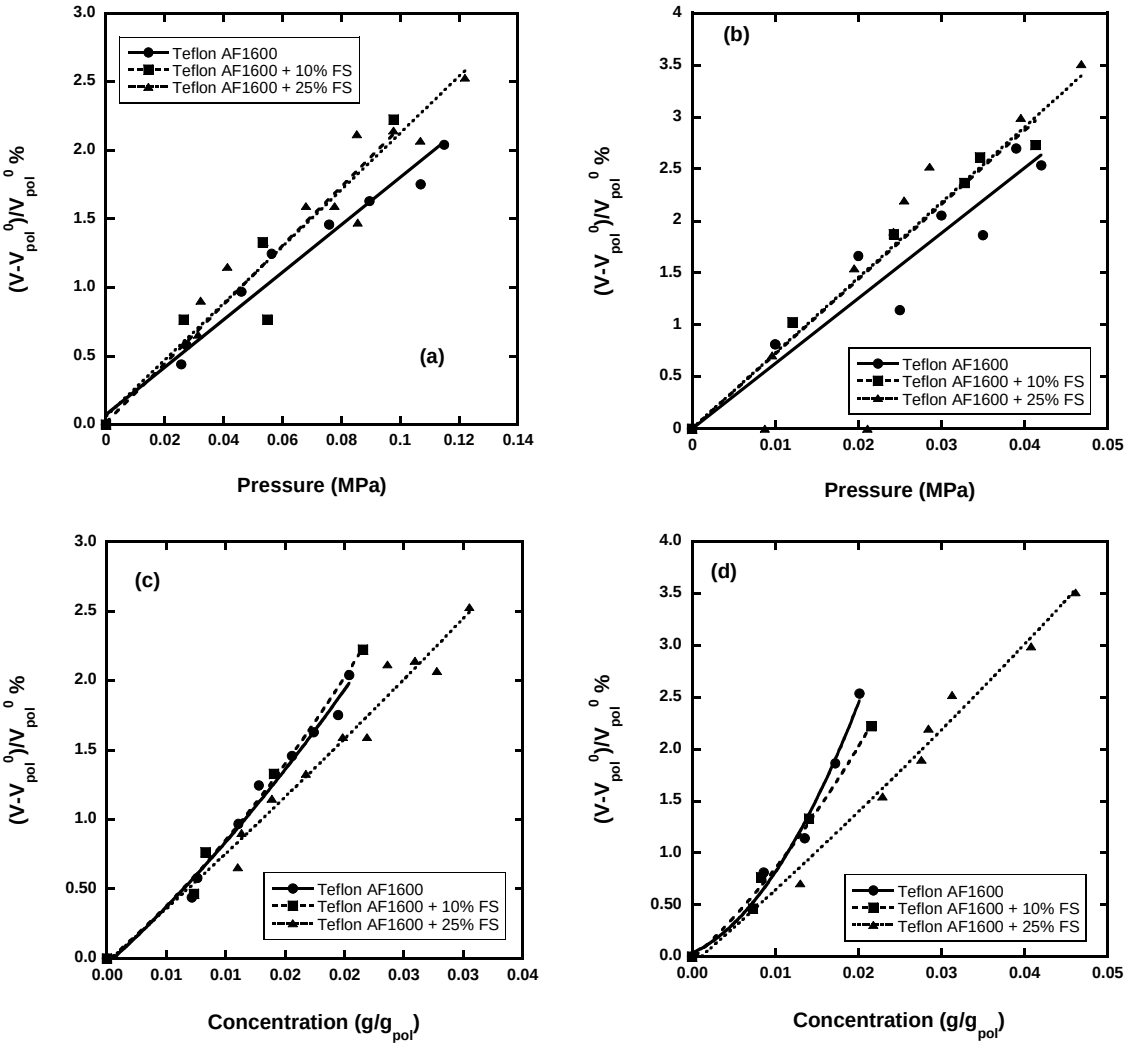

Fig 2-12: experimental dilation data at 25°C: (a) n-C_4 in mixed matrices of Teflon® AF1600 versus pressure; (b) n-C_5 in mixed matrices of Teflon® AF1600 versus pressure; (c) n-C_4 in mixed matrices of Teflon® AF1600 versus penetrant concentration and (d) n-C_5 in mixed matrices of Teflon® AF1600 versus penetrant concentration.

Considering the data for AF1600 (Fig 2-12), it is clear that, for both penetrants, the swelling of the matrices with 10 or 25% of FS is similar and slightly higher than for the pure polymer. Once again the data can also be plotted versus the concentration in

the membrane: in this case the plots show that for both penetrants, the swelling decreases with increasing filler content, and such trend is more evident in the case of n-C_5. This behavior is different than that observed in AF2400 and consistent with what one would imagine from common sense, that rigid particles increase the plasticization resistance of the polymer. The difference with what observed in AF2400 is due to the different initial free volume of the two materials, although deeper investigations are needed to clarify this aspect.

2.3 Modeling

2.3.1 Modeling solubility data

The sorption isotherms for a mixed matrix sample can be plotted not only as mass of penetrant per mass of total solid but also as mass of penetrant per mass of polymeric phase, using equation (2.15). In Fig 2-13 data for AF2400 are reported together with the results obtained with the NELF model. In the modeling procedure we considered n-butane as the test penetrant and the sorption isotherms for this vapor were fitted to the model adjusting the initial density of the polymer on the low-activity data and the swelling coefficient on the high-activity data. The density values measured with the volume method were not considered in this procedure, because they did not show a monotonic decrease with the filler content and they were affected by a large experimental error. The binary parameter requested by the model is already available in literature for this penetrant-polymer pair, as well as the characteristic parameters for pure components [30], recalled in Table 2-2.

	p^* (bar)	ρ^* (kg/L)	T^* (K)
AF 2400	2500	2.13	624
AF 1600	2800	2.16	575
n-C₄	2900	0.720	430
n-C₅	3050	0.749	451

Table 2-2: Characteristic parameters used for the NELF model [30].

From the initial density, the fractional free volume has been calculated and the results are reported in Table 2-3. As expected the addition of the impermeable filler introduces new void spaces in the polymer at the interface between the particles and the matrix; this results in an increasing value of FFV with the increase of FS in the membrane.

Penetrant	**Matrix**	**Ψ**	$\rho_{polymer}$ (g/cm^3)	*FFV*	k_{sw} (MPa^{-1})
n-C4	AF 2400	0.14	1.740	0.320	0.13
n-C4	AF 2400+25% FS	0.14	1.714	0.330	0.20
n-C4	AF 2400+40% FS	0.14	1.680	0.344	0.21
n-C5	AF 2400	0.14	1.740	0.320	0.85
n-C5	AF 2400+25% FS	0.14	1.714	0.330	1.20
n-C5	AF 2400+40% FS	0.14	1.680	0.344	2.00
n-C4	AF 1600	0.14	1.844	0.302	0.20
n-C4	AF 1600+10% FS	0.14	1.841	0.303	0.32
n-C4	AF 1600+25% FS	0.14	1.801	0.319	0.33
n-C5	AF 1600	0.14	1.844	0.302	0.40
n-C5	AF 1600+10% FS	0.14	1.841	0.303	0.70
n-C5	AF 1600+25% FS	0.14	1.801	0.319	1.85

Table 2-3: Model parameters Ψ, FFV and k_{sw} for n-C_4 and n-C_5 in AF2400 and AF1600 containing various amounts of FS.

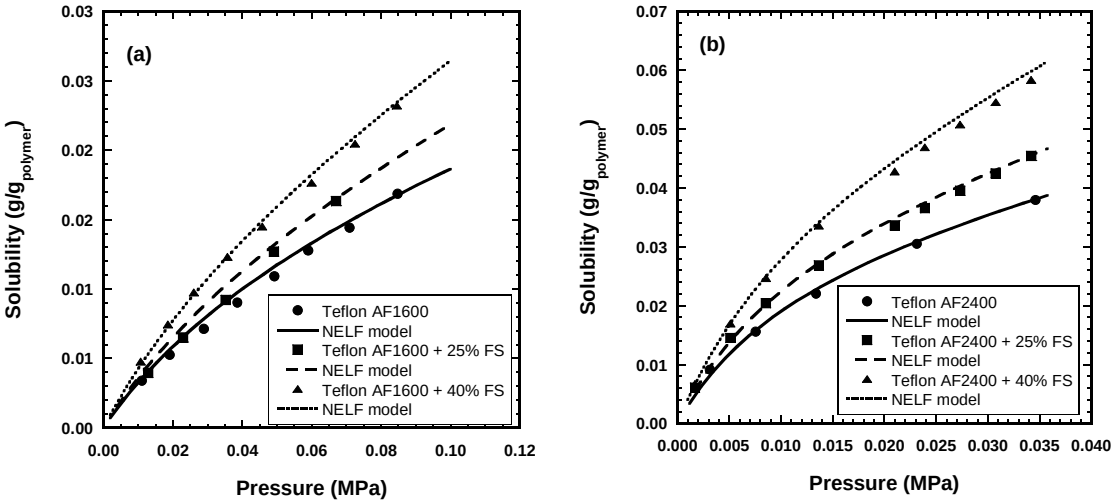

Fig. 2-13: Experimental solubility in the polymeric phase of Teflon® AF2400-based MMM at 25° C and comparisons with NELF model: (a) n-C_4 (b) n-C_5.

The FFV calculated has then been used to predict the sorption isotherm for a second penetrant, n-pentane in this case, adjusting only the swelling coefficient, while the

binary parameter can reasonably be considered the same since the penetrants are similar. The agreement between the experimental points and the predicted curve is really good and this proves our procedure to be effective. The FFV calculated by fitting the model to the experimental isotherm could also be compared to the one determined from the experimental measurement of the density and reported in Table 2-1 but there are some discrepancies especially for the sample with 25 % wt of silica, probably due to uncertainty present in the density measurements.

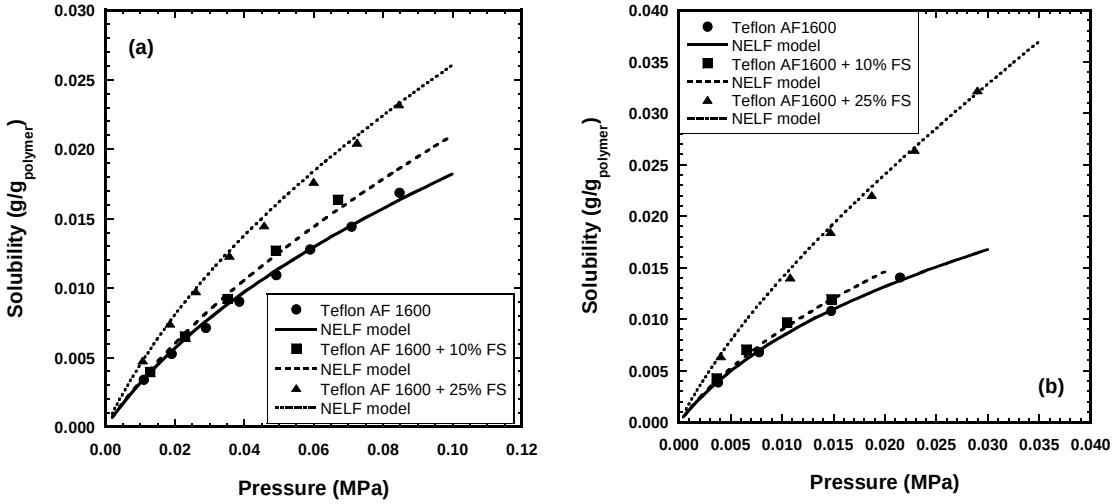

Fig. 2-14: Experimental solubility in the polymeric phase of Teflon® AF1600-based MMM at 25° C and comparisons with NELF model: (a) n-C_4 (b) n-C_5.

In the case of AF1600, a more reliable comparison between the FFV values can be made, because in this case more reliable data of density are available. In this case in particular we tested the compatibility of the density data by evaluating the sorption isotherms for n-butane in pure and filled AF1600 with the NELF model using literature values for the characteristic parameters and binary parameter [30] and the values measured with the MSB for the initial density. The swelling coefficient was adjusted onto high activity data . The same FFV has also been used to predict the sorption isotherms for n-pentane. Even in this case the model agrees very well with the experimental points collected with the pressure decay and reported as mass of vapor per mass of polymeric phase as shown in Fig 2-14, proving the potentiality of our procedure. From the data for only one penetrant in mixed matrix condition, the isotherm for any other penetrant can be predicted on the base of the characteristic of the

pure substances, reducing considerably the amount of experimental work needed. The experimental value of density, directly measured, is perfectly consistent with this procedure.

2.3.2 Modeling diffusivity data

The FFV calculated from the sorption isotherm through the NELF model or from the experimental density data, can also be used to correlate the diffusivity data collected during sorption tests.

The infinite dilution diffusion coefficient in the polymeric phase $D_P(0)$ determined from the experimental average diffusivity data can be related to the FFV that is initially present in the matrix. As shown in Fig. 2-15(a) for diffusion of n-butane in both AF2400 and AF1600, there is a correlation between the inverse of the FFV and infinite dilution diffusion coefficient that is well represented by equation (2.20). It is interesting to note that both materials can be represented by the same law with a correlation coefficient R^2 of 0.96 and this is reasonable since the two polymers contains the same monomers in different percentage and the main difference between them is in the FFV.

The same considerations can be made for the case n-pentane (Fig. 2-15(b)) even if the values of the parameters A and B differ slightly.

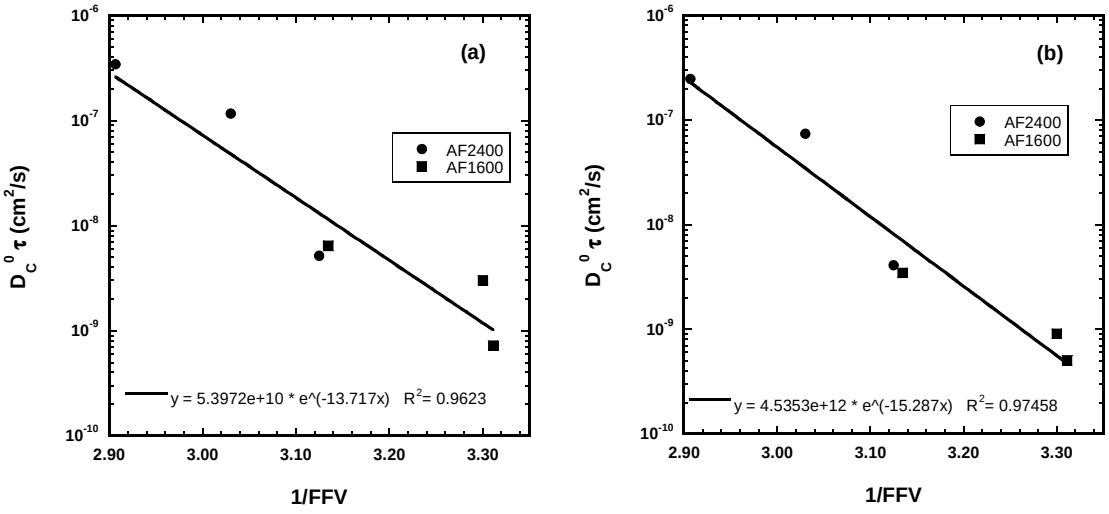

Fig. 2-15 Infinite dilution diffusion coefficient in the polymeric phase of mixed matrices based on AF2400 and AF1600 as a function of FFV for (a) n-C_4 and (b) n-C_5.

From the slope of the correlation in Fig. 2-15 (parameter *B*) also the ratios $D_C(0)/D_P(0)$ can be calculated through equation (2.21) and in Table 2-4 the values are compared to the ones that come from experiments. The model results are more satisfactory for the case of AF1600.

	n-C_4H_{10}		*n*-C_5H_{12}	
	$D_C(0)/D_P(0)$ (exp.)	$D_C(0)/D_P(0)$ (calc.) *(B=13.7)*	$D_C(0)/D_P(0)$ (exp.)	$D_C(0)/D_P(0)$ (calc.) *(B=15.3)*
AF2400	1	1	1	1
AF2400/25%wt FS	22.2	3.3	15.0	3.8
AF2400/40%wt FS	50.7	17.0	56.4	23.9
AF1600	1	1	1	1
AF1600/10%wt FS	3.5	1.1	1.7	1.1
AF1600/25%wt FS	8.1	10.1	6.2	13.4

Table 2-4: Comparison between calculated and experimental values of the ratio of the infinite dilution diffusion coefficient in the composite and in the pure polymer.

It has been seen that also the coefficient β that appears in equation (2.16) is related to the FFV (Fig. 2-16), and in particular it decreases with increasing FFV through an exponential law:

$$\beta = E \exp\left(-F \cdot FFV\right) \tag{2.23}$$

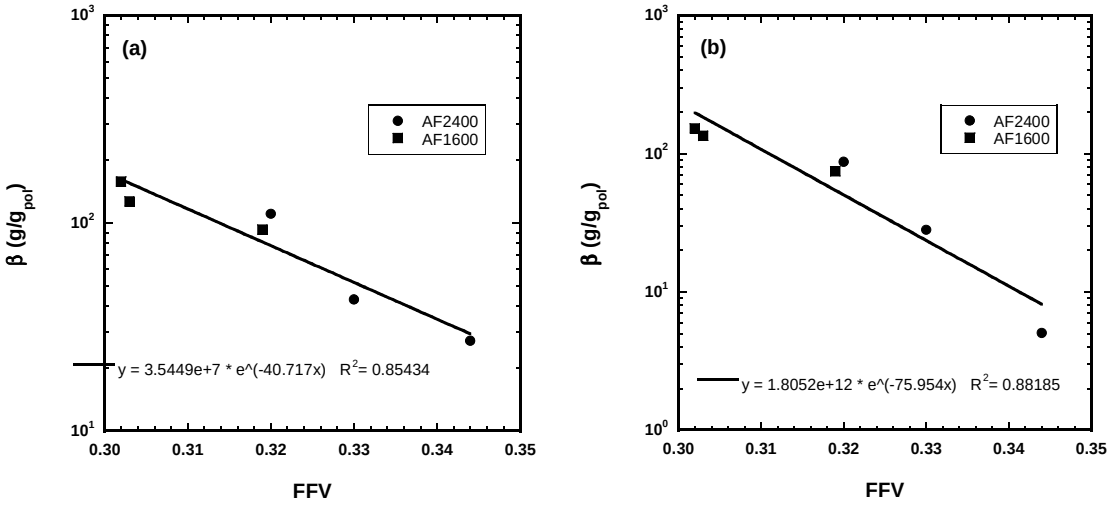

Fig. 2-16: β coefficient in the polymeric phase of mixed matrices based on AF2400 and AF1600 as a function of FFV for (a) n-C_4 and (b) n-C_5.

A single plot for the two polymers can be drawn, obtaining a rather high value of the correlation parameter R^2 equal to 0.85. The parameters E and F are different for the two penetrants. This correlation can be motivated by the fact that the higher the initial free volume of the matrix, the lower the effect of swelling on the penetrant diffusion.

2.3.3 Modeling permeability and selectivity

From the solubility and diffusivity data collected in the sorption experiments the value for the permeability of the two penetrants in the different mixed matrices was also calculated. If the solution-diffusion model is considered to hold true, and Fick's law is suitable to represent the diffusive flux, the permeability ratio can be calculated as in equation (2.22).

In Fig. 2-17 the ratio between the permeability in the composite and that in the pure polymer at infinite dilution for the two penetrants and for the two matrices is reported. It can be seen that the addition of inorganic filler to the polymer enhances the permeability of the material in all cases; in particular the increase follows a linear law for both polymers (Fig. 2-17(a)) in the case of n-butane while for n-pentane an exponential law is needed to describe the data.

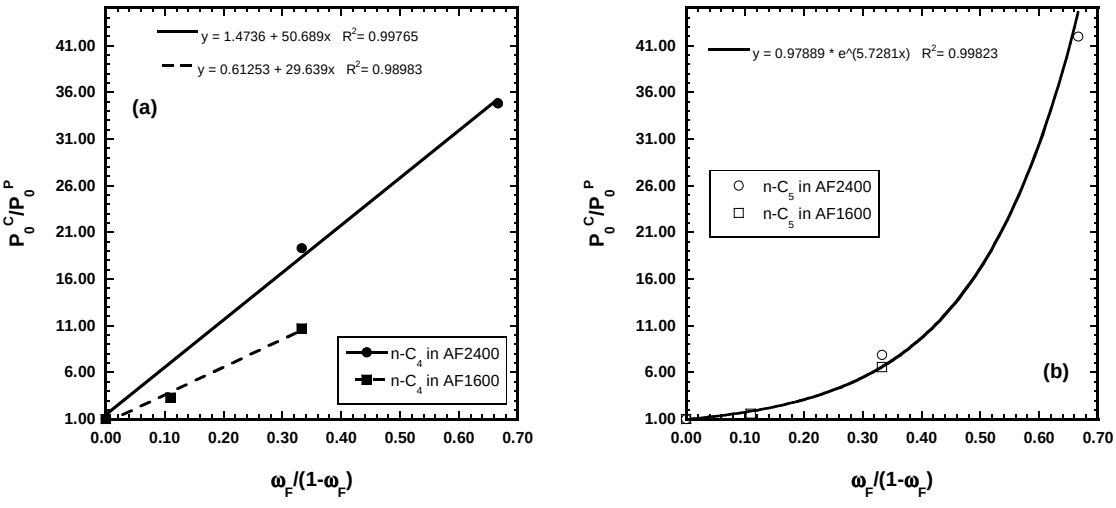

Fig. 2-17: Permeability ratio at infinite dilution in the case of (a) n-butane and (b) n-pentane

From the knowledge of the sorption and diffusivity isotherms, the behavior of the ideal selectivity of the composite can be predicted; as shown in Fig. 2-18 there is an increase

in the permeability of the larger penetrant as the initial FFV increase in the membrane. The case of 25% of filler in AF2400 is peculiar, since a change in the selectivity is observed: the membrane is n-butane selective at low activity and becomes n-pentane selective at higher activity values.

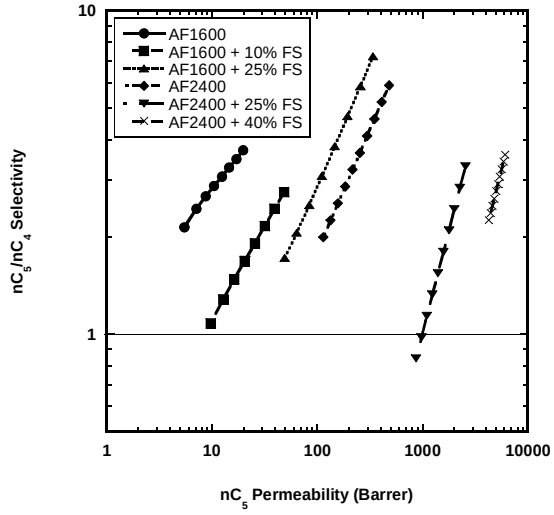

Fig. 2-18: n-pentane/n-butane selectivity for all the materials studied as a function of n-pentane permeability

It seems thus that, for the case of the n-C_4/n-C_5 pair, the matrices considered are vapor-selective, meaning that they are more permeable to the more condensable penetrant, and that the selectivity increases with increasing penetrant pressure. However, it is very clear from the plots that the selectivity of the matrices, at fixed permeability decreases with increasing filler content. However, the behavior of the matrices with the higher inorganic content would be much closer to an hypothetical trade-off curve traced for this particular mixture for vapor selective materials. It must be noticed, before concluding, that the ideal values of selectivity obtained in this work from pure vapor measurements could be different from the actual case in which interactions take place between the penetrants.

2.3.4 Swelling evaluation

The NELF model can also be used to estimate the swelling behavior of the matrix when no dilation data for the pair gas-polymer of interest are available.

In order to fit the experimental sorption isotherm the swelling coefficient of NELF model was fitted on the high-activity portion of the solubility isotherm, where the swelling is more important. In Fig. 2-19 the swelling coefficients calculated through the model as a function of the filler content in the membrane are compared to the values calculated from the dilation isotherm for both AF2400 (Fig. 2-19(a)) and AF1600 (Fig. 2-19(b)). The qualitative behavior of the model swelling coefficients agrees with the one that can be deducted from the experiments even if there is some discrepancy in the quantitative value.

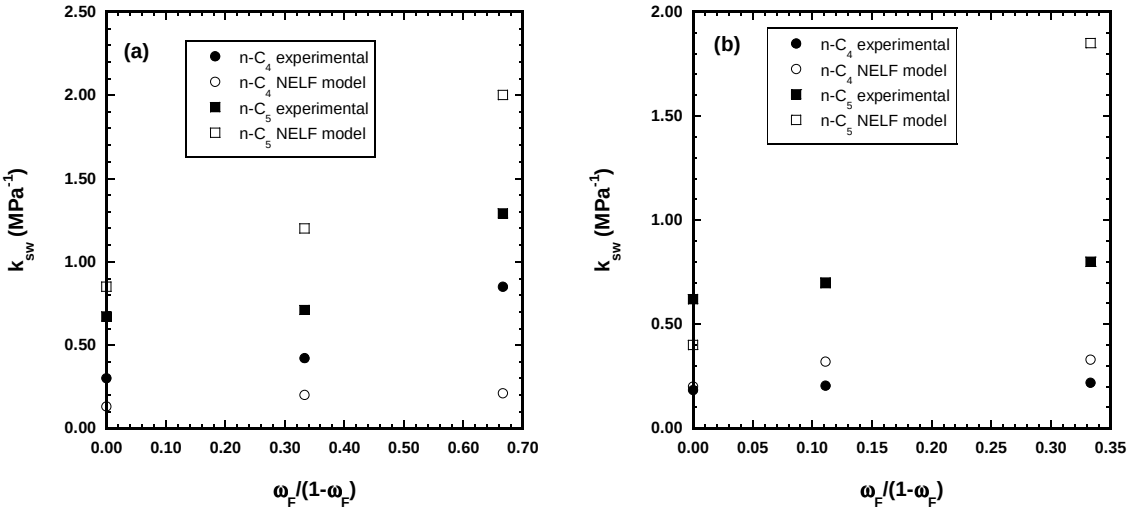

Fig. 2-19: Comparison of experimental and calculated swelling coefficients: (a) AF2400 and (b) AF1600.

In the absence of specific dilation data, not very common in literature, NELF model can be used to estimate the qualitative swelling behavior of the matrix even after the addition of particles. This is a rather important parameter that quantifies the extent of plasticization undergone by the membrane.

Conclusions

Mixed matrix membranes based on fluorinated, high free volume matrices show attractive separation performances, especially if compared to neat polymeric membranes. However, materials selection is still an open problem since the understanding of the behavior of the composite membranes is still limited compared to the knowledge of the behavior of polymer membranes. Therefore, there is a need for deeper investigation of the influence of inorganic filler on selectivity properties of polymeric materials. This study was devoted to MMMs formed by non-porous inorganic filler in a high free volume polymer. In particular two classes of membranes based on amorphous Teflon® and fumed silica were experimentally characterized to evaluate solubility, diffusivity and swelling due to two model penetrants. The density of the materials with different content of inorganic filler was also measured. The data were used to test a new procedure that allows to predict solubility of every penetrant on the basis of data for one vapor. The method has proved to be useful also for the determination of the diffusion coefficient and for an estimation of the permeability in the composite materials. The evaluation of the contributions of the permeability can hence be used to determine the ideal selective behavior of the composite membrane. The NELF model can also be used to have a qualitative idea of the swelling induced by the diffusion process of a penetrant in the polymer.

References

1. Robeson, L.M., *Correlation of Separation Factor Versus Permeability for Polymeric Membranes.* J. Membr. Sci., 1991. **62**: p. 165-185.
2. Robeson, L.M., *The upper bound revisited.* Journal of Membrane Science, 2008. **320**(1-2): p. 390.
3. Chung, T.-S., Jiang, L.Y., Li, Y. and Kulprathipanja, S., *Mixed matrix membranes (MMMs) comprising organic polymers with dispersed inorganic fillers for gas separation.* Progress in Polymer Science, 2007. **32**(4): p. 483.
4. Paul, D.R. and Kemp, D.R., *The Diffusion Time Lag in Polymer Membranes containing Adsorptive Fillers.* Journal of Polymer Science: Symposium, 1973. **41**: p. 79-93.
5. Perez, E.V., Balkus Jr, K.J., Ferraris, J.P. and Musselman, I.H., *Mixed-matrix membranes containing MOF-5 for gas separations.* Journal of Membrane Science, 2009. **328**(1-2): p. 165.
6. Yong, H.H., Park, H.C., Kang, Y.S., Won, J. and Kim, W.N., *Zeolite-filled polyimide membrane containing 2,4,6-triaminopyrimidine.* Journal of Membrane Science, 2001. **188**(2): p. 151.
7. Gür, T.M., *Permselectivity of zeolite filled polysulfone gas separation membranes.* J. Membr. Sci., 1994. **93**: p. 283-289.
8. Kim, S., Marand, E., Ida, J. and Guliants, V.V., *Polysulfone and Mesoporous Molecular Sieve MCM-48 Mixed Matrix Membranes for Gas Separation.* Chem. Mat, 2006. **18**: p. 1149-1155.
9. Li, Y., Guan, H.-M., Chung, T.-S. and Kulprathipanja, S., *Effects of novel silane modification of zeolite surface on polymer chain rigidification and partial pore blockage in polyethersulfone (PES)–zeolite A mixed matrix membranes.* J. Membr. Sci., 2006. **275**: p. 17-28.
10. Süer, M.G., Baç, N. and Yilmaz, L., *Gas permeation characteristics of polymer-zeolite mixed matrix membranes.* J. Membr. Sci., 1994. **91**: p. 77-86.
11. Vu, D.Q., Koros, W.J. and Miller, S.J., *Mixed matrix membranes using carbon molecular sieves I. Preparation and experimental results.* J. Membr. Sci., 2003. **211**: p. 311-334.
12. Maxwell, C., *Treatise on Electricity and Magnetism.* Vol. 1. 1873, London: Oxford University Press.

13. Merkel, T.C., Freeman, B.D., Spontak, R.J., He, Z., Pinnau, I., Meakin, P., et al., *Ultrapermeable, Reverse-Selective Nanocomposite Membranes.* Science, 2002. **296**: p. 519-522.
14. Merkel, T.C., He, Z., Pinnau, I., Freeman, B.D., Meakin, P. and Hill, A.J., *Sorption and Transport in Poly (2,2-bis(trifluoromethyl)-4,5-difluoro-1,3-dioxole-co-tetrafluoroethylene) Containing Nanoscale Fumed Silica.* Macromolecules, 2003. **36**: p. 8406-8414.
15. Merkel, T.C., He, Z., Pinnau, I., Freeman, B.D., Meakin, P. and Hill, A.J., *Effect of Nanoparticles on Gas Sorption and Transport in Poly(1-trimethylsilyl-1-propyne).* Macromolecules, 2003. **36**: p. 6844-6855.
16. Merkel, T.C., Freeman, B.D., Spontak, R.J., He, Z., Pinnau, I., Meakin, P., et al., *Sorption, Transport, and Structural Evidence for Enhanced Free Volume in Poly(4-methyl-2-pentyne)/Fumed Silica Nanocomposite Membranes.* Chem. Mater., 2003. **15**: p. 109-123.
17. De Angelis, M.G. and Sarti, G.C., *Solubility and Diffusivity of Gases in Mixed Matrix Membranes Containing Hydrophobic Fumed Silica: Correlations and Predictions Based on the NELF Model.* Industrial & Engineering Chemistry Research, 2008. **47**(15): p. 5214-5226.
18. Giacinti Baschetti, M., De Angelis, M.G., Doghieri, F. and Sarti, G.C., in *Chemical Engineering: Trends and Developments*, M.A. Galan and E.M.d. Valle, Editors. 2005, Wiley: Chichester (UK). p. 41-61.
19. Giacinti Baschetti, M., Doghieri, F. and Sarti, G.C., *Solubility in Glassy Polymers: Correlations through the Nonequilibrium Lattice Fluid Model.* Ind. Eng. Chem. Res., 2001. **40**: p. 3027-3037.
20. Sarti, G.C. and Doghieri, F., *Predictions of the solubility of gases in glassy polymers based on the NELF model.* Chemical Engineering Science, 1998. **19**: p. 3435-3447.
21. Sanchez, I.C. and Lacombe, R.H., *An Elementary Molecular Theory of Classical Fluids. Pure Fluids.* J. Phys. Chem., 1976. **80**: p. 2352-2362.
22. Sanchez, I.C. and Lacombe, R.H., *Statistical Thermodynamics of Polymer Solutions.* Macromolecules, 1978. **11**: p. 1145-1156.
23. Lacombe, R.H. and Sanchez, I.C., *Statistical Thermodynamics of Fluid Mixtures.* J. Phys. Chem., 1976. **80**: p. 2568-2580.
24. Doghieri, F., Quinzi, M., Rethwisch, D.G. and Sarti, G.C. in *ACS Symposium*. 2004.
25. Astarita, G., *Thermodynamics*. 1989, New York: Plenum Press.

26. Grassia, F., Giacinti Baschetti, M., Doghieri, F. and Sarti, G.C. *Solubility of gases and vapors in glassy polymer blends*. in *ACS Symposium series 876.* 2004. Washington, DC: American Chemical Society.
27. Van Krevelen, W., *Properties of polymers*. 1990, Amsterdam: Elsevier.
28. Cohen, M.H. and Turnbull, D.J., *Molecular Transport in Liquids and Glasses.* J. Chem. Phys., 1959. **31**: p. 1164-1169.
29. Fujita, H., *Diffusion in Polymer-Diluent Systems.* Fortschr.Hochpolym. Forsch., 1961. **3**: p. 1-47.
30. De Angelis, M.G., Merkel, T.C., Bondar, V.I., Freeman, B.D., Doghieri, F. and Sarti, G.C., *Gas Sorption and Dilation in Poly(2,2-bistrifluoromethyl-4,5-difluoro-1,3-dioxole-co-tetrafluoroethylene): Comparison of Experimental Data with Predictions of the Non Equilibrium Lattice Fluid Model.* Macromolecules, 2002. **35**: p. 1276-1288.

3 Oxygen scavenger systems for barrier application

The poor oxygen barrier properties of common polymers has always ruled against their employment in oxygen-sensitive applications like food and pharmaceutical packaging, or in the manufacture of electronic components, like displays based on organic light emitting diodes (LED). The processability and lightness of polymeric materials, however, makes appealing the idea of using them also in those applications. In this view, there is the need to improve the properties, with particular regard to the barrier ability against oxygen. There has been a long effort to synthesize polymers with very low intrinsic permeability to oxygen and other small molecules. In recent years there has been much interest in incorporating plate-like particles into polymers that reduce permeability by making the penetrant diffusion path more tortuous. Each of these approaches seeks to reduce the oxygen transport in a steady state situation for the permeation process [1].

Another approach, that has been recognized since the 1960s, is to delay the time required to achieve steady-state transmission of the penetrant, increasing the time lag, θ, by scavenging or immobilizing the penetrant as it diffuses through the film [2-4]. The earliest examples involve adsorption by filler particles: sachets of systems based mainly on iron oxidation are added to the packaging to reduce the oxygen content during storage life of the product [5,6]; however in more recent times interest has turned to incorporation of reactive components, typically an oxygen scavenging polymer (OSP), that irreversibly consume oxygen in the packaging material. This approach is specific to oxygen, and large quantities of gas can be consumed in this way. A number of patents have been issued describing variations on this idea for food and beverage packaging [7-13].

One of these patents regards a material commercialized with the name Oxbar^{TM} by Constar International Inc. [12,14]; this patent regards a multilayer bottle with a layer of reacting polymer (based on an aromatic polyamide, MXD6) sandwiched between two layers of Polyethylene(terephtalate), a typical material used in beverage industry.

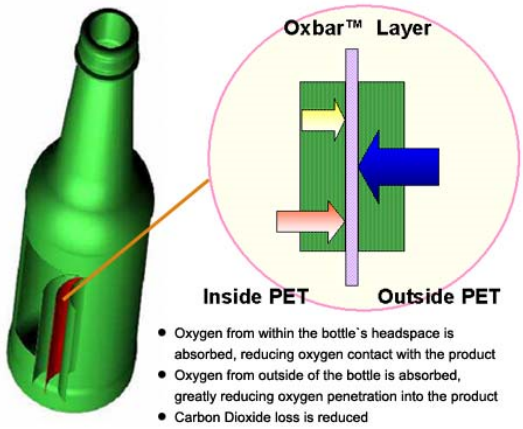

Fig. 3-1: Example of commercial Oxygen Scavenger material: Oxbar® (Constar International Inc.) [14].

Polybutadiene is another example of a polymer that readily oxidizes [15,16] particularly in the presence of certain metal catalysts [17]. This study involves the experimental characterization of several block copolymers containing butadiene to explore the possibility of using them as components in new systems with improved oxygen barrier properties. Besides the experimental campaign, a modeling work was developed in order to analyze the experimental data and find the best layout for composite membranes.

This work was completed at The University of Texas at Austin under the supervision of Prof. Benny Freeman and Prof. Don Paul and it is part of a project funded by CLiPs (Center for Layered Polymeric System) whose aim is to find the best structure for a multilayer material that optimizes the barrier performance against oxygen.

3.1 Experimental

3.1.1 Materials

The material used in this study is a block copolymer SBS (styrene-butadiene-styrene) (Fig. 3-2) that, due the presence of the double bond in the Butadiene phase, can scavenge oxygen once doped with a proper catalyst.

In Table 1-1 the materials object of the experimental campaign are reported with their composition, in terms of percentage of the two possible forms of butadiene (1,2 or 1,4 PB, Fig. 3-3). They were supplied by Eastman Chemical Company in the form of 20 %wt solution of the polymer in Cyclohexane; the same company also provided some commercial products in pellets with similar composition but with the presence of additives as antioxidant. The work was focused mainly on the so-called SBS II that contains 21 % wt of Polystyrene and for the Polybutadiene fraction is mainly constituted of 1,4-PB form (90.7 % wt). For comparison also some data regarding SBS I samples (12.5 % wt of PS and 24 % wt of 1,4 in the PB fraction) will be shown and commented.

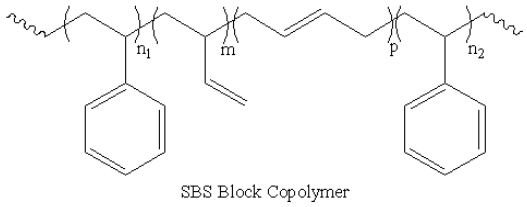

Fig. 3-2: Molecular structure of SBS block copolymer.

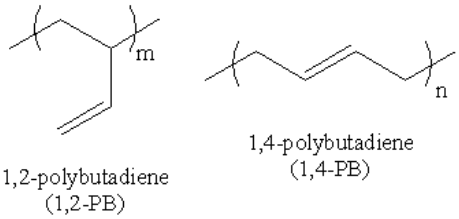

Fig. 3-3: Molecular structures of the two forms of Polybutadiene: 1,2-PB and 1,4-PB

Block Copolymer	PS Wt%	Butadiene Wt%	1,2 PBD Wt%	1,4 PBD Wt%	S Block MW	B Block MW	S Block MW
SBS I	*12.5*	*87.5*	*76*	*24*	*6400*	*102000*	*6400*
SBS II	***21***	***79***	***9.3***	***90.7***	***9000***	***67000***	***9000***

Table 1-1: Polymers object of study.

The optimal procedure to form the membranes was already established by previous work on the same materials in the group [18]. It consists in pouring a 2 % wt solution of the polymer in Cyclohexane into glass casting rings. The glass plates were then let to dry under nitrogen for 24 hours and then moved into a vacuum oven where they

were kept overnight at 35°C under vacuum to completely remove the solvent and to obtain the same initial condition for all the samples. The catalyst used was Cobalt in the form of Cobalt Neodecanoate (Fig. 3-4) (Sheperd Chemical Company, Norwood, OH), added in different amounts to the pre-cast solutions.

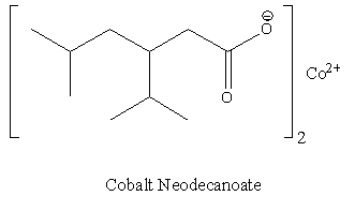

Fig. 3-4: Molecular structure of the catalyst.

Indeed, the reaction of the polymer with oxygen has to be catalyzed either by UV light or by a transition metal. Cobalt was chosen since it is reported to have the best performance [17]. The reaction is a radical one and involves the butadiene fraction due to the presence of the double bond. The mechanism is not yet completely clear but one possible reaction scheme was proposed by Beaven [16] and is reported in Fig. 3-5 for the case of 1,4 Polybutadiene (there is a similar scheme for 1,2-PB).

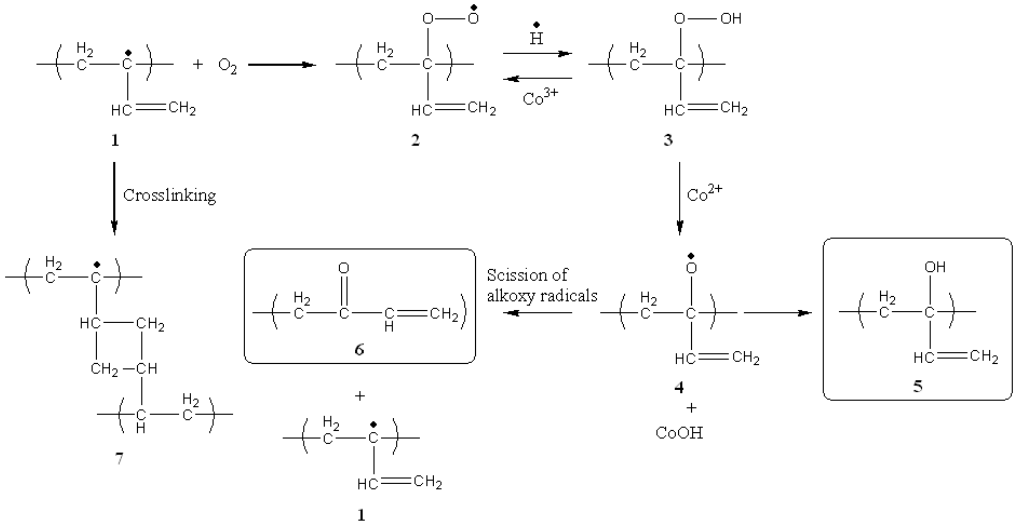

Fig. 3-5: Reaction scheme of the oxygen scavenging action by 1,4 Polybutadiene [16].

The main reaction is catalyzed by the Cobalt salt and leads to the consumption of oxygen and to the formation of an alkoxy group (component 6 in Fig. 3-5) and a new radical that can continue the reaction. It is worth noting that there is also a parallel

crosslinking reaction that consumes the double bonds of the polymer and therefore prevents further consumption of oxygen; this reaction is not catalyzed and happens in all conditions: for this reason it is really important to control the formation protocol of the membranes.

3.1.2 Sorption measurements

Equipments

The oxygen uptake of the membranes was measured with different techniques: besides an analytical balance with a precision of 10^{-5} g, a non invasive headspace measurement was used [18].

The OxySense® 200T [19] is a non invasive oxygen sensor that can measure the oxygen content inside a sealed, transparent container. A schematic of the system is shown in Fig. 3-6 while in Fig. 3-7 there is a picture of our set up.

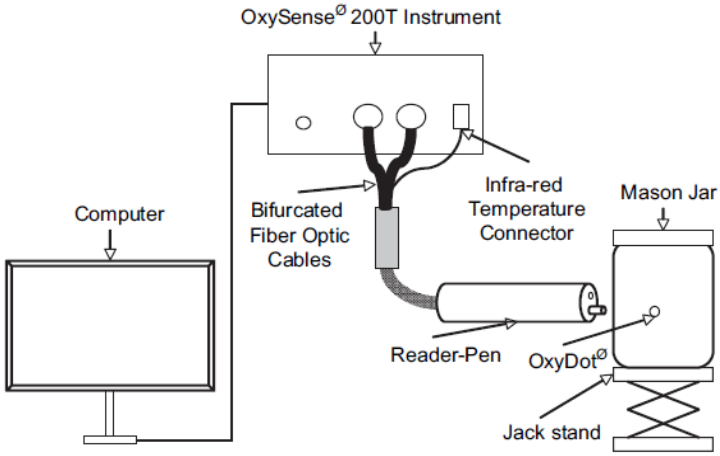

Fig. 3-6: Schematic diagram of OxySense® system [18].

The oxygen content is measured through an optical method, using oxygen sensitive sensors (OxyDot®) fixed inside a transparent container with silicon rubber. The system is constituted by a reader-pen with a fiber optic cable bundle that can illuminate the OxyDot® and an integrated infrared temperature sensor. The reader-pen can detect the fluorescence energy released by the illuminated sensors that is proportional to the

oxygen partial pressure in the Mason jar where the sample is placed at the beginning of the experiment.

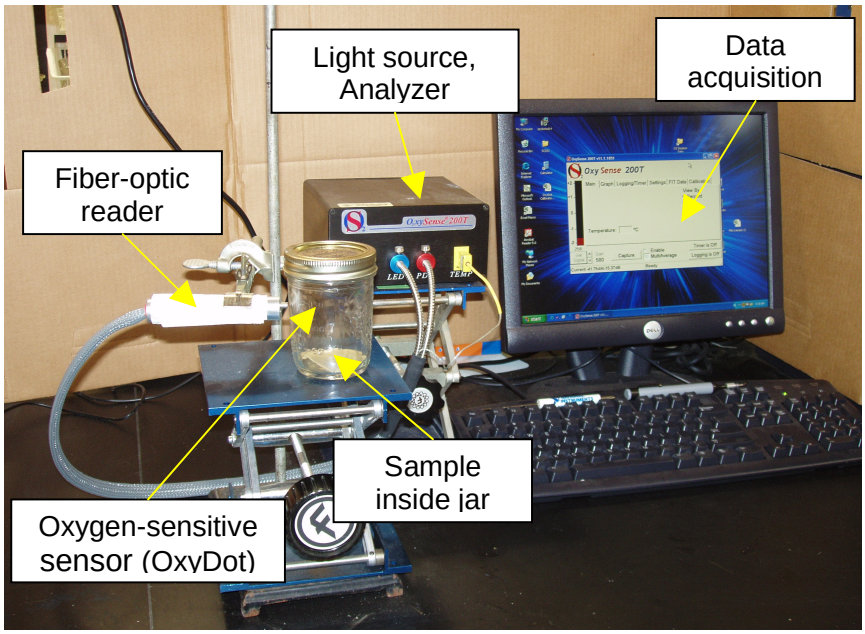

Fig. 3-7: Set up of the OxySense® system.

This instrument is very convenient for our purpose since it allows the simultaneous measurement of a large number of samples; moreover the simple headspace analysis from outside the jar avoids any possible contamination of the original atmosphere since, after the initial placement of the sample at the desired partial pressure, the jar remains sealed. In Table 3-2, the technical features of the OxySense® 200T system are reported.

Specifications		
	In Gas	**In Liquid**
Operating Range	0-30%	0-100% saturation O_2
Detection Limits	0.03%(300 ppm) 15 ppb (15u/L)	
Accuracy	Accuracy is 5% of the reading even at low levels of oxygen, (effectively the accuracy improves at lower oxygen concentrations)	
Response Time	<5 Second	
Enclosure size	3.25"x6.125"x6.25" (8.2x15.5x15.8 cm)	
Operating Temperature	32-140°F (0-60°C)	
Power	100V-240V AC (50/60 Hz)	

Table 3-2: Technical specifications for OxySense® 200T [19].

The decay of the oxygen partial pressure inside the closed jar can be easily correlated to the amount of oxygen that has reacted with the polymer or, in other words, that has been consumed by the OSP. The number of moles of oxygen in the jar at every time can be calculated from the partial pressure measured by the OxySense® with the ideal gas law:

$$n = \frac{P_{O_2} \cdot \left(V_{jar} - V_{pol}\right)}{R \cdot T} \tag{3.1}$$

where V_{jar} is the internal volume of the Mason jar, R is the ideal gas constant and T the temperature measured with the reader-pen. The mass uptake of oxygen by OSP (usually expressed in $g/g_{polymer}$) can then be calculated by a simple mass balance:

$$M = \frac{\left(n_0 - n\right) \cdot MW}{m_{o,pol}} \tag{3.2}$$

with MW being the molecular weight of Oxygen and $m_{o,pol}$ the initial mass of polymer. An example of the experimental output is reported in Fig. 3-8, , where the pressure and the correspondent mass uptake calculated trough Equations (3.1) and (3.2) are plotted, as a function of time.

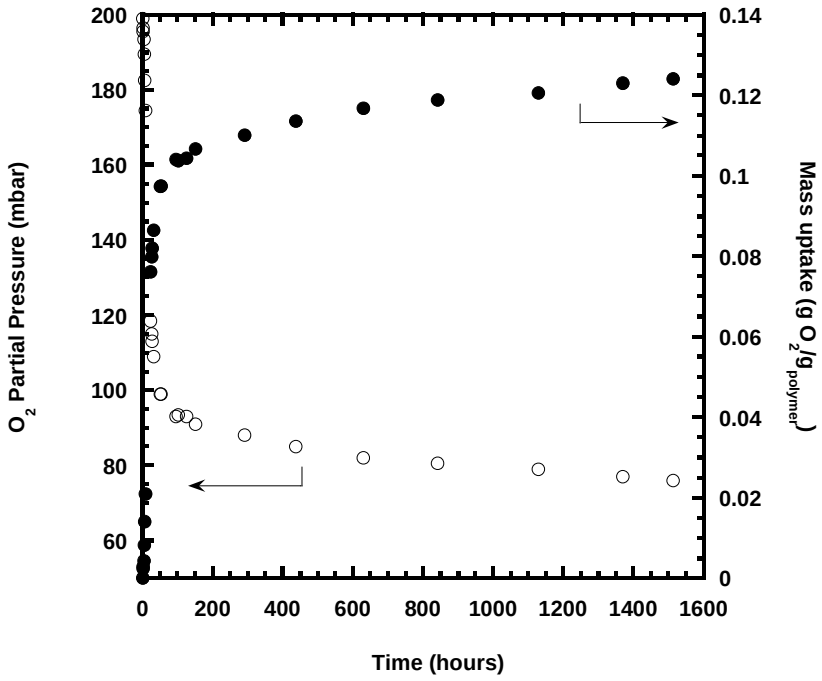

Fig. 3-8: Example of raw data collected by OxySense® and correspondent calculated mass uptake curve.

The measurement was performed every hour during the first day of the experiment and less frequently in the following days, until a constant value of the partial pressure was observed. In some cases the equilibrium was reached after several months of experiment. All the parameters (temperature, partial pressure, catalyst content, thickness) were varied in order to study their influence on the reaction of oxygen with the polymer, as it will be shown in the results section.

In the end, some solubility measurements on completely oxidized samples were performed with a Magnetic Suspension Balance (Rubotherm®) with a precision of 5 μg, since the decay in oxygen partial pressure inside jars was no longer detectable with the OxySense®.

Results

The experimental campaign involved the study of the effect of all the parameters on the oxidation process, with particular regard to the kinetics of the process and the equilibrium value of oxygen uptake. Using the OxySense® instrument, the effects of the catalyst concentration in the membrane, of the experimental temperature, of the film thickness and initial partial pressure of oxygen were studied.

First the concentration of cobalt neodecanoate in the SBS II membrane was varied, from 0 to 300 ppm in cyclohexane, to find the optimal amount of catalyst to be added to the polymer to obtain the best performance of the active membrane. The jars were filled with air and stored at 30°C between the measurements. In Fig. 3-9 the results for samples of SBS II of equal thickness and different catalyst contents are reported. It can be seen that, after two months of testing, there is no oxidation when the concentration of catalyst is equal to zero, while the highest value of oxygen consumed at equilibrium is obtained with the lowest concentration of cobalt investigated, that is 10 ppm. Then the final mass uptake decreases toward the value of 75 ppm to increase again for higher values of catalyst. The curve obtained for an amount of catalyst equal to 300 ppm was not reported in the plot since the membrane showed an anomalous behavior, most likely due to an extensive crosslinking reaction of the polymer. Since we were not able to control and measure the number of crosslinks in the membrane, we cannot

be sure that also in the other samples the O_2 uptake observed was somehow affected by this parallel reaction; however, the preparation procedure was accurately followed in order to at least have reproducible data. The mass uptake was certainly affected by the crosslinking reaction, and a more accurate measurement would be necessary for a deeper investigation of the kinetics of the oxidation that is beyond the scope of this study.

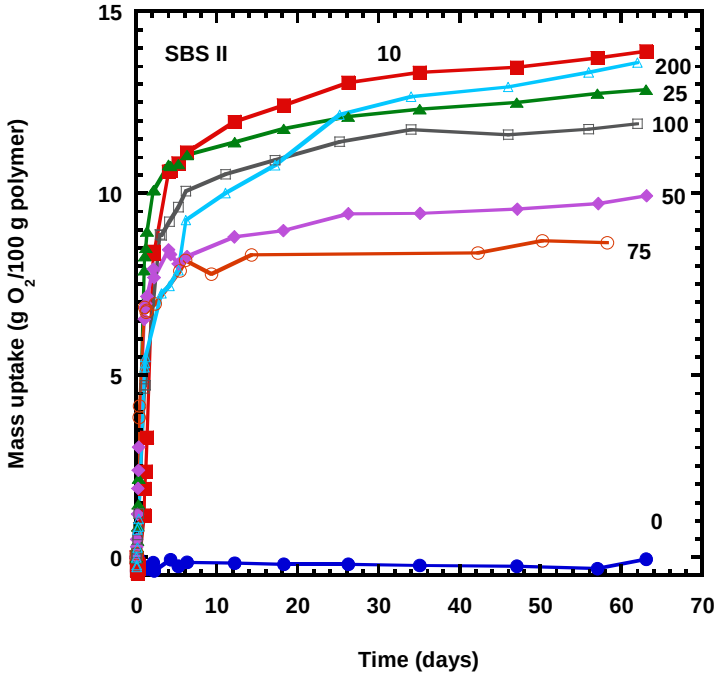

Fig. 3-9: Influence of catalyst concentration on the mass uptake of SBS II films: membranes thickness was about 100 µm; all the experiments were performed at 30°C, filling the jar with atmospheric air. All the concentrations are expressed in ppm.

The lowest cobalt concentration studied was 10 ppm and no attempts were made to decreases further the catalyst content because of a side effect that can be seen in Fig. 3-10: with the lowest concentrations of cobalt (10 and 25 ppm) an induction period appears before the reaction starts and it is not desirable that the membrane becomes active only after a period of exposure to oxygen since our purpose is to have an immediate consumption of the reactant. A good compromise between the amount of oxygen consumed by the film and the kinetics of oxidation process can be obtained by using a catalyst content of 100 ppm; the following tests were all carried on with this value of catalyst concentration.

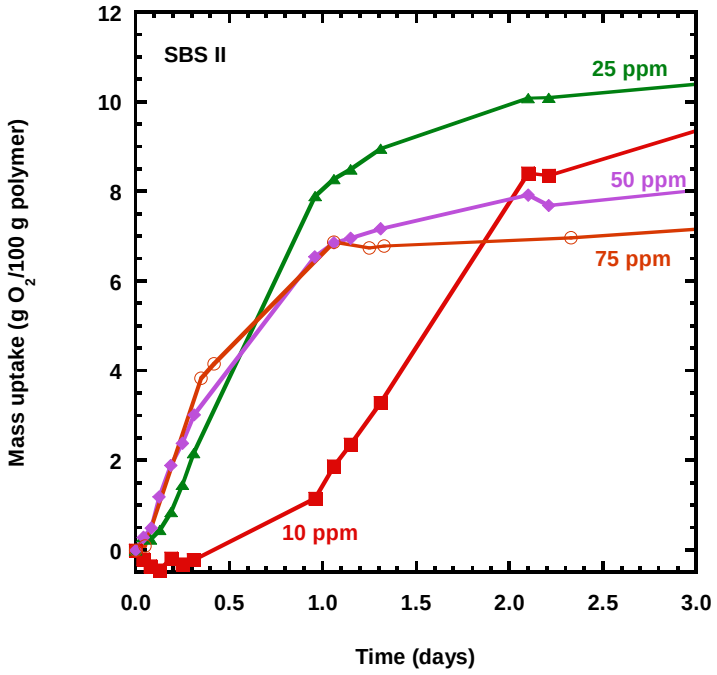

Fig. 3-10: Earliest days data point for cobalt concentration experiments.

The second parameter studied is the experimental temperature: the samples were stored, between the measurements, at the temperature of the experiment, with the exception of a small interval during which they were kept at room temperature, in order to avoid problems with the automatic temperature correction of the instrument. All the experiments were carried on with samples of about 100 μm, with a catalyst concentration fixed at 100 ppm and within jars filled with air. As expected, the increasing temperature favors the kinetics of the oxidation reaction (Fig. 3-11): no oxygen consumption can be detected for the sample stored at -20°C (the initial scattering in the data is below the experimental error) while, as the temperature increases, the reaction becomes faster as demonstrated by the Initial Oxidation Rate (IOR), calculated as the slope of the mass uptake curve 0.2 days of oxidation and reported in Table 3-3. The final mass uptake seems to be affected by temperature too, and in particular it seems to increase with temperature. However, this observation could be affected by the fact that the reaction was not complete after 60 days of measurement.

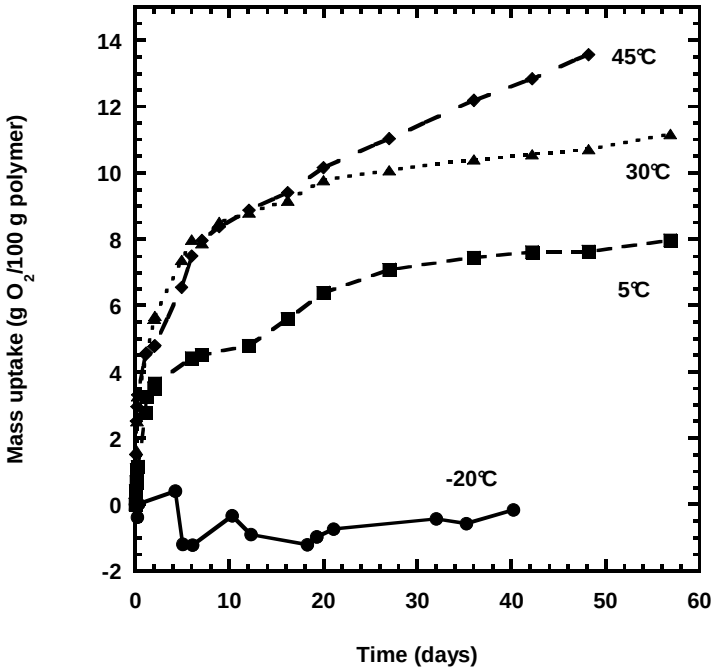

Fig. 3-11: Temperature effect on oxidation of SBS II. All samples were about 100 μm with a Cobalt concentration of 100 ppm and the jars were initially filled with air.

T (°C)	IOR (g O_2/(100 g polymer day))
5	4.75
30	12.5
45	14.5

Table 3-3: Initial Oxidation Rate as slope of the mass uptake curve at 0.2 days of oxidation in the temperature experiments.

Another variable that can be controlled in the formation of the scavenging membranes is the thickness; in this case the samples contained all the same amount of cobalt (100 ppm), they were stored at 30°C and exposed to air. If the mass uptake is reported as g of oxygen consumed per 100 g of OSP (Fig. 3-12), the final mass uptake seems to decrease as the film thickness increases; once that the mass uptake is normalized on the surface area of the sample, it is clear that all the curves overlap (Fig. 3-13). This suggests the idea that the oxygen scavenging consumption does not occur in the entire polymer at the same time but it is a heterogeneous process: the reaction front moves inside the membrane and proceeds from the surface of the film to the bulk until all the material has reacted.

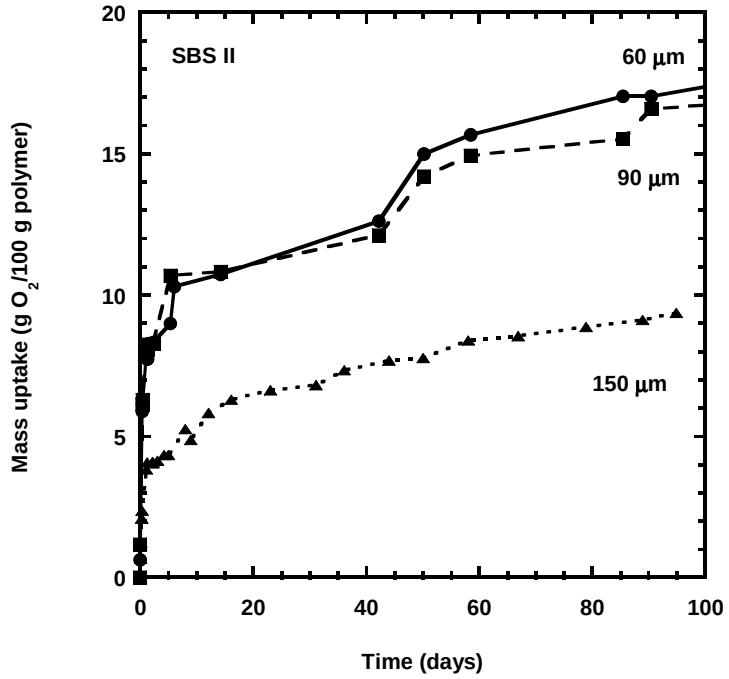

Fig. 3-12: Thickness experiment on SBS II: Mass uptake normalized on the initial mass of the sample. Jars stored at 30°C, filled with air, sample with 100 ppm of Cobalt.

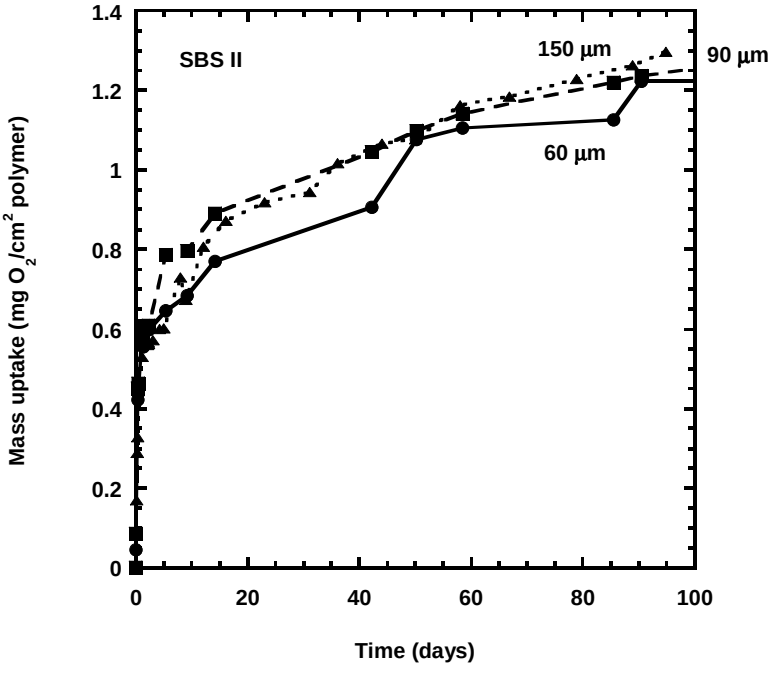

Fig. 3-13: Thickness experiment on SBS II: Mass uptake normalized on the surface of the sample. Jars stored at 30°C, filled with air, sample with 100 ppm of Cobalt.

The last parameter studied was the partial pressure of oxygen inside the Mason jars at the beginning of the experiment. The sample thickness was around 100 μm, the cobalt concentration 100 ppm and the storage temperature 30°C. The effect of initial oxygen content seems straight forward: the higher the oxygen concentration in the beginning, the higher the final value of the mass uptake as shown in Fig. 3-14.

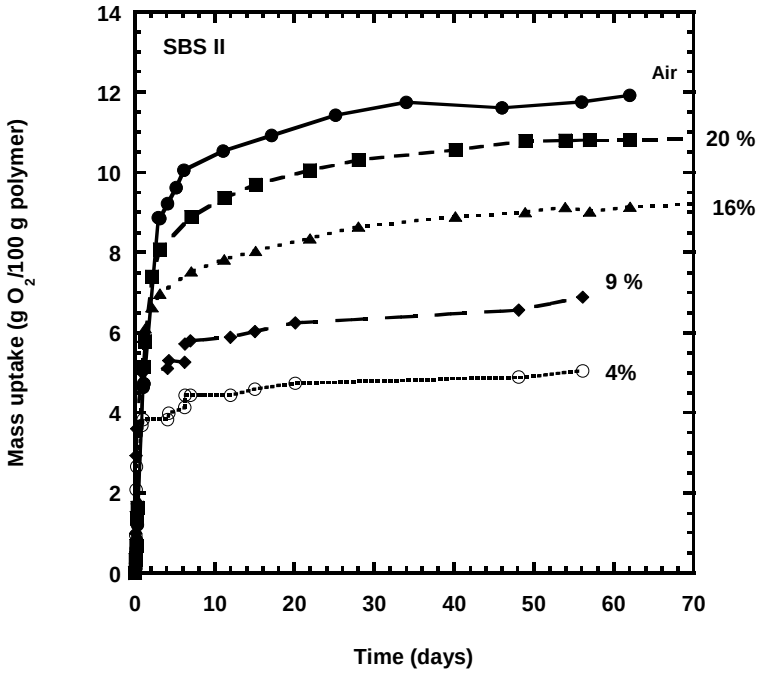

Fig. 3-14: Partial pressure experiment on SBS II. Film thickness 100 μm, Cobalt concentration 100 ppm and storage temperature 30°C.

In order to check the real completion of the reaction in all the samples, after 100 days of oxidation the jar containing the samples that had started with the lowest amount of oxygen (4%) was opened and refilled with air. At this point the jar was resealed and in Fig. 3-15 it can be seen that the oxygen content begun again to decrease (and therefore the mass uptake in the polymer to increase) symptomatic of the fact that the reaction had not been completed after the first 100 days starting at 4% of oxygen. The apparent equilibrium was observed only because the oxygen initially present in the jar had been completely consumed. This is rather important since in the usual applications these systems would be exposed to atmosphere with no lack of oxygen in any moment.

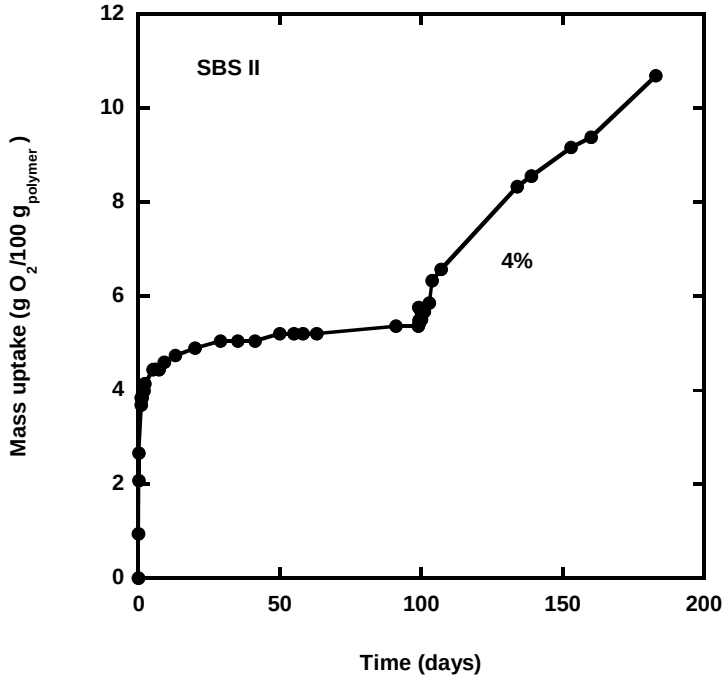

Fig. 3-15: Mass uptake curve for a sample with a 4 % of initial oxygen in the jar. After 100 days of oxidation the jar was replenished with air and the oxidation started again.

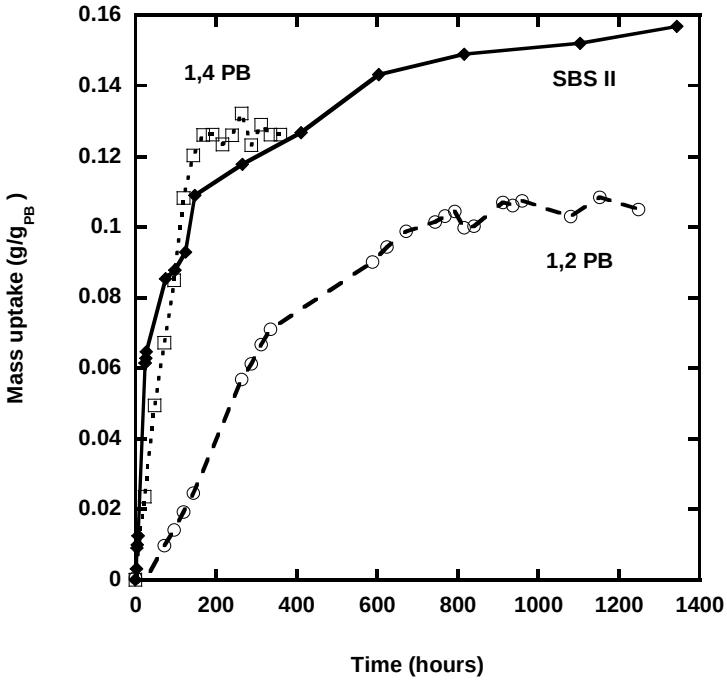

Fig. 3-16: Comparison between SBS copolymer and the homopolymers reported as grams of oxygen per grams of Polybutadiene. Measurement performed with the OxySense® on sample exposed to air of 100 µm doped with 100 ppm and stored at 30°C. Data for 1,4 Polybutadiene courtesy of Hua Li; data for 1,2 Polybutadiene courtesy of Keith Ashcraft.

Another comparison that can be done is between the copolymer and the homopolymers that were tested by my colleagues. Since the polystyrene cannot react with oxygen, the oxygen consumption was expected to be related to the fraction of butadiene present in the copolymer and therefore lower than for the homopolymers. Instead, if the oxygen uptake is normalized on the mass of Polybutadiene (Fig.3-16), the SBS II exhibits a higher consumption of gas probably due to better dispersion caused by the presence of polystyrene. The kinetic for the copolymer resembles the one for 1,4 Polybutadiene as expected since the fraction of 1,4 is prevalent in this copolymer.

The comparison between a sample with and without antioxidant was also made with experiments with an analytical balance. Since the final goal of the work is to build effective layered structures that have to be made by extrusion and therefore in the presence of antioxidant, it is important to know its effect on the reaction.

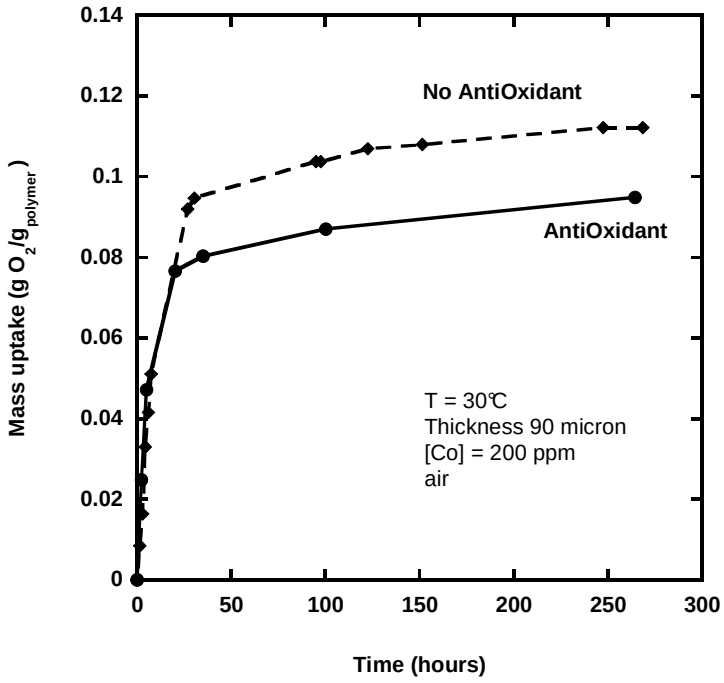

Fig. 3-17: Oxygen consumption by SBS II with or without antioxidant. Samples exposed to atmosphere and measured with an analytical balance. Data for sample with anti-oxidant courtesy of Kevin Tung.

The oxidation in the sample with antioxidant was initiated with UV light after doping the sample with benzophenone as photo initiator in high amount (10% wt). Fig. 3-17 shows that the oxidation level of the film with antioxidant remains lower compared to

the sample without additives probably due to a non homogeneous distribution of the initiator and therefore to the presence of not-reacted spots in the material.

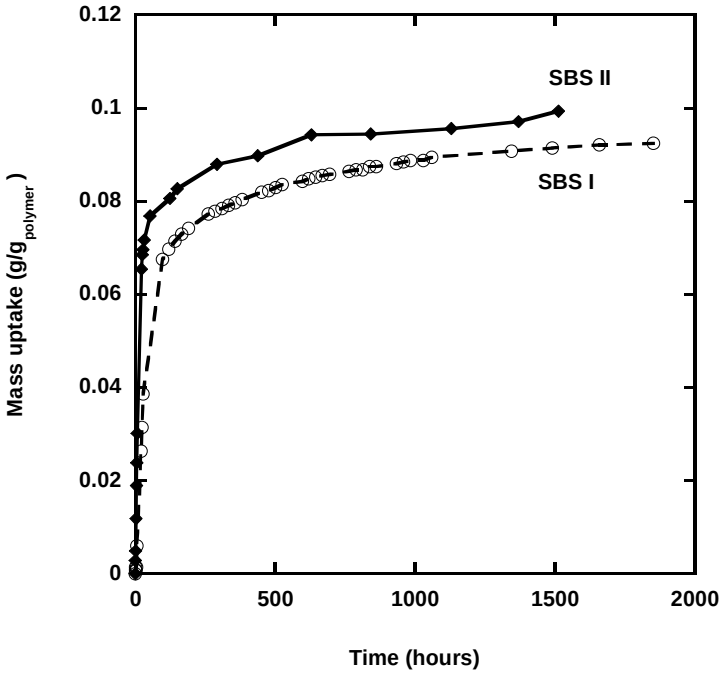

Fig. 3-18: Comparison between mass uptake of SBS I and SBS II samples in the same conditions.

In parallel to the experimentation on the SBS II, the same experiments were conducted on SBS I samples in which the butadiene part is mainly constituted by 1,2 PB (Table 3-1). In Fig. 3-18 only one comparison with SBS II (films with 50 ppm of cobalt, 100 μm thick, jar filled with air and stored at 30°C) is reported showing that the higher presence of 1,4 PB in SBS II speeds up the reaction as expected; most of the data on SBS I will be reported in the next section and used to illustrate the model developed.

As a final issue, the oxygen uptake of a "completely" oxidized membrane of SBS II, doped with 10 ppm of Cobalt neodecanoate, was measured with a Magnetic suspension Balance. The sample was let react for seven months before measuring the solubility when no further oxidation was detectable with the OxySense® measurement. The mass uptake curve measured with MSB shows a non-Fickian behavior that suggests a non-complete reaction. This residual oxidation could also have been enhanced by the experimental condition: during the sorption measurement the sample was exposed to a higher oxygen partial pressure than the other samples that can activate regions of the

material that did not react before due to lack of oxygen. For this reason the solubility datum calculated in this way (7 cm^3 STP/cm^3 atm) has to be used with great care to avoid wrong conclusions.

3.1.3 Permeation Measurements

Oxygen permeability was determined using a constant volume/variable pressure apparatus. The measurement was performed to retrieve the diffusion coefficient of oxygen in the oxidized polymer beside the permeability value. A SBS II film doped with 10 ppm of catalyst, already oxidized for seven months, was exposed to vacuum for one night on both the upstream and downstream surfaces. After degassing, the system was tested for leakages; after a successful leak test, the downstream volume was sealed at vacuum and the upstream film surface was exposed to a pure gas at 1 atm. Gas permeability ($5x10^{-12}$ cm^3(STP) cm/(cm^2 s cmHg)) was calculated from the steady state pressure increase in the downstream volume as follows:

$$P = \frac{dp}{dt}\frac{lV}{pAR} \tag{3.3}$$

where *dp/dt* is the pseudo-steady state rate of pressure increase in the downstream volume, *l* is the film thickness (cm), *p* is the upstream absolute pressure, *A* is the area of the film available for transport (cm^2), *V* is the downstream volume (cm^3), and *T* is absolute temperature (K). *R* is the gas constant.

Form the transient curve of permeation, also the diffusion coefficient for oxygen in the polymer was determined ($1x10^{-9}$ cm^2/s); in particular the diffusivity was calculated from the time lag θ_0 of the experiment, that is the intercept of the tangent to the permeate curve vs. time on the abscissa axis, following:

$$D = \frac{l^2}{6\theta_0} \tag{3.4}$$

The permeation test was repeated several times until the permeability value was reproducible in order to be sure that the membrane has been completely oxidized; in

fact the use of pure oxygen in the upstream reactivates the oxidation process even if the membrane used for the test seemed already completely oxidized in the OxySense® test. The diffusion coefficient was calculated from the time lag and not from the relation that holds true for Fickian transport and when the solution diffusion model can be applied ($P = D \times S$), because the MSB experiment did not show Fickian behaviour probably due to the non-complete oxidation of the sample and therefore the value of the solubility S calculated in that way would lead to an underestimation of D (~10^{-10} cm^2/s).

3.2 Modeling

Beside the experimental activity, a modeling work was performed in order to reduce the amount of experimental tests needed and fully understand the mechanism that rules the oxygen scavenging. The achievement of the goal regarding the reduction of oxygen permeation through the material, indeed, will lead to experimental times no more practical for the investigation and therefore to the need of a model that predicts the performance of the packaging allowing decision about its applicability in each case.
Two models were developed: one can describe the sorption experiments performed on the SBS samples and can be used to retrieve some parameters not yet completely available in literature; the second one is an attempt to describe a possible layout of a real package considering a blend of the Oxygen Scavenging Polymer in a common barrier material. In real application, in fact, the OSP will not be used by itself due to the lack of mechanical and optical characteristics that matters in the packaging industry. After the oxidation has taken place, the SBS membrane appears brittle and dark and therefore it has to be combined with other materials in order to maintain the packing intact and transparent. Furthermore, the presence of a metal catalyst will raise issues about the toxicity of the entire film.

3.2.1 Single Film model

As demonstrated by the thickness experiments (Fig. 3-13), the oxidation process is heterogeneous and proceeds from the surface to the bulk of the membrane. This is also confirmed by images of the cross section of a film after several weeks of oxidation taken both with an optic microscope and with a SEM (Fig. 3-19, Fig. 3-20). In both pictures it is evident the presence of two regions in the membrane: the external region has already reacted while the internal portion has not seen oxygen yet. The thickness of the oxidized layer is coherent with the experimental mass uptake data collected.

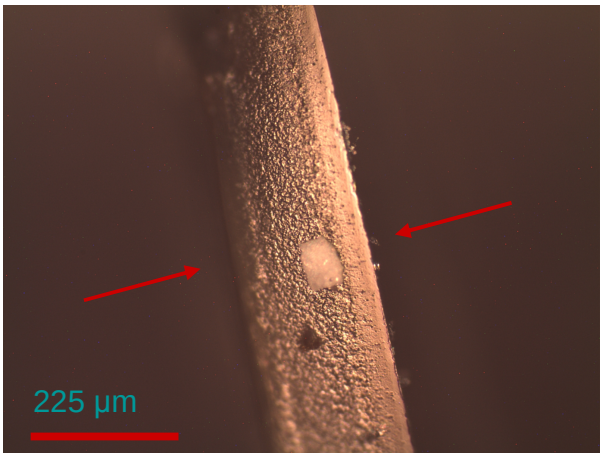

Fig. 3-19: Image of the cross section of SBS I during oxidation taken with an optic microscope. (Courtesy of Viktor Kusuma)

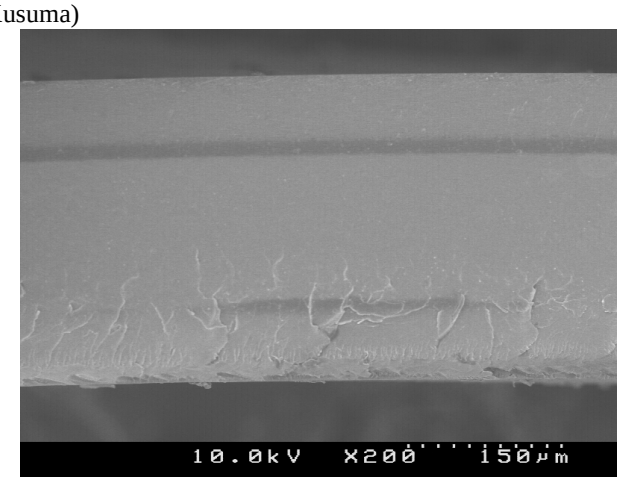

Fig. 3-20: SEM image of an SBS I membrane during oxidation. (Courtesy of Viktor Kusuma)

Physical description and mathematical formulation of the model

The results of the experiments on the mass uptake of Oxygen Scavenger Polymer can be modeled considering the geometry in Fig. 3-21.

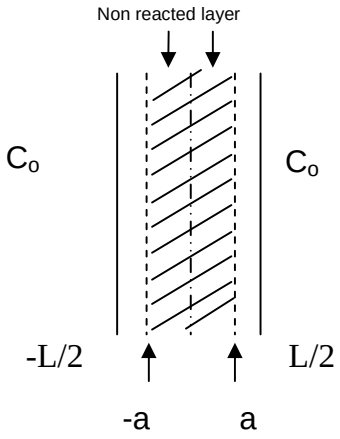

Fig. 3-21: Schematic of an OSP membrane.

The film is considered immersed in a gaseous oxygen atmosphere. The concentration at the film surface can be calculated from the partial pressure in the atmosphere p_{O_2} with the solubility coefficient S_p of the oxidized material.

The reaction is faster than the diffusion process in the already oxidized layer that grows at the external surfaces and this leads to a reaction front inside the film that moves while the reaction proceeds. Under these assumptions, there is no oxygen in the portion of film between the two reaction fronts (the sorption process proceeds symmetrically from the two surfaces, both exposed to the same atmosphere) and the mass uptake due to reaction is prevalent while the physical contribution can be neglected. When the reaction front reaches the middle plan of the membrane, the material is completely oxidized and there is no more oxygen uptake related to oxidation but only a physical sorption.

To analyze the chemical sorption, a simple first order reaction can be considered and through a mass balance between the volume variation of the oxidation layer and the oxygen consumed, expressed through the Rate of Oxygen Consumption (ROC), the following equation is obtained:

$$\frac{d}{dt}\left(A\cdot 2a\right)=-\frac{ROC}{\beta} \tag{3.5}$$

$$ROC=2A\cdot k\cdot C(a) \tag{3.6}$$

$$x=\frac{L}{2}\qquad C=C\left(\frac{L}{2}\right)=C_s=S_p\cdot P_{o_2} \tag{3.7}$$

$$x=a\qquad C=C(a) \tag{3.8}$$

where β represents the amount of oxygen consumed per volume of OSP, S_p is the solubility coefficient of the completely oxidized polymer and k is the reaction rate. Equating the reaction at the front to the flux of diffusing oxygen and using a pseudo-steady state analysis:

$$N=D_p\frac{C_s-C(a)}{L/2-a}=kC(a) \tag{3.9}$$

the concentration at the moving boundary becomes:

$$C(a)=\frac{C_s}{1+\frac{k}{D_p}\left(L/2-a\right)} \tag{3.10}$$

Substituting the concentration at the reaction front in equation (3.6), we can calculate the ROC and find the differential equation that controls the variation of the position of the reaction front with time.

$$ROC=\frac{2AkC_s(t)}{1+\frac{k}{D_p}\left(L/2-a\right)} \tag{3.11}$$

$$\frac{da}{dt}=-\frac{ROC}{2A\beta}=-\frac{C_s(t)}{\left(1+\frac{k}{D_p}\left(L/2-a\right)\right)\beta} \tag{3.12}$$

Equation (3.12) should be integrated to determine the position of the reaction front at every time:

$$a(t) = \frac{D_p}{k}\left\{\left(1+\frac{kL}{2D_p}\right)-\left(1+\frac{2k^2}{\beta D_p}\int_0^t C_s(t)dt'\right)^{1/2}\right\} \qquad (3.13)$$

For the OxySense® experiments the oxygen partial pressure outside the membrane is decreasing during the experiment and the integral in (3.13) has to be solved numerically.

The variation of mass absorbed can then be calculated integrating the ROC.

$$\frac{dM_t}{dt} = ROC = \frac{2AkC_s(t)}{1+\frac{k}{D_p}\left(L/2 - a(t)\right)} \qquad (3.14)$$

$$M_t(t) = 2Ak\int_0^t \frac{C_s(t')}{1+\frac{k}{D_p}\left(L/2 - a(t')\right)}dt' \qquad (3.15)$$

In the case of gravimetric experiments, the partial pressure of oxygen outside the membrane is constant and the integrals in equations (3.13) and (3.15) can be easily calculated:

$$a = \frac{D_P}{k}\left\{\left(1+\frac{kL}{2D_p}\right)-\left(1+\frac{2k^2C_s t}{\beta D_p}\right)^{1/2}\right\} \qquad (3.16)$$

$$M_t = \frac{2A\beta D_p}{k}\left\{\left(1+\frac{2k^2C_s\cdot t}{\beta D_p}\right)^{1/2}-1\right\} \qquad (3.17)$$

After the reaction front has reached the middle plan of the membrane ($t = t_a$), where the concentration is $C(a, t = t_a) = C_a$, the physical sorption must be considered; the concentration profile at the beginning of this period is due to the previous chemical sorption and can be approximated as:

$$C(t_a) = C_a + \frac{2(C_s - C_a)}{L}x \qquad 0 < x < L/2 \qquad (3.18)$$

$$C(t_a) = C_a + \frac{2(C_a - C_s)}{L}x \qquad -L/2 < x < 0 \qquad (3.19)$$

Applying the analytical solution suggested by Crank [20] for sorption in a semi-infinite sheet with a known initial condition, the concentration profile for the following times can be calculated:

$$C(t>t_a)=C_a+\frac{2(C_s-C_a)}{L}x \qquad 0<x<L/2$$
$$+\frac{2}{\pi}\sum_1^\infty\left\{\frac{C_s\cdot\cos(n\pi)-C_a}{n}\cdot\sin\left(\frac{2n\pi x}{L}\right)\cdot\exp\left(-\frac{4D_p n^2\pi^2 t}{L^2}\right)\right\}$$
$$+\frac{4}{L}\sum_1^\infty\left\{\sin\left(\frac{2n\pi x}{L}\right)\cdot\exp\left(-\frac{4D_p n^2\pi^2 t}{L^2}\right)\cdot\int_0^{L/2}C(t_a)\cdot\sin\left(\frac{2n\pi x'}{L}\right)dx'\right\} \tag{3.20}$$

From the concentration profile for $t>t_a$, the mass uptake associated to physical sorption can be retrieved:

$$M_t(t>t_a)=2A\int_0^{L/2}C(t>t_a)dx'+M_a \tag{3.21}$$

The results for the mass uptake as a function of time can then be compared to the experimental data.

The parameters needed by this model are the capacity of the OSP β, the diffusion coefficient in the oxidized layer D_p, the kinetic constant of the oxidation reaction k. The capacity of the polymer can actually be calculated from the final experimental mass uptake of the membrane only, considering both the chemical and the physical contribution in the limit of very long times:

$$M_\infty=AL\beta+ALS_pP_{O_2} \tag{3.22}$$

The solubility coefficient S_p of the oxidized material can be measured in a sorption experiment; the value obtained with the Magnetic Suspension Balance (7 cm^3(STP)/cm^3atm) was used even if it was measured on only one sample and is affected by experimental errors.

The diffusion coefficient D_p can be determined in a separate experiment on a completely oxidized material (for example in a time lag experiment ~ 10^{-10} cm/s, see previous section); in this case only the kinetic constant remains as a fitting parameter.

In alternative, both the diffusion coefficient and the kinetic constant can be used as fitting parameter to adjust the model curve to the experimental one.

A non dimensional group, the Damköhler number, $(Da) = kL / D_p$, can be defined in order to compare the characteristic time of the diffusion in the oxidized layer and the oxidation at the reaction front, keeping in mind that the model was developed in the limit of fast reaction.

Results

The single film model was applied to both the SBS I and SBS II experimental data. Here only data for SBS I with different content of Cobalt will be reported since the data for SBS II have already been shown and the trends for the two materials are similar.

First the capacity of the membrane was calculated through the long time expression (3.22) considering that the final value of the OxySense® experiments was the mass uptake after reaction has reached its completion and using the value measured with the MSB for the solubility coefficient of the completely oxidized polymer. It can be seen in Fig. 3-22 that as the cobalt concentration inside the membrane increases, maintaining all other variables constant, there is a decrease in the capacity β of the OSP, i.e. the moles of oxygen reacted per volume of polymer.

In order to apply the model in a complete predictive way, information about the kinetic of the oxidation reaction and the diffusion coefficient of oxygen in the oxidized material has to be known. Since no values are available for the kinetic constant of the process, in the following it was always considered as a fitting parameter; for the diffusion coefficient the permeation experiments gave a value that was first used.

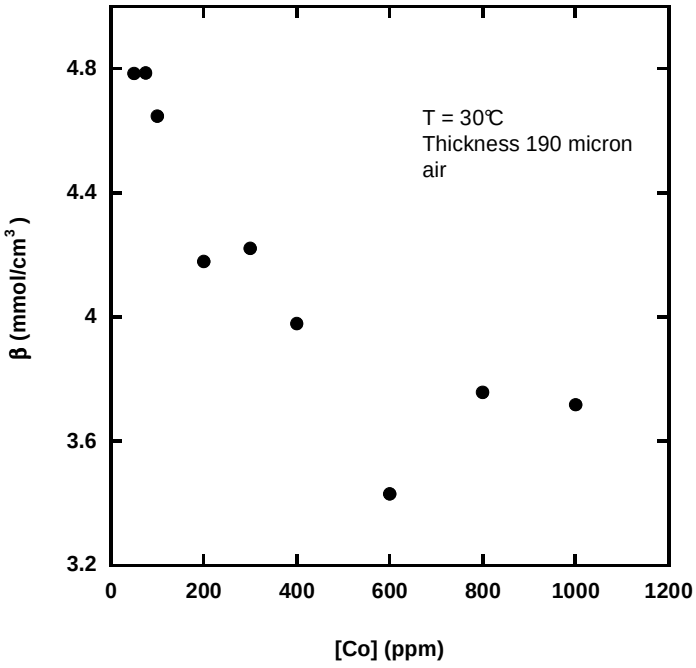

Fig. 3-22: Capacity of the OSP membranes (SBS I) varying the catalyst concentration in the initial casting solution.

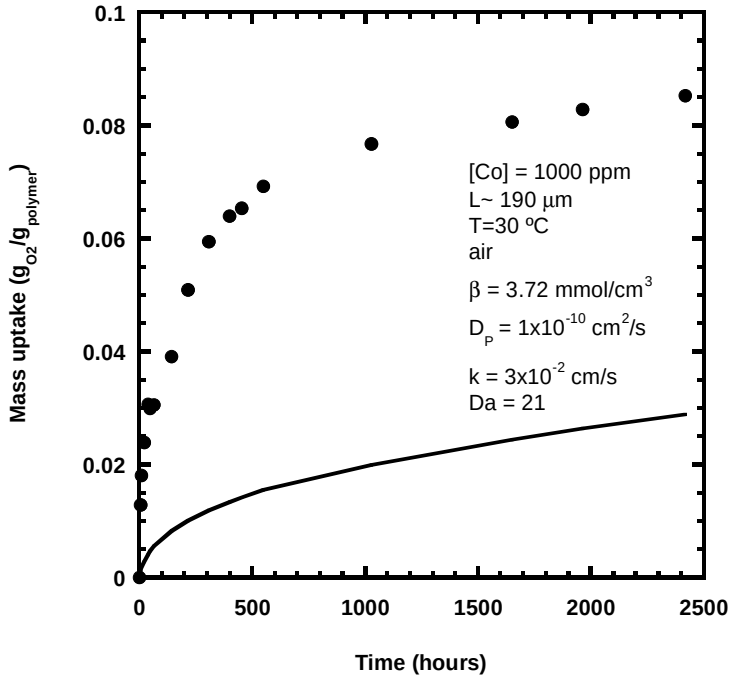

Fig. 3-23: Comparison between model curve and experimental points considering only the kinetic constant *k* as fitting parameter.

As shown in Fig. 3-23, this value leads to a model curve that is far away from the experimental data. The model was then used with two fitting variables, k and D; an

example of a fitting curve compared with experimental points is reported in Fig. 3-24 for a SBS I sample but the model has been applied to all the data for both copolymers and also to some data for the homopolymers.

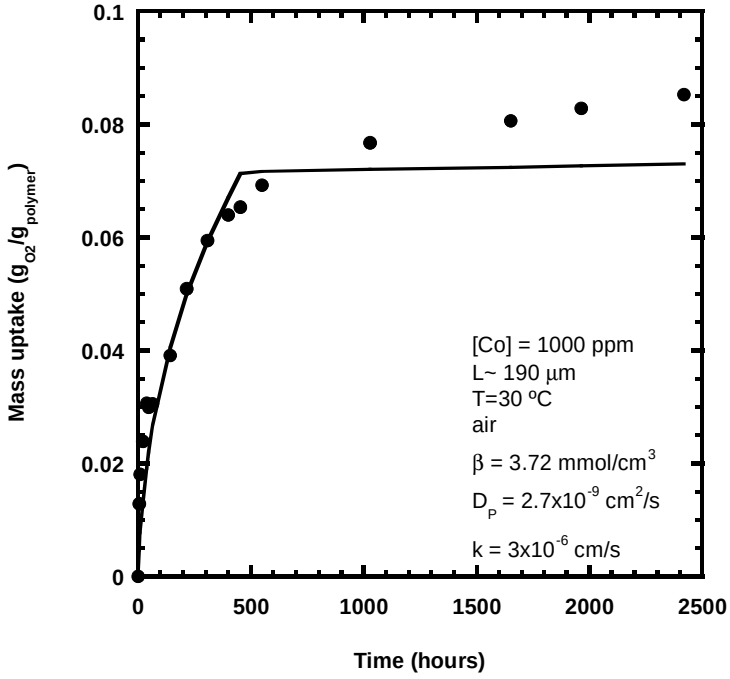

Fig. 3-24: Comparison between experimental and model curves using two fitting parameters, *k* and *D*.

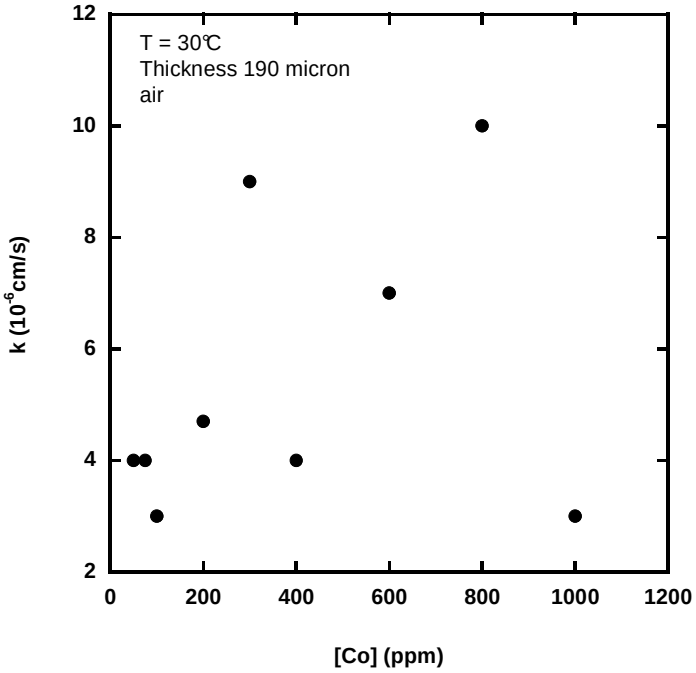

Fig. 3-25: Variation of the kinetic constant k with the Cobalt content in the OSP film.

In Fig. 3-25 and Fig. 3-26, the values of the parameters obtained from the fitting procedure applied to SBS I membranes with different content of cobalt are reported. No clear trend can be identified in the kinetic constant while the diffusion coefficient seems to decrease as the initial catalyst concentration increases. The procedure has to be optimized after a deeper experimental investigation of the diffusion coefficient in the oxidized material and of the actual kinetic of the process has been performed and no conclusion can be drawn at this point. Anyway it is important to note that this simple approach to the problem allows the determination of all the parameters needed by other models to predict the performance of more complex structures in which the OSP could be inserted. An example of a model of this kind will be presented in the next section.

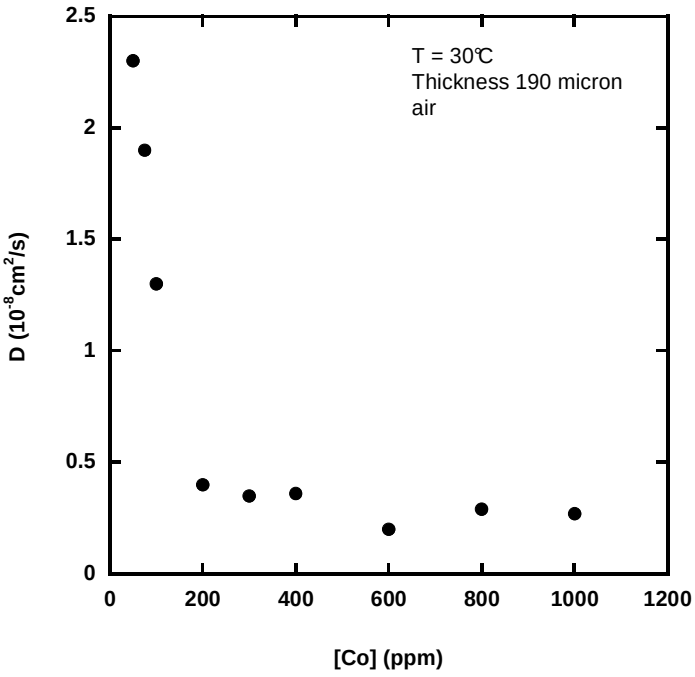

Fig. 3-26: Variation of the diffusion coefficient *D* in the oxidized layer with the Cobalt content inside the OSP film.

3.2.2 Blend films

There are many ways an oxygen scavenging polymer (OSP) can be incorporated into a barrier film or sheet. One of the most straightforward ways is to simply blend a butadiene containing polymer with a matrix polymer like poly(ethyleneterepthalate), PET, or polystyrene, PS; however, due to the immiscibility of these polymers, the OSP will form particles (spherical in the simplest case) in the matrix which size can, in theory, be controlled by rheology and compounding additions. Clearly there are many variables to consider and a model [21] was developed that describes the oxygen transport in the blended film taking into account a diffusion process in addition to reaction kinetics [22-24].

Physical description and mathematical formulation of the model

Blend films of interest consist of a matrix polymer that is melt processable and shows good barrier properties to oxygen (PET) into which particles of a readily oxidable polymer, such as one based on butadiene, are dispersed. The size of the particles is crucial for the properties and can be varied changing the mixing conditions of the components.

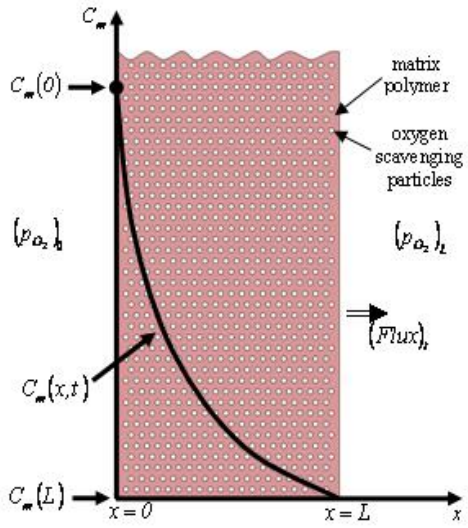

Fig. 3-27: Schematic illustration of a blend film containing particles of an oxygen scavenging polymer in a matrix polymer.

To simplify the model, all the particles are considered to be spheres of the same radius R even if in reality there will be a distribution of sizes and shapes. A schematic of the cross sectional view of the blend film is shown in Fig. 3-27.

The film is supposed to have been kept away from oxygen until ready for use: at time $t = 0$ the upstream surface is exposed to a partial pressure of oxygen (p_{O_2}), that in most cases will be air (0.21 atm) considering the main application that will involve this kind of materials. The downstream of the film is maintained at very low pressure, which for simplicity can be considered negligible. Oxygen dissolves in the matrix at the upstream boundary according to Henry's law:

$$C_m(0) = S_m(p_{O_2})_0 \qquad (3.23)$$

where $C_m(0)$ is the concentration of oxygen in the matrix polymer phase at $x = 0$ and S_m is the effective solubility coefficient; oxygen diffuses through the matrix following Fick's law

$$Flux = -D_m \frac{\partial C_m}{dx} \qquad (3.24)$$

During its diffusion, oxygen is consumed by the oxidizable particles and the kinetics of this consumption can be described by a shrinking core model illustrated in Fig. 3-28.

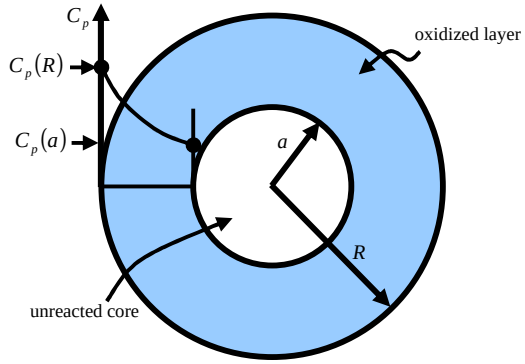

Fig. 3-28: Schematic illustration of the 'shrinking core' model for oxygen diffusion and reaction within an oxygen scavenging particle.

The reaction is assumed to be fast compared to the diffusion process in the oxidized particle shell ($R > r > a$) that at any given time will surround a completely unoxidized

core ($a < r < 0$). For a particle located in the film at position x, where the oxygen concentration in the matrix is $C_m(x,t)$, oxygen will partition into the oxidized surface:

$$C_p(R) = C_m(x,t) / H \tag{3.25}$$

where $C_p(R)$ denotes the dissolved oxygen concentration in the oxidized polymer, H is a partition coefficient that can be calculated as $H = S_m / S_p$, with S_p solubility coefficient for oxygen in the oxidized polymer. At $r = a$ there is a reaction front where oxygen is consumed rather rapidly but with a finite rate k. The amount of oxygen that arrives on the reaction front is controlled by the diffusion in the oxidized shell with a diffusion coefficient D_p. An important assumption of the model is that the oxygen transport in the matrix is considered one-dimensional avoiding the consideration of a very complex three-dimensional composition field around each particle: C_m is a continuously varying function of x only for a given time t. This hypothesis, along with the shrinking core approach for the oxygen consumption within particles, simplifies the mathematical aspects of the model.

For any OSP particle at an arbitrary location x in the film, the reaction is considered to be fast compared to the diffusion process in the article shell so that when oxygen reaches the surface of the core it reacts immediately. Due to the reaction, the scavenging material is consumed, and the radius of the reactive core decreases with time; meanwhile the shell of reacted material around the core becomes thicker.

A simple steady-state balance can be used to approximate the concentration profile inside the shell of reacted material in the same manner used for the film of OSP in the previous section:

$$\frac{D_p}{r^2}\frac{d}{dr}\left(r^2\frac{dC_p}{dr}\right) = 0 \tag{3.26}$$

where D_p is the diffusion coefficient in the oxidized OSP. Integrating (3.26) twice and applying the boundary conditions shown in Fig. 3-28:

$$\begin{aligned} C_p &= C_p(R) = \frac{C_m(x,t)}{H} \quad at\ r = R \\ C_p &= C_p(a) \quad at\ r = a \end{aligned} \tag{3.27}$$

the concentration profile in the shell can be obtained for a given concentration $C_p(R)$ at the particle surface:

$$C_p(r) = C_p(R) - \frac{C_p(R) - C_p(a)}{\left(1 - \frac{R}{a}\right)}\left(1 - \frac{R}{r}\right) \tag{3.28}$$

According to Fick's law, the radial oxygen flux within the OSP is given by

$$N = -D_p \frac{dC_p}{dr} = -D_p \frac{C_1 - C_p(a)}{\left(\frac{R}{a} - 1\right)} \frac{R}{r^2} \tag{3.29}$$

Assuming that the rate of reaction is fast relative to the rate of diffusion, the flux of oxygen and reaction at the reaction front ($r = a$) can be equated to the rate of oxygen consumption at $r = a$ which is approximated by a simple first order surface reaction:

$$-D_p \frac{dC_p}{dr} = -kC_p(a) \tag{3.30}$$

Combining equations (3.29) and (3.30), the concentration of dissolved oxygen at the reaction front, $C_p(a)$, can be expressed as

$$C_p(a) = \frac{C_p(R)}{1 + \frac{ka^2}{D_p R}\left(\frac{R}{a} - 1\right)} \tag{3.31}$$

The Rate of Oxygen Consumption, ROC, for the single particle can be determined as the product of the flux of oxygen and the surface area at $r = a$

$$ROC = 4\pi a^2 k C_p(a) = 4\pi a^2 k \frac{C_p(R)}{1 + \frac{ka^2}{D_p R}\left(\frac{R}{a} - 1\right)} \tag{3.32}$$

A simple mass balance relates the time profile of the un-reacted core radius to the ROC:

$$\frac{d}{dt}\left(\rho_{polymer} \frac{4\pi a^3}{3}\right) = -\frac{ROC}{\beta} \rho_{polymer} \tag{3.33}$$

where β takes into account the capacity of the particle to consume oxygen when fully oxidized; this parameter is defined as the moles of oxygen consumed per unit volume of OSP and can be determined by experimentally measuring the mass uptake of the Oxygen Scavenger Polymer alone [18]. Combining equations (3.32) and (3.33) and simplifying leads to the following dynamic equation for the radius of the unreacted OSP particles

$$\frac{da}{dt} = \frac{kC_p(R)/\beta}{1+\frac{ka^2}{RD_p}\left(\frac{R}{a}-1\right)} \tag{3.34}$$

It must be remembered that $C_p(R)$ is a function of x and t: it is implicitly assumed that this model describes a situation were the particle boundary condition varies with time.

It is now possible to consider the complete membrane consisting of particles dispersed within the matrix as shown in Fig. 3-27. A continuum approach, assuming that the particles are sufficiently small, numerous, and well dispersed, is used where all properties and variables are averages over a particular film volume. The transport of oxygen through the membrane can be described considering the Fickian diffusion in the matrix and the consumption due to the reaction within the particles. The latter term can be calculated from the ROC of a single particle multiplied by the number density, ρ, of particles in the film

$$\rho = \frac{3\phi}{4\pi R^3} \tag{3.35}$$

where ϕ is the volume fraction of particles of radius R. The resulting diffusion equation is given by

$$\frac{\partial C_m}{\partial t} = D_m\frac{\partial^2 C_m}{\partial x^2} - \frac{3\phi}{R^3}\cdot a^2\cdot k\cdot\frac{C_m}{H}\cdot\left[1+\frac{ka^2}{RD_p}\left(\frac{R}{a}-1\right)\right]^{-1} \tag{3.36}$$

This equation must be solved simultaneously with the following equations describing the decrease in the radius of the unreacted core, a, of scavenging particle for all x and t.

$$\frac{da}{dt}=\begin{cases}-\dfrac{k}{\beta}\dfrac{C_m}{H}\cdot\left[1+\dfrac{ka^2}{RD_p}\left(\dfrac{R}{a}-1\right)\right]^{-1} & for\ a\geq 0\\ 0 & for\ a=0\end{cases} \tag{3.37}$$

This system of equations must be solved for the following initial and boundary conditions, representing the typical transient permeation experiment:

$$I.C.:\quad C_m(x,t=0)=0,\quad a(x,t=0)=R \tag{3.38}$$

$$B.C.:\quad C_m(0)\equiv C_m(x=0,t)=S_m p_{O_2},\quad C_m(L)\equiv C_m(x=L,t)=0 \tag{3.39}$$

The equations can be expressed in a more convenient non-dimensional form by defining the following dimensionless variables

$$\tilde{C}=\frac{C_m}{C_m(0)},\quad \tilde{x}=\frac{x}{L},\quad \tilde{a}=\frac{a}{R},\quad \tilde{t}=\frac{t}{L^2/D_m} \tag{3.40}$$

The differential equations plus initial and boundary conditions become

$$\frac{\partial\tilde{C}}{\partial\tilde{t}}=\frac{\partial^2\tilde{C}}{\partial\tilde{x}^2}-3\phi\frac{(Da)\Delta}{\varepsilon^2 H}\left[\frac{\tilde{a}^2}{1+(Da)\left(\tilde{a}-\tilde{a}^2\right)}\right]\tilde{C} \tag{3.41}$$

$$I.C.:\quad \tilde{C}(\tilde{x},\tilde{t}=0)=0 \tag{3.42}$$

$$B.C.:\quad \tilde{C}(\tilde{x}=0,\tilde{t}>0)=1,\quad \tilde{C}(\tilde{x}=1,\tilde{t}>0)=0 \tag{3.43}$$

$$\frac{d\tilde{a}}{d\tilde{t}}=\begin{cases}-\dfrac{C_m(0)}{\beta}\dfrac{(Da)\Delta}{\varepsilon^2 H}\left[\dfrac{1}{1+(Da)\left(\tilde{a}-\tilde{a}^2\right)}\right]\tilde{C} & for\quad \tilde{a}\geq 0\\ 0 & for\quad \tilde{a}=0\end{cases} \tag{3.44}$$

$$I.C.:\quad \tilde{a}(\tilde{x},\tilde{t}=0)=1 \tag{3.45}$$

where $(Da)=kR/D_p$ is the Damköhler number for the OSP particle, the ratio between the time scale of diffusion and the time scale of reaction, $\varepsilon=R/L$ is the ratio of the radius of the OSP and the film thickness, and $\Delta=D_p/D_m$ is the ratio of the diffusion coefficient of the OSP to the diffusion coefficient of the film matrix. The term $C_m(0)$ is

the concentration of oxygen in the matrix at the upstream surface of the membrane and was define in equation (3.38).

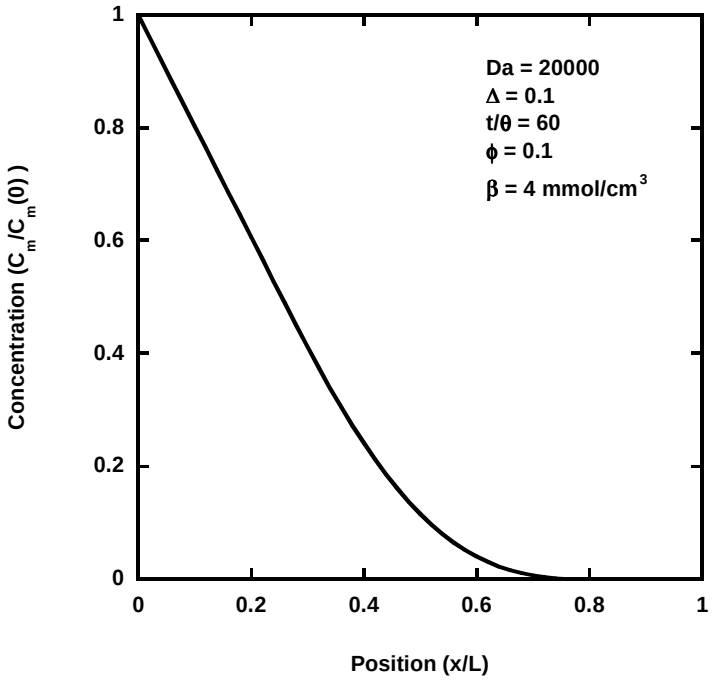

Fig. 3-29: Example of the oxygen concentration profile inside the membrane.

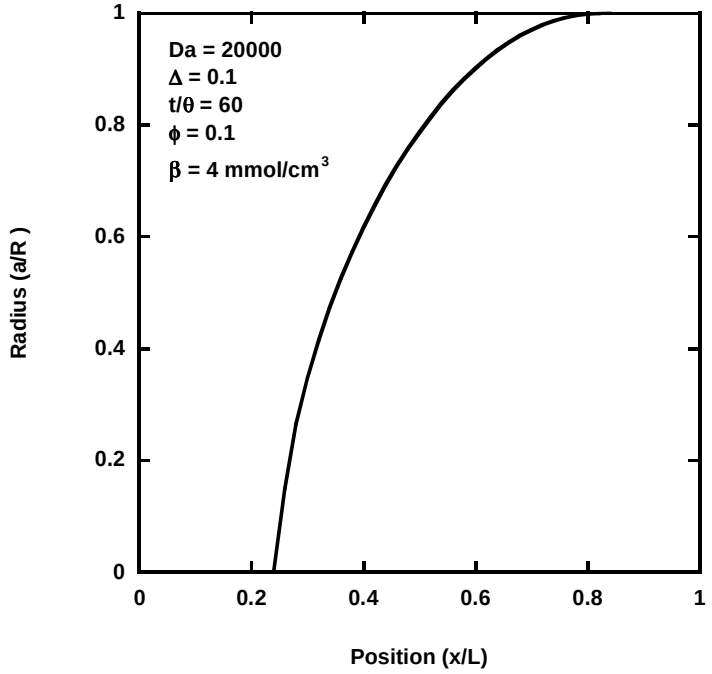

Fig. 3-30: Example of the OSP particle radius profile inside the membrane.

The non-dimensional equations (3.41) and (3.44) were solved numerically using an explicit finite difference method. The equations were discretized using a three point central difference for the spatial derivatives and two point forward difference for the time derivatives. For this problem, the early transient as well as steady state behavior are of interest. The numerical solution utilized variable time steps to capture the behavior over the entire time span while keeping computational times within practical limits. While the numerical solution was developed in MatLab for convenient matrix manipulation, it did not rely on any specialized solvers. When there are no reactive particles in the matrix, the solution should reduce to the classical transient diffusion in a membrane film; the numerical results for the case with no particles was found to be in excellent agreement with the analytical solution given by Crank [20].

The solution of equations (3.41) and (3.44) provides space and time profiles for the dimensionless oxygen concentration, $\tilde{C}(\tilde{x},\tilde{t})$ (Fig. 3-29) and the dimensionless radius of the unreacted core of the OSP particles, $\tilde{a}(\tilde{x},\tilde{t})$ (Fig. 3-30).

For barrier applications, it is important to know the time evolution of the oxygen flux and the cumulative amount of permeate, Q, exiting the downstream surface of the barrier film. Both quantities can be derived from the concentration profile. The flux is given by

$$\left(Flux\right)_t \equiv N\left(x=L,t\right) = -D_m \left.\frac{dC}{dx}\right|_{x=L} = -D_m \frac{C_m(0)}{L}\left.\frac{d\tilde{C}}{d\tilde{x}}\right|_{\tilde{x}=1} \tag{3.46}$$

$$\tilde{N}\Big|_{\tilde{x}=1} = \frac{\left(Flux\right)_t}{\left(Flux\right)_{SS}} = -\left.\frac{d\tilde{C}}{d\tilde{x}}\right|_{\tilde{x}=1} \tag{3.47}$$

where $D_m C_m(0)/L$ is the flux at steady state. The cumulative amount of permeate is given by

$$Q_t = \int_0^t N\Big|_{x=L} dt = \left(Flux\right)_{SS} \frac{L^2}{D_m}\int_0^{\tilde{t}} -\left.\frac{d\tilde{C}}{d\tilde{x}}\right|_{\tilde{x}=1} d\tilde{t} = \left(Flux\right)_{SS} 6\theta_0 \int_0^{\tilde{t}} -\tilde{N}\Big|_{\tilde{x}=1} d\tilde{t} \tag{3.48}$$

$$\frac{Q_t}{\left(Flux\right)_{SS}\theta_0} = 6\int_0^{\tilde{t}} -\left.\frac{d\tilde{C}}{d\tilde{x}}\right|_{\tilde{x}=1} d\tilde{t} = 6\int_0^{\tilde{t}} -\tilde{N}\Big|_{\tilde{x}=1} d\tilde{t} \tag{3.49}$$

where $\theta_0 = L^2 / 6D_m$ is the diffusion time lag for the matrix without any OSP. From the dimensionless equations we see that $\tilde{C}$ is a function of $\tilde{x}$ and $\tilde{t}$ plus the dimensionless parameters ϕ, $C_m(0)/\beta$, Δ, ε, H and (Da). Consequently, $\frac{(Flux)_t}{(Flux)_{SS}}$ and $\frac{Q_t}{(Flux)_{SS}\,\theta_0}$ are functions of $\tilde{t}$ and the same dimensionless parameters.

The dimensionless flux presented in the results section was obtained numerically from equation (3.47) using the five-point backward difference at $\tilde{x} = 1$. The dimensionless oxygen permeate was obtained numerically from equation (3.49) using the trapezoidal rule of integration. Note that the dimensionless time used in the derivation is defined as $\tilde{t} = t/\left(L^2 / D_m\right)$; however, for comparison with diffusion time scales, all graphs presented in the result section use $t/\theta_o = 6\tilde{t}$.

Results

The mathematical model developed for the blend films contains numerous parameters that are listed in Table 3-4 and must be specified to make the model predictive.

The thickness, L, of typical barrier film would generally be in the range of 50 to 500 μm. One can expect that polymer particles dispersed in a polymer matrix prepared by melt compounding and extrusion would have diameters in the range of 1 to 10 μm [25]. The volume fraction of these particles in the blend might be expected to be within the range of 0.05 to 0.20.

A typical matrix polymer might be poly(ethyleneterepthalate), PET, which is used extensively for conventional barrier applications. Literatures values of S_m and D_m [26] are shown in Table 3-4. Values for polystyrene [27], which is not such a good barrier material, are also included in Table 3-4. At the moment there are no reported values of S_p and D_p for butadiene-based polymer (our Oxygen Scavenging Polymer) in the fully oxidized state, and all the following calculations were based on the

evaluations made on the experimental data collected using the single film model illustrated in the previous section 3.2.1. The parameter β characterizes the ultimate oxygen scavenging capacity of the butadiene-based polymer and it has been found experimentally to be in the range of 8 to 31% by weight.

Parameter	Estimated Range	Base Case for Calculations	Ref
L	50 to 500 μm	250 μm	
R	0.5 to 5 μm	2.5 μm	
ϕ	0.05 to 0.20	0.1	
S_m	0.098 cm^3(STP)/cm^3 atm for PET 0.19 cm^3(STP)/cm^3 atm for PS	0.098 cm^3(STP)/cm^3 atm	[26] [27]
D_m	5.6 x 10^{-9} cm^2/sec for PET 1.0x 10^{-7} cm^2/sec for PS	5.6 x 10^{-9} cm^2/sec	[26] [27]
S_p	measurements needed, probably ~ S_m	0.098 cm^3(STP)/cm^3 atm	
D_p	estimated to be ~(1 to 6) x 10^{-9} cm^2/sec	2 x 10^{-9} cm^2/sec	
k	estimated to be 10^{-5} to 10^{-3} cm/sec	8 x 10^{-5} cm/sec	
β	2.5 to 10 mmol O_2/cm^3 OSP	250 cm^3 OSP/mol O_2	
$H = \frac{S_m}{S_p}$	~1	1	
$\varepsilon = \frac{R}{L}$	10^{-3} to 50 x 10^{-3}	10^{-2}	
$\Delta = \frac{D_p}{D_m}$	10^{-2} to 100	2/5.6 for PET	
$(Da) = \frac{kR}{D_p}$	0.1 to 500	10	

Table 3-4: Range of model parameters of interest.

The physical parameters described above were used to estimate the range of values the various dimensionless group in the model might be expected to have. Table 3-4 also lists the "base case" set of parameters that will be used to illustrate the model

predictions; this case considers PET as the matrix and uses mid-range values of the geometrical parameters.

The diffusion time lag for a PET film with a thickness of 250 μm without scavenging particles would be $\theta_0 = \frac{L^2}{6D_m} \sim 5.2$ hours. For polystyrene, θ_0 at this thickness would be only 0.3 hours.

It should be noted that in this model, the physical effects of the particles on the oxygen diffusion process has been ignored. In the extreme case, the particles might be considered impermeable in which case Maxwell's equation [28] would predict the following relationship between the steady-state permeability of the blend, P_{blend}, to that of the matrix, P_m

$$\frac{P_{blend}}{P_m} = \frac{1-\phi}{1-\phi/2} \tag{3.50}$$

which for $\phi = 0.2$ amounts to about an 11% reduction for the blend. This is of no consequence for the current considerations.

The model involves a considerable parameter space so the strategy is to use the "base case" values and then systematically explore the trends produced by varying each parameter individually within the "estimated range" shown in Table 3-4.

Fig. 3-31 explores the effect of varying the loading of oxygen scavenging polymer in a matrix of PET; in Fig. 3-31(a) the results in terms of the dimensionless cumulative amount of oxygen exiting the downstream surface of the film versus dimensionless time (defined here as t/θ_0) for several values of ϕ all plotted on arithmetic coordinates. After an initial transient period, a linear asymptote is approached which can be extrapolated to the time axis to define the time lag θ with scavenging particles. Note that scavenging extends the time lag by several thousand-fold. However, such plots do not give a full picture of what is happening for time less than θ; as explained earlier, the "leakage" through the film for $t < \theta$ is of great interest. To see this, it is useful to plot the oxygen flux exiting the film normalized by the steady state value on a logarithmic scale versus time, also on dimensionless logarithmic scale, as shown in

Fig. 3-31(b). In this case, the fluxes for times $t < \theta$ area t least 10^{-4} times smaller that the steady state values. However as seen later, this may not always be the case.

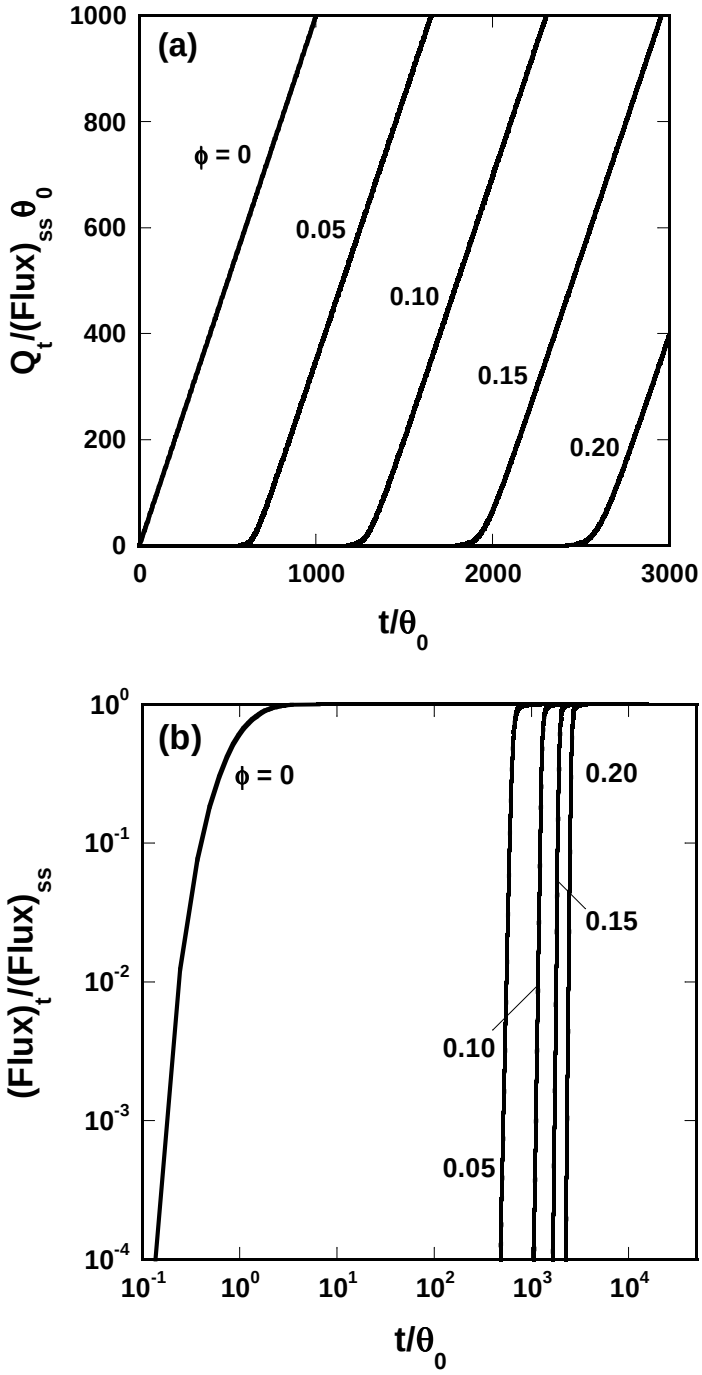

Fig. 3-31: Predicted transient permeation behavior for a blend film containing various volume fractions of oxygen scavenging polymer shown as (a) cumulative amount of oxygen and (b) flux of oxygen exiting the downstream film surface. All parameters set at base case values except for ϕ as noted.

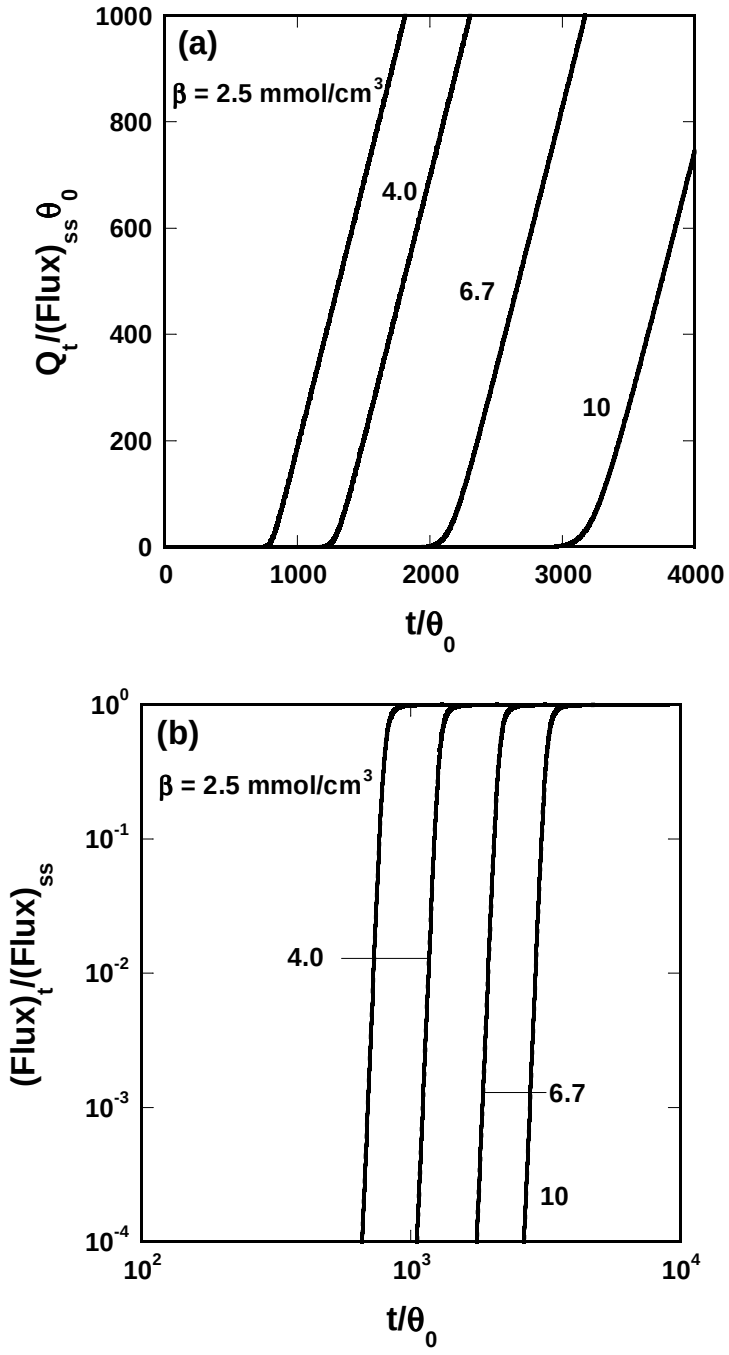

Fig. 3-32: Predicted transient permeation behavior for a blend film containing oxygen scavenging polymer with various oxygen reaction capacity shown as (a) cumulative amount of oxygen and (b) flux of oxygen exiting the downstream film surface. All parameters set at base case values except for β as noted; β is given in unit of millimoles O_2/cm^3 OSP.

Fig. 3-32 shows analogous plots as in Fig. 3-31 where β is varied rather than ϕ. Increasing the capacity of the oxygen scavenging polymer to take up oxygen for a fixed loading $\phi = 0.10$ by increasing β has somewhat similar effects as increasing ϕ. Interestingly, the asymptotic solution illustrated in Fig. 3-32 and Fig. 3-33, and consequently θ, are independent of the kinetics of the scavenging reactions and all the parameters that affect the rate of reaction. Thus θ / θ_0 depends only on the capacity to absorb oxygen, ϕ and β, and the solubility of oxygen in the polymer matrix or $C_m(0)$. The method of Frisch [29] can be used to develop the following analytical expression for θ / θ_0:

$$\frac{\theta}{\theta_0} = 1 + \frac{3\beta}{C_m(0)} \tag{3.51}$$

This equation can be derived from the combination of equation (3.41) for concentration and (3.44) for radius:

$$\frac{\partial \tilde{C}}{\partial \tilde{t}} - \frac{3\phi\beta}{C_m(0)} \tilde{a}^2 \frac{d\tilde{a}}{d\tilde{t}} = \frac{\partial^2 \tilde{C}}{\partial \tilde{x}^2} \tag{3.52}$$

Integrating equation (3.52) from an arbitrary position along the film, $\tilde{x}$, to 1 gives

$$\int_{\tilde{x}}^{1} \left[\frac{\partial \tilde{C}}{\partial \tilde{t}} - \frac{\phi\beta}{C_m(0)} \frac{\partial \tilde{a}^3}{\partial \tilde{t}} \right] dy = \left. \frac{\partial \tilde{C}}{\partial \tilde{x}} \right|_1 - \frac{\partial \tilde{C}}{\partial \tilde{x}} \tag{3.53}$$

Integrating again in space, now from 0 to 1, gives

$$\int_0^1 \int_{\tilde{x}}^{1} \left[\frac{\partial \tilde{C}}{\partial \tilde{t}} - \frac{\phi\beta}{C_m(0)} \frac{\partial \tilde{a}^3}{\partial \tilde{t}} \right] dy d\tilde{x} = \left. \frac{\partial \tilde{C}}{\partial \tilde{x}} \right|_1 \int_0^1 d\tilde{x} - \int_0^1 \frac{\partial \tilde{C}}{\partial \tilde{x}} d\tilde{x} \tag{3.54}$$

The double integral in the left hand side can be simplified to a single integral, by reversal of the integration order:

$$\int_0^1 \tilde{x} \left[\frac{\partial \tilde{C}}{\partial \tilde{t}} - \frac{\phi\beta}{C_m(0)} \frac{\partial \tilde{a}^3}{\partial \tilde{t}} \right] d\tilde{x} = \left. \frac{\partial \tilde{C}}{\partial \tilde{x}} \right|_1 - \tilde{C}(1,\tilde{t}) + \tilde{C}(0,\tilde{t}) = \left. \frac{\partial \tilde{C}}{\partial \tilde{x}} \right|_1 + 1 \tag{3.55}$$

Integrating equation (3.55) over time results in the following:

$$\int_0^{\tilde{t}}\int_0^1 \tilde{x}\left[\frac{\partial \tilde{C}}{\partial \tilde{t}} - \frac{\phi\beta}{C_m(0)}\frac{\partial \tilde{a}^3}{\partial \tilde{t}}\right]d\tilde{x}d\tilde{t} = \int_0^{\tilde{t}}\left.\frac{\partial \tilde{C}}{\partial \tilde{x}}\right|_1 d\tilde{t} + \int_0^{\tilde{t}} d\tilde{t} \qquad (3.56)$$

The time lag is determined at steady state, therefore each term has to be evaluated as time goes to infinity. At steady state the concentration profile becomes linear and the radius, a, of the core of every oxidized particle approaches 0, except at the downstream boundary. Using the cumulative oxygen permeate defined in (3.49) and evaluating each term, equation (3.56) becomes

$$\int_0^1 \tilde{x}(1-\tilde{x})d\tilde{x} + \frac{\phi\beta}{C_m(0)}\int_0^1 \tilde{x}d\tilde{x} = -\frac{Q_{t,SS}}{6\left(Flux\right)_{SS} C_m(0)} + \tilde{t} \qquad (3.57)$$

$$\frac{1}{6} + \frac{1}{2}\frac{\phi\beta}{C_m(0)} = -\frac{Q_{t,SS}}{6\left(Flux\right)_{SS} C_m(0)} + \tilde{t} \qquad (3.58)$$

The time lag is determined by finding the point where the steady-state asymptote of the cumulative permeate crosses the time axis, i.e., by setting $Q_{t,SS} = 0$ in equation (3.58), and in this way expression (3.51) is obtained.

Fig. 3-33 shows how the time lag relative to the case of no scavenging depends on ϕ and β for PET (Fig. 3-33(a)) and PS (Fig. 3-33(b)) matrices calculated by numerical solution of the model described above; these values of θ/θ_0 are in excellent agreement with those calculated by (3.51). These plots are linear and could be collapsed into master plots for all matrix polymers using the dimensionless ratio $C_m(0)/\beta$ rather than β as parameter, as predicted by equation (3.51). Note that owing to the lower solubility of oxygen in PET than PS, the extension of the time lag caused by scavenging is greater for PET than PS by almost a factor of two.

What happens during the times less than θ can be critically dependent on factors affecting the rate of oxygen consumption. The responses to the variation of the reaction rate parameter k are shown in Fig. 3-34; the parameter is varied in a range of values much lower than what experiments suggest would be reasonable. For this case, $\theta/\theta_0 \sim 1250$ and all the plots of the cumulative amount of oxygen exiting the film

downstream surface versus time would eventually approach a single asymptote, except of course for the case of no scavenging ($k = 0$).

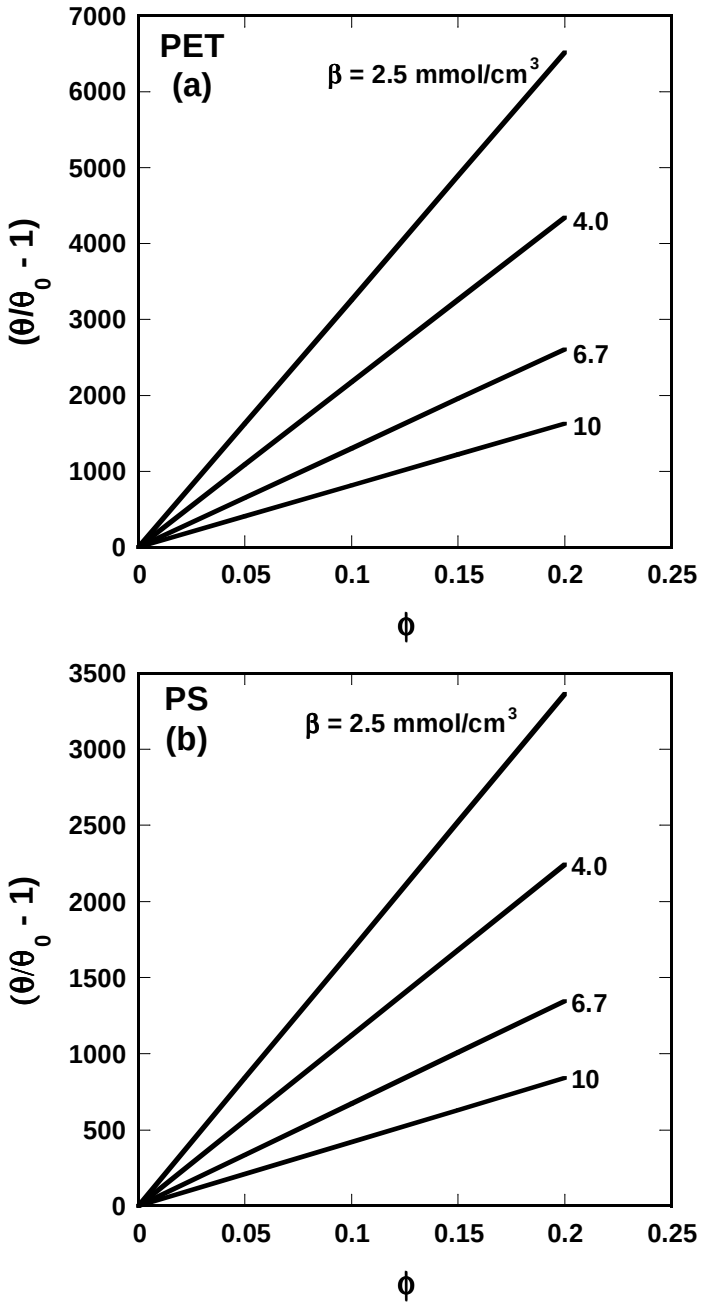

Fig. 3-33: Predicted extension of the transient permeation time lag, θ, caused by scavenging as a function of ϕ and β for (a) PET and (b) PS as the matrix polymer. All parameters set at base case values except as shown.

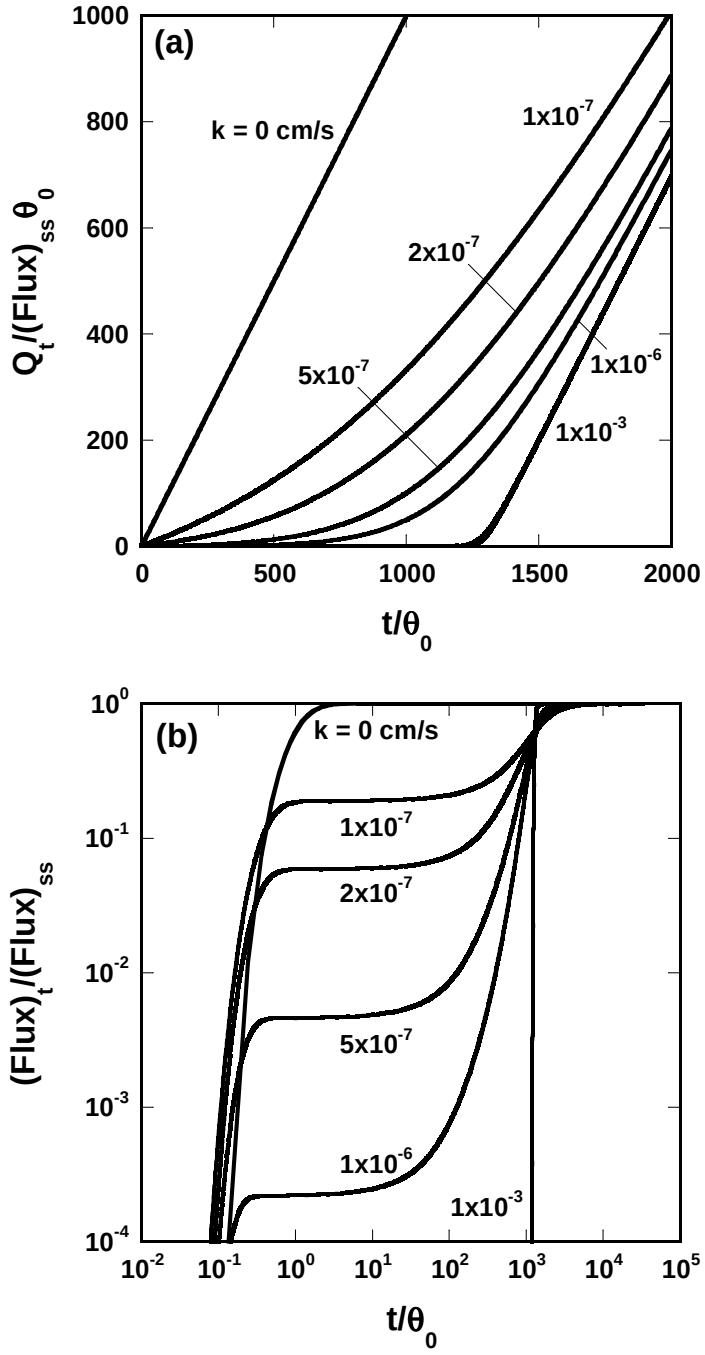

Fig. 3-34: Predicted transient permeation behavior for a blend film for different values of the oxygen scavenging rate parameter shown as (a) cumulative amount of oxygen and (b) flux of oxygen exiting the downstream film surface. All parameters set at base case values except for *k* as noted.

Clearly the approach to this asymptote depends strongly on k. This "leakage" is better seen by examining the flux versus time using logarithmic scales. Such flux plots (Fig.

3-34(b)) show two rapid rises; the first occurs at times of the order of θ_0 and the second at times of order of θ with a plateau region between these limits. The value of the flux relative to the steady-state case is lower the larger the value of k, that means the faster is the scavenging reaction. Note that these plateaus are only seen for values of k that are at the least an order of magnitude less than the expected range.

Fig. 3-35 shows for the base case, on a more expanded time scale near $t \sim \theta$ and beyond, how the size of oxygen scavenging polymer particles, R, affects the flux of oxygen exiting the film. For a given time, the flux increases as the particles become larger owing to the coupling of mass transfer within the particle with the reaction. Clearly, there is some advantage to having the OSP finely dispersed in the matrix polymer.

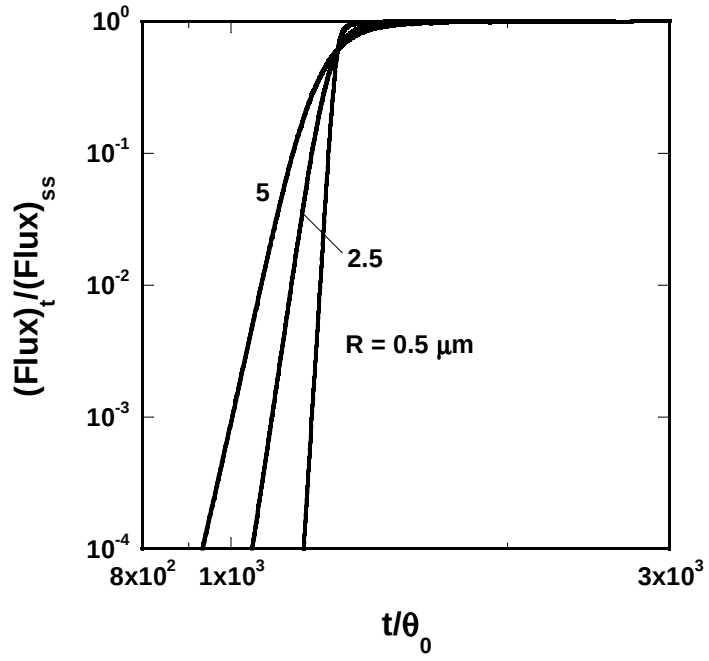

Fig. 3-35: Predicted effect of oxygen scavenging polymer particle radius on the flux of oxygen exiting the blend film. All parameters set at base case values except *R* as noted.

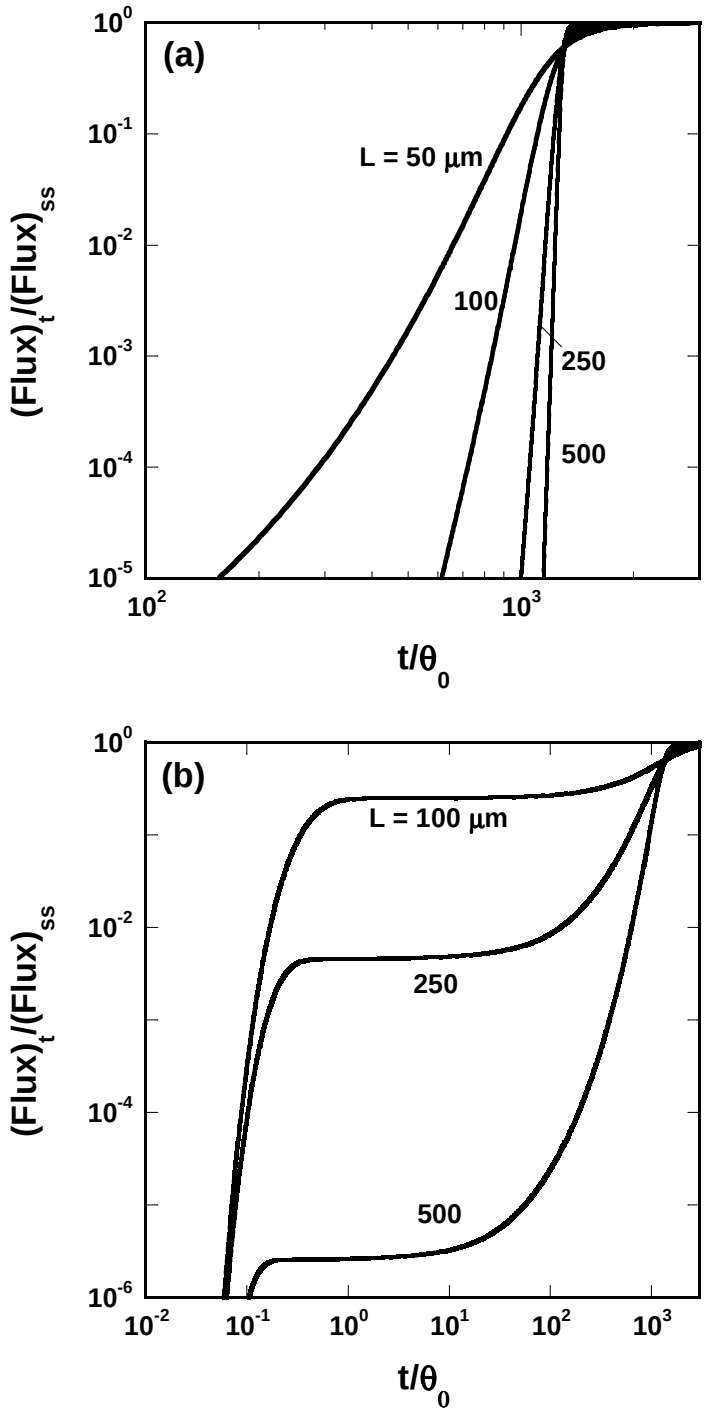

Fig. 3-36: Predicted effect of blend film thickness on oxygen flux exiting the downstream surface for (a) $k=8x10^{-5}$ cm/sec and (b) $k=5x10^{-7}$ cm/sec. All other parameters set at base case values except *L* as noted.

The variation of the overall membrane thickness, L, affects the dimensionless flux at a given dimensionless time as shown in Fig. 3-36(a). Interestingly, the dimensionless flux becomes larger as the film becomes thinner; the time scale for diffusion is proportional to L^2 but the time scale for reaction does not depend on L and thus, for thinner film there is less time for the scavenging reaction to occur before oxygen breakthrough. However, in interpreting these dimensionless plots it is important to remember that $(Flux)_{SS} \sim L^{-1}$ and $\theta_0 \sim L^2$. As the value of k becomes lower the extent of "leakage" in the time range $\theta_0 < t < \theta$ relative to $(Flux)_{SS}$ becomes more significant and strongly dependent on L as illustrated in Fig. 3-36(b) for $k = 5\times10^{-7}$ cm/sec for various values of L with all other parameters corresponding to the base case. The effect on the absolute flux leakage is even greater since $(Flux)_{SS} \sim L^{-1}$.

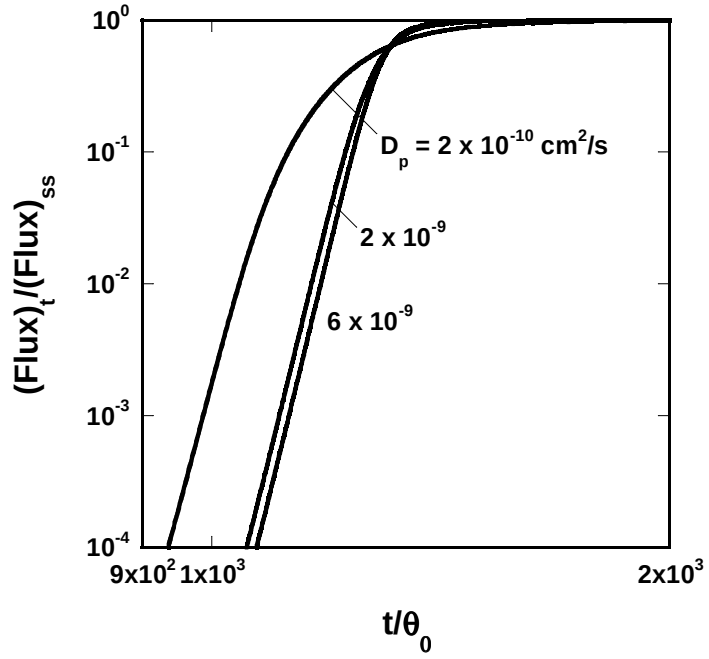

Fig. 3-37: Predicted effect of diffusion coefficient in the oxidized layer of the oxygen scavenging particle on the oxygen flux exiting the downstream surface of the blend film. All parameters set at base case values except for D_p as noted.

The effect of diffusion coefficient within the oxidized layer of the butadiene containing particles, D_p, over the expected range values (2 to 6) x 10^{-9} cm^2/sec turns out to be very small as illustrated in Fig. 3-37 where the dimensionless flux is plotted versus an

expanded time scale in the vicinity of θ. Reducing the values of D_p by an order of magnitude to 2 x 10^{-10} cm^2/sec produce a more noticeable effect but overall, D_p is not a very influential parameter in the barrier performance of blend films as represented by this model.

As a final issue, the effect of varying the matrix polymer is explored by comparing the performance of membranes based on PS versus PET as the matrix; all the parameters are kept a the base case values except for changing S_m and D_m to the value of PS. Because of the higher oxygen solubility in PS, the dimensionless time lag θ / θ_0 is smaller for PS than for PET (Fig. 3-38(a)); because of the higher D_m of PS than PET, the value of θ_0 is about 18 times smaller for PS. Considering the effect of both S_m and D_m, the absolute value of θ for PET is about 37 times that of PS. Furthermore, the slope of the dimensionless flux-time plots for PET is much steeper than for PS in the region of θ (Fig. 3-38 (b)). PS is prone to show greater "leakage" permeation in the region $t < \theta$ than PET.

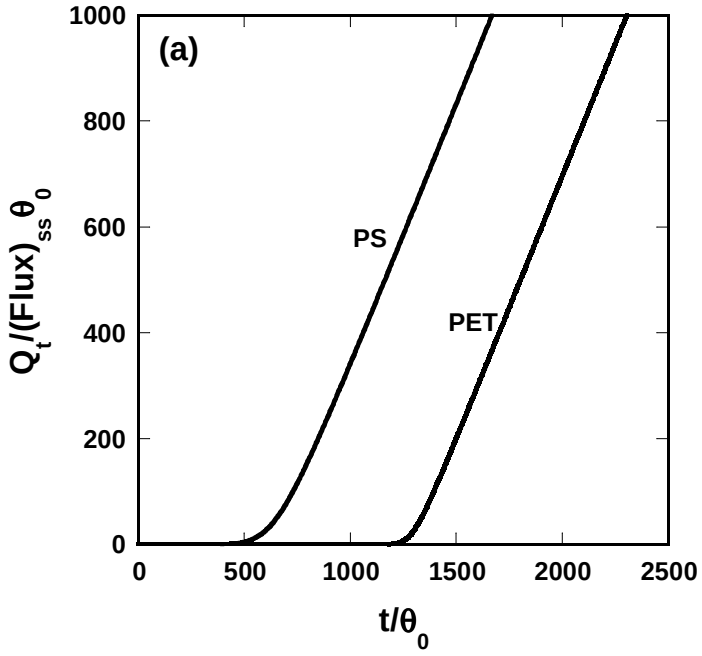

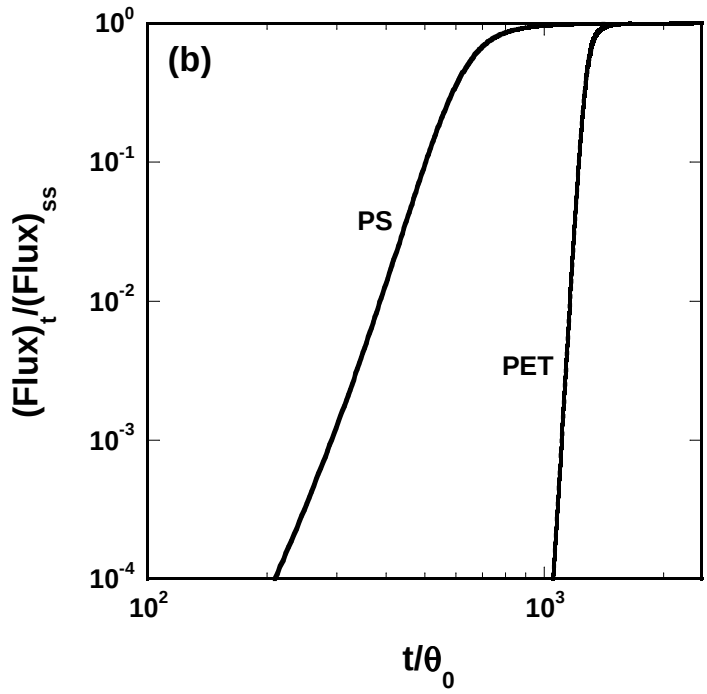

Fig. 3-1: Comparison of predicted transient permeation behavior for PET versus PS as the matrix polymer shown as (a) cumulative amount of oxygen and (b) flux of oxygen exiting the downstream surface of blend film. All parameters set at base case values except as needed for Polystyrene.

The effects illustrated quantitatively above by actual numerical solution of the model equations can be understood qualitatively, within certain limitations, by examining the scavenging terms in the model, the last term in equation (3.41) and equation (3.44). As seen earlier, θ/θ_0 is a function of ϕ and $C_m(0)/\beta$ only, and they affect the outcome in opposite directions. Increasing $C_m(0)/\beta$, which appears only in equation (3.44) accelerates the rate of change of the shrinking core radius, a, and results in a decrease of θ/θ_0. Conversely, increasing ϕ, which appears only in equation (3.41), accelerates the rate of change of the oxygen concentration, $\tilde{C}$, and results in an increase of θ/θ_0. The constant factor

$$\frac{(Da)\Delta}{\varepsilon^2 H} = \frac{kR}{D_p}\frac{D_p}{D_m}\frac{L^2}{R^2}\frac{1}{H} = \frac{kL^2}{RD_m H} = (Da)_{eff} \tag{3.59}$$

where $(Da)_{eff}$ is an effective Damköhler number, comparing the time scale of diffusion in the matrix and the time scale of the reaction in the OSP, appears in both equations (3.41) and (3.44) and plays a dominant role in the extent of leakage flux prior to reaching the asymptotic steady-state flux. However the first defined Damköhler number, (Da), appears in the variable term in braces, and plays a more limited role since it is damped by the $(\tilde{a}-\tilde{a}^2)$ term. In general, the extent of leakage flux prior to reaching the asymptotic steady-state flux can be reduced by making choices (materials, formulation and geometry) that maximize the term $\phi(Da)_{eff}$.

Conclusions

The interest in oxygen scavenging system is constantly increasing due the ability of these systems to improve the barrier properties of common polymers that, for other characteristics, are desirable materials for certain applications. The final goal of obtaining a membrane almost impermeable to oxygen leads to experimental times out of reach. Hence, this study involved both experimental and modeling efforts and it explored the performance of SBS block copolymer with oxygen. All the variables that affect the reaction were taken into account to discover their influence in the mass uptake of the film and therefore have information on the oxidation reaction. In order to describe the experimental data, a simple model was developed considering a single first order reaction that is faster than the diffusion process in the oxidized material. The application of this single film model to the data allows the determination of the capacity of the oxygen scavenging polymer that depends on the catalyst concentration in the membrane: furthermore the values for the kinetic constant and for the diffusion coefficient can be calculated through a fitting procedure that has to be optimized. The accurate measurement of the diffusion coefficient in the oxidized materials and the collection of more precise details on the reaction mechanism can lead to a pure predictive use of the model that has not been completely tested up to date. In the end, a model for predicting the oxygen barrier behavior of a more complex situation was

presented: a blend of OSP in a common packaging material was considered with particles capable of reactions with oxygen embedded in a non-reactive matrix. This geometry represents one of the possible solutions that can be developed to use the OSP in the packaging industry. Some characteristic of the oxygen scavengers (like poor mechanical and optical properties and the presence of a toxic catalyst) inhibit their use in pure form and the final goal is to find of the optimal way to incorporate them in the packaging in order to obtain the best performance in consuming oxygen. It is assumed that the oxygen scavenging by the particles can be described by a "shrinking core" model while the diffusion of oxygen in the matrix can be approximated as a function only of the coordinate axis in the thickness direction and of time. The model equations have been solved numerically for the cases where the matrix polymer is either poly(ethylene terephthalate) or polystyrene. Scavenging extends the time lag, θ, for transient permeation by a factor that depends only on the loading of the oxygen scavenging polymer and its capacity to consume oxygen relative to the capacity of the matrix polymer to dissolve oxygen; the time lag can easily be increased by factors of thousands. However, for demanding applications, the flux of oxygen exiting the downstream surface of the film on time scales of the order of θ and less may be the limiting criteria for the utility of this technology. This model was used to estimate this leakage flux for $t < \theta$, which depends on the factors that affect the rate of oxygen consumption relative to the rate of oxygen diffusion and can be summarized in terms of an effective Damköhler number.

Future work will focus on more detailed analysis of the kinetics of oxygen scavenging by polymers based on butadiene, experimental validation of the current model for blend films, and extension of this approach to layered polymer films.

References

1. Lape, N.K., Yang, C. and Cussler, E.L., *Flake-filled reactive membranes.* J. Membrane Sci., 2002. **209**: p. 271-282.
2. Paul, D.R., *The effect of Immobilizing Adsorption on the Diffusion Time Lag.* Journal of Polymer Science: Part A-2, 1969. **7**: p. 1811-1818.
3. Paul, D.R. and Kemp, D.R., *The Diffusion Time Lag in Polymer Membranes containing Adsorptive Fillers.* Journal of Polymer Science: Symposium, 1973. **41**: p. 79-93.
4. Paul, D.R. and Koros, W.J., *Effect of partially immobilizing sorption on permeability and the diffusion time lag.* J. Polym. Sci., 1976. **14**: p. 675-685.
5. Vermeiren, L., Devlieghere, F., van Beest, M., de Kruijf, N. and Debevere, J., *Developments in the active packaging of foods.* Trends in Food Science & Technology, 1999. **10**(3): p. 77.
6. Dainelli, D., Gontard, N., Spyropoulos, D., Zondervan-van den Beuken, E. and Tobback, P., *Active and intelligent food packaging: legal aspects and safety concerns.* Trends in Food Science & Technology, 2008. **19**(Supplement 1): p. S103.
7. Blinka, T.A., Edwards, F.B., Miranda, N.R., Speer, D.V. and Thomas, J.A., *Zeolite in packaging film*, in *US Patent*. 1998, W.R. Grace.
8. Cochran, M.A., Folland, R., Nicholas, J.W. and Robinson, E.R., *Packaging*, in *US Patent*. 1991, CMB Foodcan.
9. Katsumoto, K. and Ching, T.Y., *Multi-component oxygen scavenging composition*, in *US Patent*. 1998, Chevron Chemical Company.
10. Speer, D.V., Morgan, C.R. and Roberts, W.P., *Methods and compositions for oxygen scavenging*, in *US Patent*. 1993, W. R. Grace.
11. Speer, D.V., Roberts, W.P., Morgan, C.R. and VanPutte, A.W., *Multylayer structure for a package for scavenging oxygen*, in *US Patent*. 1996, W.R. Grace.
12. Stewart, M.E., Estep, R.N., Gamble, B.B., Clifton, M.D., Quillen, D.R., Buehrig, L.S., et al., *Blends of oxygen scavenging polyamides with polyesters wich contain zinc and cobalt*, in *US Patent*. 2006, Constar International Inc., Eastman Chemical Company.
13. Cahill, P.J. and Chen, S.Y., *Oxygen Scavenging condensation copolymners for bottles and packaging articles*, in *US Patent*. 2000, BP AMoco Corporation.

14. *http://www.constar.net/*.
15. Bauman, R.G. and Maron, S.H., *Oxidation of polybutadiene. I. Rate of oxidation.* J. Polym Sci., 1956. **22**: p. 1-12.
16. Beavan, S.W. and Philips, D., *Mechanist Studies on the Photo-Oxidation of commercial Poly(Butadiene).* European Polymer J., 1974. **10**: p. 593-603.
17. Sheldon, R.A. and Kochi, J.M., *Metal-catalyzed oxidations of organic compounds*. 1981: Academic Press: New York.
18. Li, H., Ashcraft, D.K., Freeman, B.D., Stewart, M.E., Jank, M.K. and Clark, T.R., *Non-invasive headspace measurement for characterizing oxygen-scavenging in polymers.* Polymer, 2008. **49**(21): p. 4541.
19. *http://www.oxysense.com/products_and_accessories/detail/oxysense_210t/*.
20. Crank, J., *The mathematics of diffusion*. 2nd Ed. ed. 1975, Oxford: Oxford University Press.
21. Ferrari, M.C., Carranza, S., Bonnecaze, R.T., Tung, K.K., Freeman, B.D. and Paul, D.R., *Modeling of oxygen scavenging for improved barrier behavior: Blend films.* Journal of Membrane Science, 2009. **329**: p. 183-192.
22. Coquillat, M., Verdu, J., Colin, X., Audouin, L. and Neviere, R., *Thermal oxidation of polybutadiene. Part 1: Effect of temperature, oxygen pressure and sample thickness on the thermal oxidation of hydroxyl-terminated polybutadiene.* Polymer Degradation and Stability, 2007. **92**: p. 1326-1333.
23. Coquillat, M., Verdu, J., Colin, X., Audouin, L. and Neviere, R., *Thermal oxidation of polybutadiene. Part 2: Mechanistic and kinetic schemes for additive-free non-crosslinked polybutadiene.* Polymer Degradation and Stability, 2007. **92**: p. 1334-1342.
24. Coquillat, M., Verdu, J., Colin, X., Audouin, L. and Neviere, R., *Thermal oxidation of polybutadiene. Part 3: Molar mass changes of additive-free non-crosslinked polybutadiene.* Polymer Degradation and Stability, 2007. **92**: p. 1343-1349.
25. Paul, D.R. and Bucknall, C.B., eds. *Polymer Blends*. Vol. 1, Formulation. 2000, John Wiley: New York.
26. Polyakova, A., Liu, R.Y.F., Schiraldi, D.A., Hiltner, A. and Baer, E., *Oxygen-Barrier Properties of Copolymers Based on Ethylene Terephthalate.* Journal of Polymer Science Part B: Polymer Physics, 2001. **39**: p. 1889-1899.
27. Hodge, K., Prodpran, T., Shenogina, N.B. and Nazarenko, S., *Diffusion of Oxygen and Carbon Dioxide in Thermally Crystallized Syndiotactic*

Polystyrene. Journal of Polymer Science: Part B: Polymer Physics, 2001. **39**: p. 2519-2538.

28. Maxwell, C., *Treatise on electrical and magnetism*. Vol. I, London: Oxford University Press.
29. Frisch, H.L., *The time lag in diffusion*. J. Phys. Chem, 1957. **61**: p. 93-95.

4 Water transport in short side chain PFSI

Perfluorosulphonic acid ionomeric (PFSI) membranes are capturing greater and greater attention because of their high thermal and chemical resistance, and very peculiar transport properties that make them appropriate to be used in many demanding separation fields, such as in the chloro-alkali industry, and more generally in the electrochemical field. The first perfluoroionomer, Nafion®, was developed by DuPont Company in the late 1960s as polymer electrolyte in GE fuel cell designed for NASA spacecraft mission. Such materials are composed of a polytetrafuoroethylene backbone and perfluorinated pendant side chains terminated by a sulphonate ionic group, and are thus characterized by a hydrophobic backbone with many hydrophilic ion domains attached on it. This structure is responsible for particular characteristics and many types of PFSI have been synthesized and studied for their ion transport properties. In the early 90s, it has been discovered the potentiality of such membranes as electrolytes in Proton Exchange Membrane Fuel Cells (PEMFC) (Fig. 4-1, [1]), devices that convert chemical energy to electrical energy, provided two feeds of humidified hydrogen and oxygen.

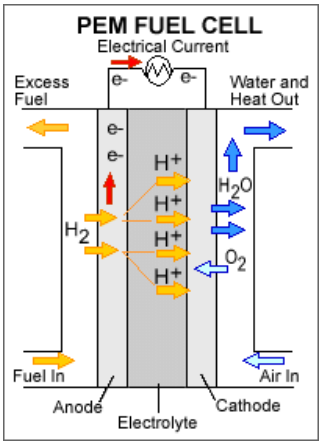

Fig. 4-1: Schematic of a PEM fuel cell

Fuels are fed continuously to the anode and an oxidant is fed continuously to the cathode. At the surface of the anode catalyst, fuels are converted into protons (H^+) and electrons (e^-). The protons travel through a PEM, which prohibits electrons crossing, to

the cathode side. The electrons (e^-) are forced to travel through an external wire and deliver part of their energy to a 'load' on their way to the cathode. At the cathode, the transferred protons and the energy depleted electron combine with oxygen to produce water. Theoretically, any substance capable of chemical oxidation that can be supplied continuously can be used as a fuel at the anode of the fuel cell. More recently, fuels alternative to hydrogen have been considered, the most attractive for low temperature processes being methanol, such as in Direct Methanol Fuel Cells (DMFC). Similarly, the oxidant can be any fluid that can be reduced at a sufficient rate. Gaseous oxygen in air is the most common choice for the oxidant because it is readily and economically available. The electrochemical reaction takes place at the surface of the electrodes that are attached to a carbon paper or carbon cloth. The carbon is conductive and porous and allows the flow of gases and electrons through it. The membrane, instead, allows protons to travel through but inhibits the electrons from passing. The protons transfer through the membrane by virtue of the electric field created across the membrane. The streams fed to the electrodes of the fuel cells must be humidified since in fuel cell operations the higher the water absorbed by the membrane, the higher the proton conductivity, as show in many studies [2,3]. Therefore, the knowledge and determination of water vapor transport parameters in the PFSI membranes is of essential importance for determining the water profile and controlling it during FC operation. Other applications of this membrane are in the separation of aqueous solutions through pervaporation [4].

Hyflon® Ion H [3,5] is a new PFSI membrane that has a shorter side chain compared to Nafion®, that is still the leading material in this field. This feature gives peculiar characteristics to the ionomer that makes it very competitive. For example the shorter chain makes the material more stable at high temperature, increasing the temperature at which the first transition (α transition) occurs from 110 to 160°C and therefore makes it suitable for high temperature fuel cell operations. Moreover the ionomer results more crystalline at the same equivalent weight (EW expressed as g_{pol}/mol SO_3H); therefore lower EW (i.e. higher ionic content) membranes can be prepared with the same cristallinity that means the same mechanical properties.

The history of the membrane can dramatically influence its properties and therefore the effect of the different preparation procedures was studied qualitatively with a Fourier Transform Infrared-Attenuated Total Reflectance (FTIR-ATR) spectrometer and then quantitatively through the water uptake of the different membranes. The swelling induced by the sorption process was also studied at various temperatures on extruded membranes. As a final issue, the water sorption isotherm at 30°C for an extruded membrane was measured with a Time Resolved FTIR-ATR spectrometer that has been already applied [6] to the study of water transport in another PFSI membrane (Nafion® 117). The FTIR-ATR technique can provide a deeper insight into the process of water diffusion and absorption into PFSI membranes, because it allows to distinguish among different classes of water molecules based on the extent of their hydrogen bond interactions with the sulphonic groups, and to monitor simultaneously the concentration of the different populations over time. The total water uptake determined with the FTIR-ATR method is in good agreement with previous data obtained on the same membrane with a manometric method. Furthermore, the water solubility isotherm was decomposed into the various contributions corresponding to the different populations of water and the sorption behavior can be modeled invoking a scheme of equilibrium acid dissociation reactions.

4.1 Experimental

4.1.1 Materials

Hyflon-Ion® H is a short-side-chain PFSI membrane that can be used as electrolyte in Proton Exchange Membranes Fuel Cells (PEMFCs). The material consists of a hydrophobic poly(tetrafluoroethylene) backbone with perfluorovinyl ether short side chains terminated by sulphonic acid ($-SO_3H$) groups and its repeating unit is reported in Fig. 4-2.

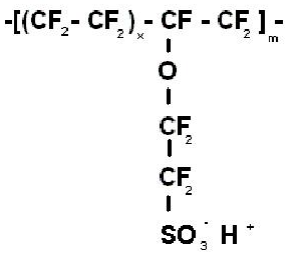

Fig. 4-2: Molecular structure of Hyflon® Ion H.

Studies have shown that, during hydration of PFSI membranes, two phases separate inside the polymer, an hydrophobic one, made by the perfluorinated chains, and an hydrophilic one, made by the sulphonic acid groups and by the water molecules (Fig 4-3) [7]. The number, size and shape of the water domains affect dramatically the water transport properties.

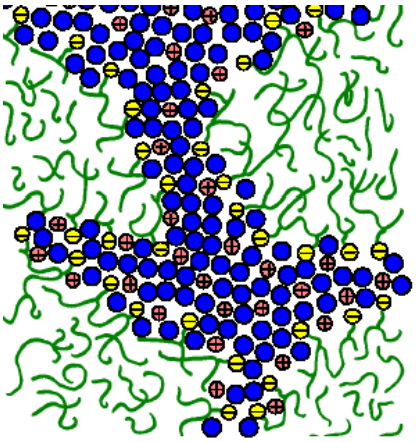

Fig. 4-3: Schematic molecular structure of hydrated Hyflon® Ion H [1].

The sulphonyl fluoride (SO_2F) form of the polymer is obtained from the free radical copolymerization of tetrafluotoethylene (TFE) and perfluorosulphonylfluorodevinyl ether (SFVE) [3]; after synthesis, the material is transformed to an ionomer converting the $-SO_2F$ groups to $–SO_3H$. This conversion is usually performed in alkaline aqueous solutions at medium temperature (80°C) and then the polymer is finally treated with a strong acid solution.

The ionomer was provided by Solvay Solexis S.p.A., in various forms: first a 150 μm thick extruded membranes with an equivalent weight of 800 g_{pol}/mol SO_3H, was used for the dilation experiments and for FTIR-ATR water sorption measurements. In order to study the effect of the formation procedure on the mass uptake, the results for extruded membranes were compared to experimental data for cast film obtained from two different solutions: one contained water, methanol, H-Galden® and dimethyl acetamide (DMA) (EW 1000 g_{pol}/mol SO_3H) while the other one was an hydroalcoholic solution with only water, n-propanol and isopropanol (EW 800 g_{pol}/mol SO_3H). The solution was cast at atmospheric condition on a quartz crystal for the QCM measurement (with resulting thickness around 1 μm) and on a glass plate for the quartz spring and pressure decay measurements. After evaporation of the solvents, the films were dried in a vacuum oven at 160°C for 1 hour, and then at 120°C overnight to completely remove any residual solvent. The extruded membranes for the dilation experiments were evacuated in the cell at 120°C for 4 hours before the test to completely remove water, while the samples for the FTIR-ATR sorption experiments were evacuated at the experimental temperature.

4.1.2 FTIR-ATR spectroscopy

FTIR-ATR spectroscopy is a powerful analytical tool recently applied to the study of mass transport in polymers; due to the microscopic insight achievable from the spectroscopic analysis, this methodology allows a deeper inspection of the sorption processes with respect to the classical techniques. In particular, the FTIR-ATR methodology is extremely convenient when multi-component diffusion needs to be monitored [8] or when the diffusion is accompanied by strong interactions between the polymer and the penetrant (e.g. hydrogen bonding or chemical reactions) [9-15].
The technique is based on the fact that a light beam traveling in a medium interacts with the medium and alters its path; the radiation can be reflected, refracted or selectively absorbed by the different chemical compounds present in the material. Spectroscopy is the science that studies the interactions between matter and light [16-

19]; in infrared spectroscopy the energy source is an infrared light beam. Absorption involves variations of the vibrational energy of the molecules that form matter, since every chemical bond in a molecule vibrates around an equilibrium state with a fixed energy and can jump from one state to another if it has enough energy [16,20].

From a macroscopic point of view, there is a relationship between the chemical bonds present in a molecule and the wavelength of the light it can interact with. Any given functional group absorbs energy almost at the same wavenumber (the inverse of wavelength) regardless of the structure of the rest of the molecule. The spectrum of a component, that is the trace left in the light, is related to the chemical structure and practically unique. The IR spectrum can be thus used to recognize compounds in a mixture of unknown composition or to evaluate their concentration in a known solution [16,17]. With the development of modern computer and thanks to the Fast Fourier Transform (FFT) algorithm introduced by J.W.Cooley and J.W. Tukey [21], this technique became practical and the FFT is now used to process the data [22,23].

A general limitation of this powerful analysis tool is that infrared spectroscopy can detect only those elements that interact with light and absorb it; atoms or monoatomic ions that have no vibrational motions are invisible, as well as those element that do not absorb infrared light as for example N_2, O_2 and other simple symmetric molecules. Spectroscopy can fail also in the analysis of complex mixtures, since the spectra often have many overlapping bands. A specific limitations of the FTIR spectroscopy is that it is a single beam technique: the background spectrum, which measures the contribution of the instrument and of the environment, is taken at a different time than the spectrum of the sample. If something changes between the acquisition of the background and of the sample spectrum, spectral artifacts can appear as, for example, absorption bands of CO_2 or water vapor.

ATR sampling

A simple scheme of an FTIR-ATR spectrometer is shown in Fig. 4-4; the light beam arrives to an interferometer that modulates the light. An example could be the Michelson's interferometer [19] that consists in four arms: one containing the source

of light, one with a stationary mirror, another one with a moving mirror and the last open in the direction of the sample and of the detector. In the middle of the four arms there is a beam splitter that transmits half the radiation that interacts with it and reflects the other half. The light is split into two beams that are reflected by the mirrors and recombine in the beamsplitter after having traveled two different distances, and thus interferes in different ways related also to their wavelength. The light passed through the interferometer is thus modulated and its intensity is a periodic function of the optical path difference, δ, that is determined by the position of the moving mirror. The intensity of the light beam can be plotted for one scan, which is a complete translation back and forth of the moving mirror. The plot, called interferogram, is a sinusoidal wave if the light is monochromatic (with a single wavelength), but, for a normal light beam where many wavelengths are present, it has a more complex form and is a sum of sinusoidal functions, each related to a determined wavelength.

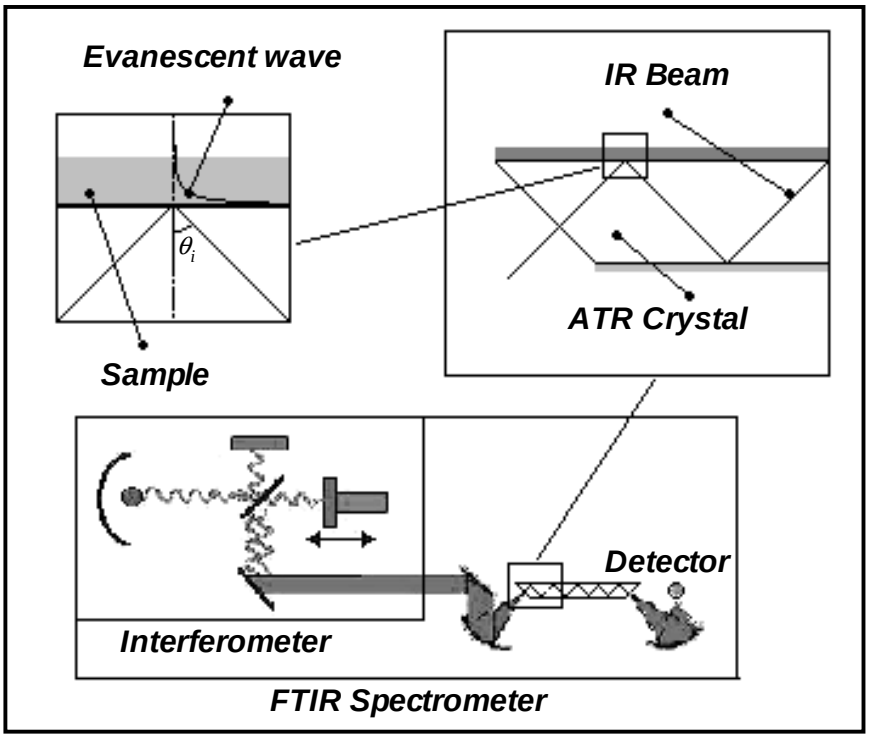

Fig. 4-4: The ATR sampling technique: the modulated light leaving the spectrometer is focused in the ATR crystal with a suitable angle to obtain the internal reflection. At each reflection the evanescent wave propagates in the sample which is in contact with the crystal and acts as the rarer medium. After multiple reflections the beam leaves the crystal and is focused on the detector to give an interferogram and then the spectrum [26].

After the interferometer, the modulated light beam reaches the sample: in normal transmission spectroscopy the spectra are calculated from the transmitted light that has physically passed through the sample; in attenuated total reflection (ATR) a different feature is exploited [24]. When total reflection occurs at the interface between two media an evanescent wave [24,25] propagates in the rarer medium (that has a higher refractive index), and can be absorbed by the components present in it. The modulated light in ATR is focused on a crystal where it remains entrapped due to the occurring of a total reflection process (Fig. 4-4). In each reflection inside the crystal an evanescent wave propagates into the optically rarer medium and is absorbed by the functional groups typical of the sample. When the beam reaches the other end of the crystal, it is allowed to leave the ATR element and is focused on the detector that registers the interferogram that is then processed by using the Fourier Transform to obtain the single functions from their sum so that the spectrum can be built.

The ATR technique can be considered a surface analysis method since the evanescent wave decays rapidly inside the specimen and only a depth of few microns of the material is effectively investigated. The good contact between the sample and the crystal is very important to obtain an effective absorption of the light from the rarer material, and it becomes particularly critical when quantitative analyses are made.

The spectrum is usually plot as the ratio between the intensity I of the beam entering the detector and the intensity I_0 of the beam incident to the sample. For quantitative analysis the absorbance A, related to the intensity through [16-19]:

$$A = -\log_{10}\left(\frac{I}{I_0}\right) \tag{4.1}$$

is often considered since it is proportional to the concentration of a given species in the sample. The Beer-Lambert law states that the absorption of electromagnetic waves is related to the quantity of absorbing material:

$$dI = \alpha I dz = -\varepsilon C I dz \tag{4.2}$$

where α is the absorption coefficient, ε the molar extinction coefficient of the functional group considered, C is the concentration of the absorbing species at the

position z and I is the beam intensity integrated along the absorption band of interest. Integrating equation (4.1) on a thickness L gives:

$$A = \int_0^L \frac{\varepsilon C}{\ln 10} dz \qquad (4.3)$$

that reduces to a linear relationship when both ε and C are constant through the sample.

It is well known from the optics principles that when a light beam propagating in a given medium strikes the interface between this one and another uniform medium, it is partially reflected from the interface and partially transmitted in the second medium. The law of reflection and the Snell law for the refraction allow to evaluate the direction of the reflected and transmitted beams in the plane of incidence. From the electromagnetic theory of light it is also possible to have information about the energy of the reflected and transmitted light and it is possible to evaluate the amplitude of the electric field (E) associated to each polarized waves forming the light beam (both reflected and transmitted) through the Fresnel laws [24,25,27,28]:

The energy is related to E:

$$I = const \cdot E^2 \qquad (4.4)$$

where I is the intensity of the light, that is the energy per unit of time and area of a given beam and the constant is related to the medium in which the wave propagates.

There is a limit for the light beam incident angle defined as critical angle ($\theta_c = \arcsin(n_i/n_t)$ with n_i and n_t refractive indexes of the two media, the one containing the incident light, and the one containing the transmitted beam respectively) beyond which the transmitted beam travels parallel to the interface and its energy vanishes and the process of the total internal reflection occurs. No energy is transmitted but the continuity of the tangential electric field at the interface implies that there should be however a transmitted wave. This electromagnetic field decays exponentially as it penetrates in the medium and, on average, does not carry any energy:

$$E = E_0 e^{-z/d_p} \qquad (4.5)$$

where E_0 is the amplitude of the electric field of the incident beam, z is the distance from the interface and d_p is the penetration depth of the evanescent wave defined as:

$$d_p = \frac{\lambda}{2\pi n_i \sqrt{\sin^2 \theta_i - (n_t / n_i)^2}} \tag{4.6}$$

Even for angles of incidence greater than θ_c, the electric field propagates across the interface between the two media and can thus be absorbed by the rarer medium. The reflection is no more total, but attenuated and the energy of the reflected beam is not equal to that of the incident ray, but shows in its spectrum the typical absorption bands of the less dense medium.

When an attenuated total reflection takes place the Fresnel laws continue to hold and are theoretically able to describe the process and to estimate the absorption occurring in the rarer medium because of the evanescent wave propagation. However an approximated approach can be used limiting the description to those cases in which only a low absorption takes place with intensity losses not exceeding 10% [24,25]. The approximation consists in treating the ATR spectra as transmission spectra in which the light beam passes through a sample of thickness *L* instead of being reflected on the surface of it. If the reflection losses are neglected, the intensity decreases exponentially so that:

$$\frac{I}{I_0} = e^{-\alpha L} \tag{4.7}$$

Therefore, an effective thickness can be defined as the thickness of a theoretical sample that should be used in a transmission experiment to obtain the same absorption. In the assumption of weak absorption and considering that the real thickness is much grater of the penetration depth, the effective thickness can be expressed as:

$$d_e = \frac{n_2}{n_1 \cos\theta_i} \int_0^\infty E^2 dz = \frac{n_2 E_0^2 d_p}{2 n_1 \cos\theta_i} \tag{4.8}$$

where E is the evanescent field given in equation (4.5) and where the values of both E_0 and d_p can be assumed equal to those of non-absorbing media.

The parameters that affect absorption in the attenuated total reflection process are the penetration depth, the refractive indexes of the two media, the angle of incidence and the electric field amplitude at the interface where the ATR takes place. It can be shown that the only key parameters to control the interaction between the evanescent wave and the sample are the refractive indexes of the two media involved in the reflection, n_1 and n_2, and the angle of incidence θ_i of the light on the reflecting surface. Since the rarer medium is the sample inspected, its refractive index cannot be varied and there are three parameters that can be practically changed with the experimental set up: n_1 and θ_i, plus the number of reflections, N, occurring inside the ATR crystal. In fact when multiple reflections experiments are considered the effective depth of penetration will be *N* times the value obtained from equation (4.8). The material of the internal reflection element determines the refractive index n_1, and can influence the angle of incidence θ_i, while the shape and dimension of it allows to fix both θ_i and the number of reflection N. For a given optical path outside the crystal in fact, θ_i depends on the relative position of the reflecting surface with respect to that in which the beam enter the crystal, as well as on the angle of incidence of light on this latter surface.
Commercial ATR cells are designed for crystals of a given shape and dimension, and also the angle of incidence is generally fixed so that the choice of a given cell allows to set all the parameters but the refractive index of the crystal. The various materials used for the crystal differs not only in the value of the refractive index but also in the range of wavenumbers in which they can be used and in the chemical properties.

Application to the study of mass transport in polymers

For the Beer-Lambert law, the absorbance of a given component is related to its concentration in the sample inspected, so that it is theoretically possible to monitor the changes of penetrant content in the polymer during a diffusion process simply by observing the time evolution of the absorbance peaks typical of the solvent, in the ATR spectra of the polymer itself. From a quantitative analysis of the progressive increasing

solvent absorbance peaks area, it is possible to evaluate both diffusion coefficient and solubility of the considered penetrant in the polymer.

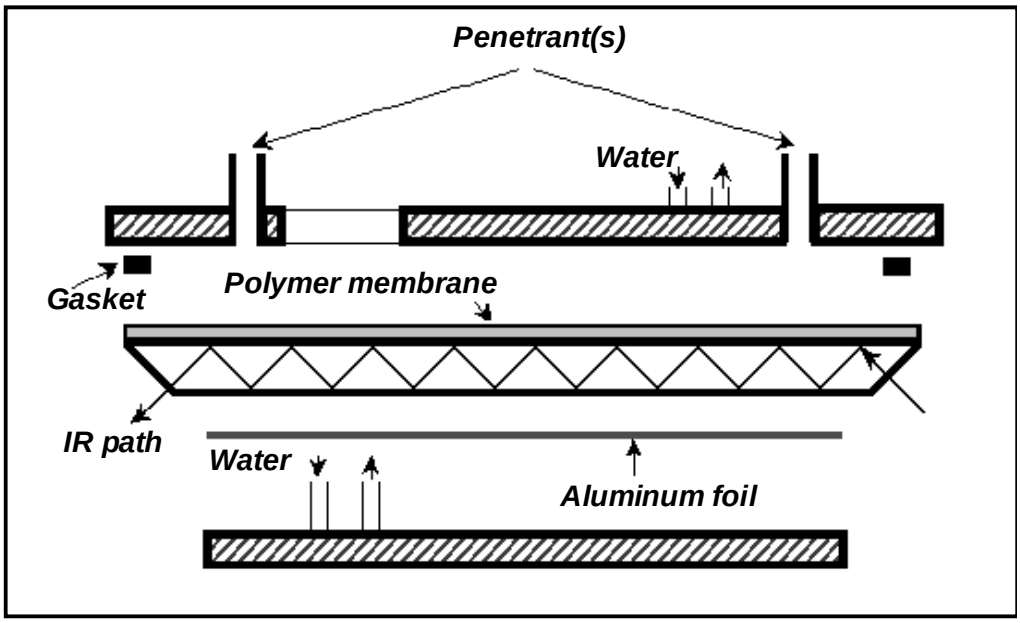

Fig. 4-5: Schematic of the ATR cell: the polymer is attached onto the ATR crystal, the penetrant enters from the ducts in the upper part of the cell and diffuses in the film. The IR beam is entrapped in the crystal so that only the diffused penetrant can be detected from the instrument [26].

A scheme of the experimental ATR cell used during the experiments is shown in Fig. 4-5; the polymer film is placed on a trapezoidal crystal while the penetrant comes from the special duct provided on the upper part of the cell. A gasket prevents every possible contact between the penetrant and the ATR crystal so that only the species that had diffused into the sample are detected from the spectrometer. The cell is also provided with a heating system that allows temperature control through the use of circulating water. To effectively use the ATR technique, the adhesion between the internal reflection element and the sample must be insured; the most common solution consists in directly casting the polymer on the ATR crystal from a solution but this technique can be used only when the polymer can be dissolved. Other methods are the hot pressing of the polymer on the crystal [29] or the use of the same penetrant to pressurize the chamber [30].

The dilation of the sample can also be detected due to the decrease of the absorption peaks typical of the polymer [14,15,30,31]. During diffusion the polymer swells to

accommodate the incoming penetrant, as a consequence the thickness of the sample increases and parts of the polymer that interacted with the evanescent wave at the beginning of the experiment cannot be detected anymore from the spectrometer when the equilibrium is attained.

To obtain a quantitative description of the penetrant concentration in the sample, the Beer-Lambert law (equation (4.2)) can be used; the integration of such equation is not trivial since both intensity and concentration are space dependent. The behavior of the intensity, that is related to the electric field, can be obtained directly from equation (4.5) describing the evanescent wave in the rarer medium, so that equation (4.4) can be rewritten as:

$$I = E_0^2 \exp\left(-\frac{2z}{d_p}\right) dz \tag{4.9}$$

The absorbance cannot be considered simply proportional to the concentration of the absorbing species but the relationship can be easily obtained if only weak absorption is assumed [24]:

$$\frac{I}{I_0} = e^{-A\ln 10} \approx \left(1 - A\ln 10\right) \tag{4.10}$$

so that

$$dI = -I_0 \ln 10 \, dA \tag{4.11}$$

Substituting equation (4.11) in equation (4.2) and using (4.9) one obtains:

$$A = \int_0^L \frac{N\varepsilon C}{\ln 10} \frac{E_0^2}{I_0} \exp\left(-\frac{2z}{d_p}\right) dz \tag{4.12}$$

where N is the number of reflections inside the ATR crystal.

To calculate the relationship between absorbance and concentration with equation (4.12) it is necessary to know the concentration profile in the film. As far as the mass transport problem is concerned, the system can be considered one-dimensional and therefore, assuming Fickian diffusion, the concentration of the diffusing component C can be described with:

$$\frac{\partial C}{\partial t} = D_{eff}\frac{\partial^2 C}{\partial z^2} \tag{4.13}$$

where D_{eff} is the effective diffusion coefficient considered constant with the concentration. In the case of the ATR cell, the boundary and initial conditions are:

$$\begin{aligned} &C = C_{eq} && z = L, \quad \forall t \\ &\frac{\partial C}{\partial z} = 0 && z = 0, \quad \forall t \\ &C = C_{eq} && 0 < z < L, \quad t = 0 \end{aligned} \tag{4.14}$$

where L is the thickness of the film C_{eq} is the concentration in the membrane when the equilibrium is attained.

The concentration profile in the film during mass transport determined through equation (4.13) can thus be substituted in equation (4.12) to obtain the relationship between absorbance and concentration profile in the case of Fickian diffusion [31]:

$$\frac{A_t - A_0}{A_{eq} - A_0} = 1 - \frac{8}{\pi d_p\left[1 - \exp\left(-2\frac{L}{d_p}\right)\right]}\sum_{n=0}^{\infty}\left[\frac{\exp(g_n)\left[f_n \exp\left(-2\frac{L}{d_p}\right) + (-1)^n\left(\frac{2}{d_p}\right)\right]}{(2n+1)\left(\frac{4}{d_p{}^2} + f_n{}^2\right)}\right] \tag{4.15}$$

where A_0 represents the initial absorbance of the peak considered and g_n and f_n are described by the following relationships:

$$\begin{aligned} g_n &= \frac{-D_{eff}(2n+1)^2\pi^2 t}{4L^2} \\ f_n &= \frac{(2n+1)\pi}{2L} \end{aligned} \tag{4.16}$$

In an ATR experiment, the refractive indexes of the polymer and of the crystal as well as the geometry of the system are given, so that the only unknown is the effective diffusion coefficient that can be estimated from the comparison between the model (4.15) and the experimental data.

Considering now the evaluation of the solubility, it is worthwhile to notice that all the data obtained in the FTIR-ATR spectroscopy are absorbances. While the kinetic analysis can be conducted directly through the use of the dimensionless variables, to obtain the solubility of a given penetrant in a polymer a calibration is required [32]. Once the relationship between C and A is known, the value of equilibrium concentrations and thus the solubility isotherm can be directly calculated from the equilibrium values of the absorbance in the FTIR-ATR experiments. For long times, when the equilibrium between polymer and penetrant is attained, the value of the concentration in the sample is no longer a function of space and equation (4.12) can be directly integrated:

$$A_{eq} = \frac{N\varepsilon C_{eq}}{\ln 10}\frac{E_0^2}{I_0}\frac{d_p}{2}\left[1-\exp\left(-\frac{2L}{d_p}\right)\right] \qquad (4.17)$$

The value of the molar extinction coefficient ε can be easily obtained with a sufficient number of equilibrium data for both absorbance and concentration in the same experimental conditions and then equation (4.12) can be integrated at any time giving the calibration curve during all the diffusion experiment. Anyway, the simple A_{eq} vs. C_{eq} plot is usually sufficient to know the equilibrium value of the solubility in any experimental condition assuming the linearity of the calibration curve due to a constant molar extinction coefficient.

When more complex phenomena are concerned and the diffusion involves multiple penetrant the equation describing the mass transport process have to be rewritten for each component and the generative terms due to the reaction have also to be considered leading to a non linear system of multiple differential equations.

The spectrometer available in the laboratory is an AVATAR spectrometer (Nicolet Instrument Corporation) with a horizontal, temperature-controlled ATR cell manufactured by Specac. Inc.; a liquid nitrogen-cooled Mercury-Cadmium-Telluride detector is used with 32 scan per sample at a resolution of 4 cm^{-1} and a multiple reflection trapezoidal zinc selenide (ZnSe) crystal with 45° beveled faces. The automatic data acquisition of time evolving spectra was possible through a software (OMNIC) that was also used to process the results.

4.2 Results and discussion

A spectrum of the Hyflon® Ion H extruded membrane is reported in Fig. 4-6 together with a spectrum of a Nafion® 117 extruded membrane of similar thickness (190 μm), both collected at room temperature and humidity, in the wavenumber interval of 820 - 1500 cm^{-1} , in which the peaks characteristic of the polymer are located.

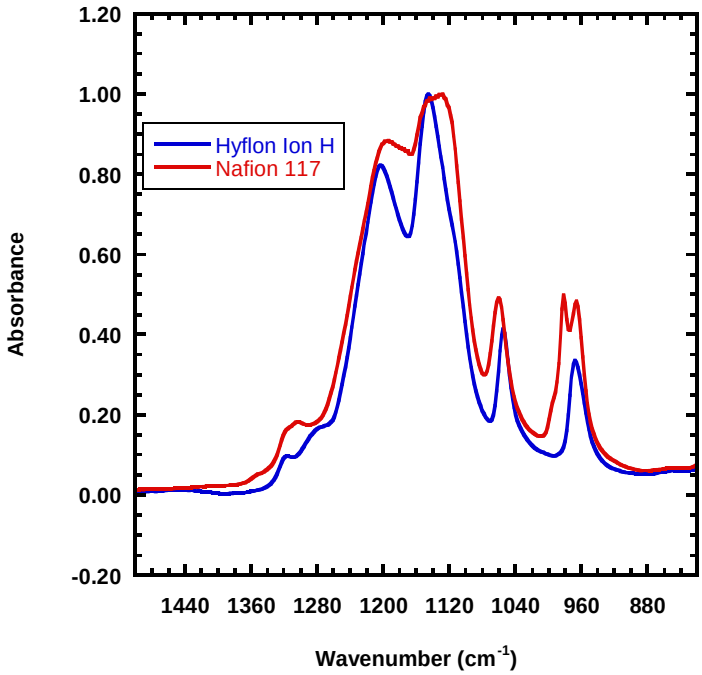

Fig. 4-6: Spectrum of Hyflon® Ion H and Nafion® 117 at 30°C, collected with a ZnSe crystal as background, membrane evacuated at sampling temperature.

The two spectra are quite similar and in both cases it is easy to recognize the characteristic and fairly intense bands at wavenumbers 1155 and 1220 cm^{-1} that are related to the stretching vibrations of CF bonds already reported in literature [33,34]. Another distinct feature of the spectra is a shoulder around 1300 cm^{-1} due to the asymmetric stretching of the SO_3^- bonds (as the band at 1060 cm^{-1}) that tends to increases with water sorption. The other distinguished band at 970 cm^{-1} is associated to the stretching modes of the C-O-C and CF bonds together.

4.2.1 Effects of solvent on the water sorption

In the case of Nafion 117, literature data [35] show that the water transport properties can be very different for cast or extruded membranes. In order to study the effect of formation conditions on the water sorption behavior of Hyflon® Ion films, the water solubility isotherms of the solution-cast films were compared to the ones relative to extruded films. All the data were collected after evacuating the membrane at the temperature of the experiment even though it is known that the membrane is completely dry only after evacuating at 120°C [36]. First a membrane cast from the solution containing H-Galden® and DMA was considered: it was observed that the amount of water absorbed is lower than that measured on the "as received" extruded film. The measurement on the cast film was first performed with a quartz crystal microbalance (QCM) [37]. The data obtained with this technique usually match well with data from other techniques after being treated with the Sauerbrey's equation [38], that relates the mass uptake Δm to the measured frequency shift ΔF and to the polymers and quartz crystal parameters:

$$\Delta F = -\frac{2nF_0^2}{A\rho_Q^{1/2}\mu_Q^{1/2}}\Delta m \qquad (4.18)$$

with n order of harmonic, F_0 base frequency of the crystal, A area of the electrode, ρ_Q and μ_Q respectively density and shear modulus of the crystal. It can be seen in Fig. 4-7 that the mass uptake measured for cast membranes with the QCM [39] is significantly lower than the one observed for extruded membranes; the measurement was also repeated with a quartz spring balance to exclude that the behavior is due to the specific experimental technique.

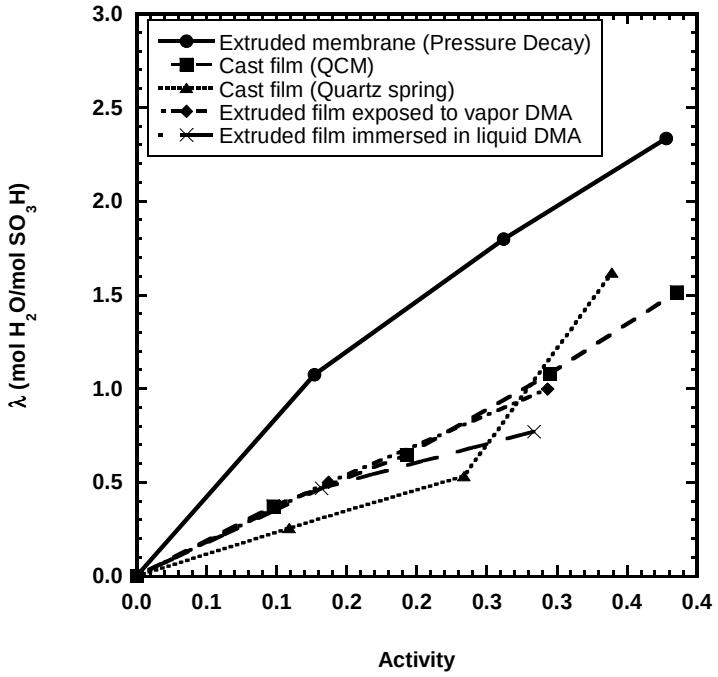

Fig. 4-7: Effects of DMA on the mass uptake at 35°C of cast and extruded membrane of Hyflon® Ion.

In order to explain the experimental results, likely due to the different solvent treatment experienced by the two samples, experiments were performed on extruded samples pretreated with DMA vapor or after immersion in DMA liquid and also these data are reported in Fig. 4-7. It is clear that the DMA affects the sorption capacity of the ionomer lowering it also in the case of extruded membrane: this could be related to a permanent modification induced on the polymer structure by the solvent. In order to check this hypothesis, the IR spectra of all the samples used in the sorption experiments were collected at room temperature. In Fig. 4-8 the spectra for the membrane cast from the solution with DMA and for the "as received" extruded membrane are compared: in the solution cast film two more peaks appear at a wavenumber of 1460 cm^{-1} and of ~1020 cm^{-1} that are clear sign of a modification of the polymer structure induced by the DMA. A spectrum of a film cast from the hydroalcoholic solution is also plotted in Fig. 4-8 to show this is indistinguishable from the extruded sample as far as the spectra are considered..

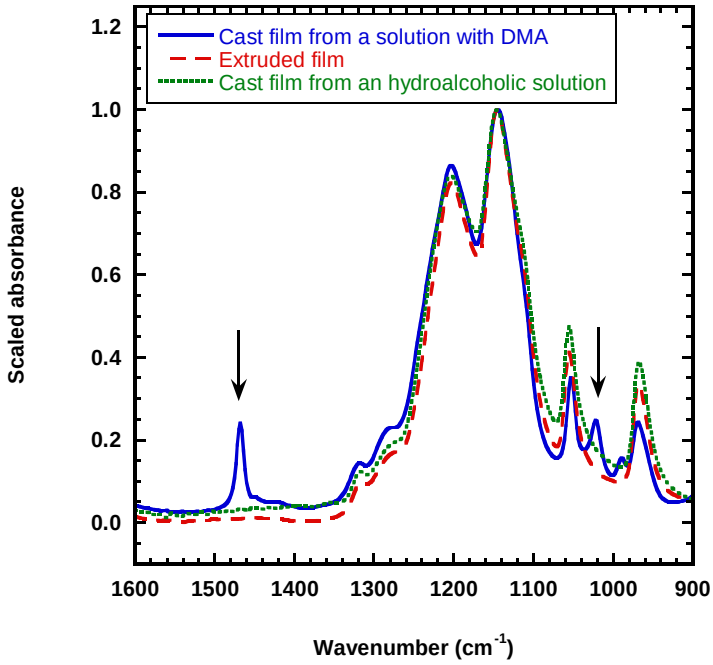

Fig. 4-8: Effects of DMA on the spectrum of Hyflon® Ion H cast membranes. Also the spectrum of an extruded membrane is reported for the sake of comparison.

4.2.2 Dilation

The swelling behavior of ionomers employed in fuel cell is really important since it can affect the overall performance of the system. In fact, an excessive dimensional variation of the membrane is not desired since it can result in the buildup of stresses during transitory hydration states (as start up or shut down).

The dilation of extruded membranes (EW 800 g_{pol}/mol SO_3H, 150 μm thick) was measured at three different temperatures (35, 95 and 120 °C) in the cell already used for the bending beam measurements (see Chapter 1), following with the micrometer the relative position of two points of the film. Before the experiments the samples where evacuated at 120°C for 4 hours to remove all the water adsorbed by the membranes due to atmospheric humidity. It is indeed well know [36] that Hyflon® Ion H (as Nafion® 117) is completely dry only after being evacuated at this temperature, while treatments at room temperature leave approximately one molecule of water bonded to every sulphonic group. The swelling was measured in both main dimensions

since the behavior was expected to be different due to the extrusion process. In Fig. 4-9 it is clear that the dilation is higher in the direction perpendicular to extrusion.

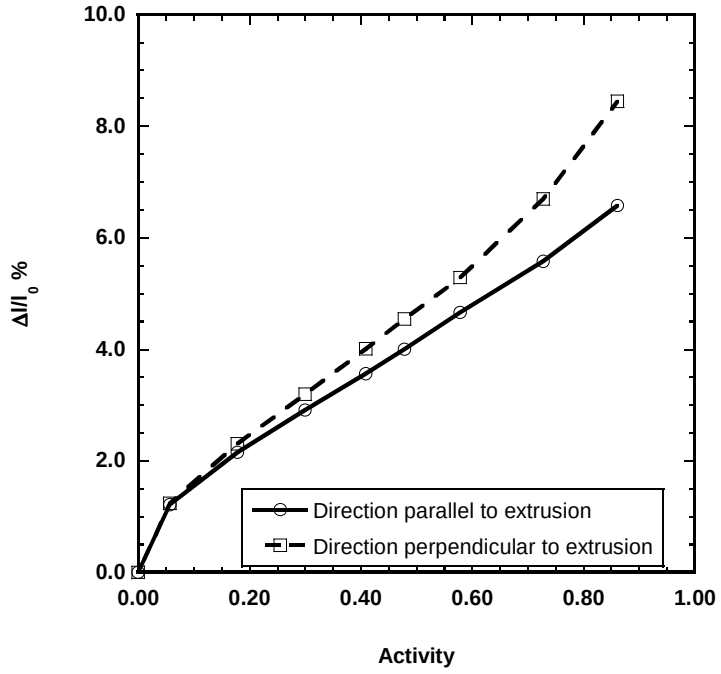

Fig. 4-9: Dilation in the two main dimensions of a Hyflon® Ion extruded film (150 μm); data collected at 35°C

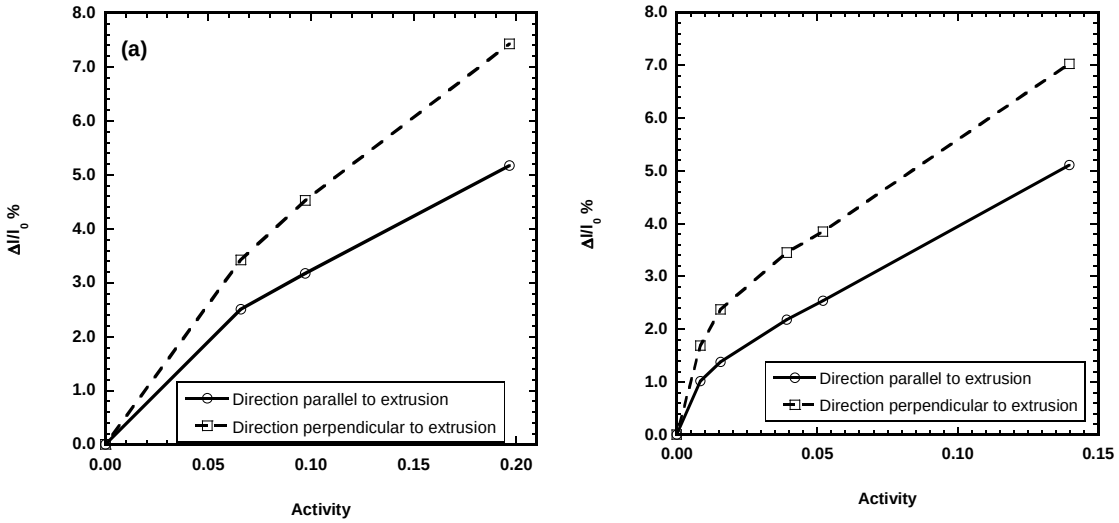

Fig. 4-10: Dilation in the two main dimensions of a Hyflon® Ion H extruded film (150 μm); data collected at 95 (a) and 120°C (b).

In Fig. 4-10 the data for other temperatures are reported; at 95 and 120°C the activity range inspected is narrower, due to condensation problems in the tubes that did not

allow to further increase the water vapor pressure in the cell. It is still evident, however, that the swelling is different in the two directions and, as expected, lower in the direction of extrusion that has already been stretched during the formation process.

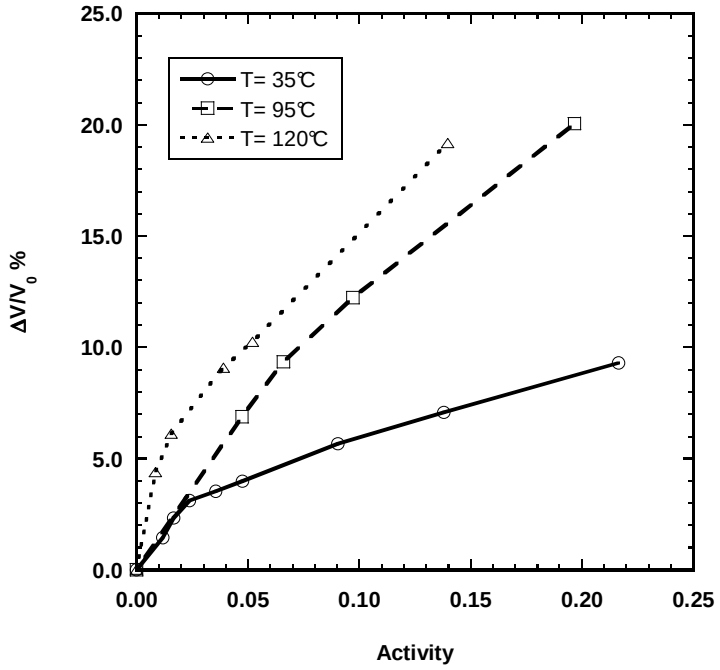

Fig. 4-11: Comparison between volumetric swelling on extruded membrane of Hyflon® Ion H at different temperature.

The volumetric dilation of the samples can also be compared (Fig. 4-11); in order to calculate the overall swelling of the membrane, the anisotropy of the film has to be considered, and assuming the dilation in the thickness direction (z) equal to the one perpendicular to extrusion, the relationship is:

$$\frac{\Delta V}{V_0} = \frac{\Delta x}{x_0} + 2\frac{\Delta y}{y_0} \qquad (4.19)$$

where y is the direction perpendicular to the extrusion one.

The increase in temperature dramatically affects the overall swelling of the membrane even at low values of water vapor activity and this has to be taken in account since the desired operation temperature for fuel cell usually is the highest possible in order to have the highest proton conductivity.

4.2.3 Water sorption with FTIR-ATR spectrometer

The FTIR-ATR spectrometer has been used not only to characterize the membrane before performing the sorption measurements in other apparatuses, but also to measure the water diffusion and sorption in situ. The experiments were carried out on extruded membranes and since the intimate contact between the crystal and the polymer is crucial in this kind of test, a different method [6] had to be used to guarantee the adhesion of the ionomer onto the crystal. Before every diffusion experiment, a background spectrum of the ATR crystal was collected. Then a wet sample of Hyflon® Ion H, precut in the hydrated condition, was placed onto the crystal and the cell was tightened. The sample was dried flowing dry air overnight, and then evacuated for 4 hours at the test temperature, 30°C. The water vapor partial pressure was then increased stepwise allowing for the attainment of the equilibrium after every increase.

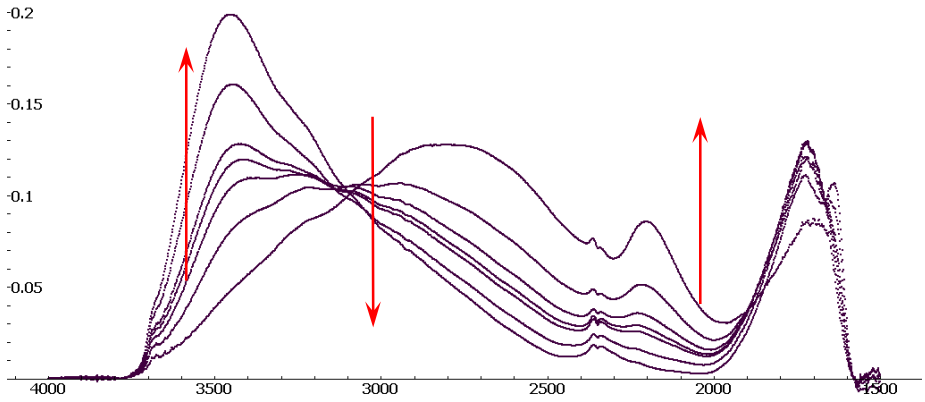

Fig. 4-12: Spectra of Hyflon® Ion H in the stretching (2400-3800 cm^{-1}) and bending (1500-2000 cm^{-1}) regions of the hydrogen bonding at increasing water content

The portion of the spectra related to water sorption is between the wavenumbers 1500 and 3800 cm^{-1} where there are the regions for the bending vibrations (1500-2000 cm^{-1}) and for stretching vibrations (2400-3800 cm^{-1}) of hydrogen bonds [12,13]. In Fig. 4-12 this region of the spectra of the polymer is reported after each differential hydration step. It can be seen that increasing the water content in the membrane, the spectrum undergoes some modifications with the increase of the bands related to the hydrogen bonds and the decrease of a large band centered around 2720 cm^{-1}: this decrease could be related to the dissociation of $-SO_3H$ in presence of water but could also be the result

of an Evans window that is a local decrease of a band in the spectrum due to the rapid increase of other bands in this case caused by water uptake [33,34].

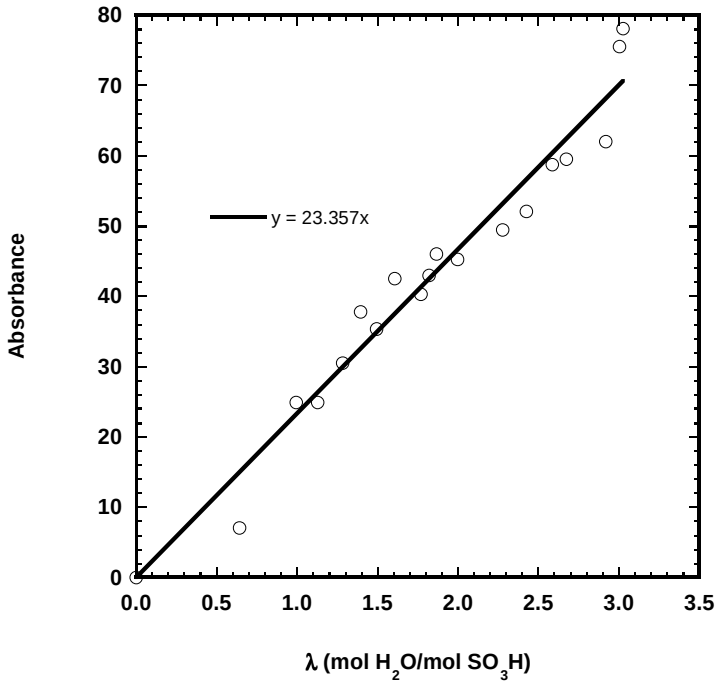

Fig. 4-13: Calibration curve between absorbance and water concentration in the polymer for the FTIR-ATR experiment

To estimate the water uptake of the membrane at equilibrium after every step, the region of the stretching vibrations of water molecules (2400-3800 cm^{-1}) was considered but the same calculations can be done on the region of bending vibrations. As already said, the data measured by the spectrometer are in terms of absorbance and a calibration curve is needed in order to obtain the value of the water concentration in the sample after each step. Two experiments on two different samples were performed and then compared. In Fig. 4-13 the calibration curve used to relate the absorbance value to the concentration for all the data is reported; it was calculated using sorption data collected on the same material in a pressure decay apparatus at 35°C. The sorption isotherms, obtained using the calibration curve, are reported in Fig. 4-14 together with the pressure decay data used to obtain the conversion factor.

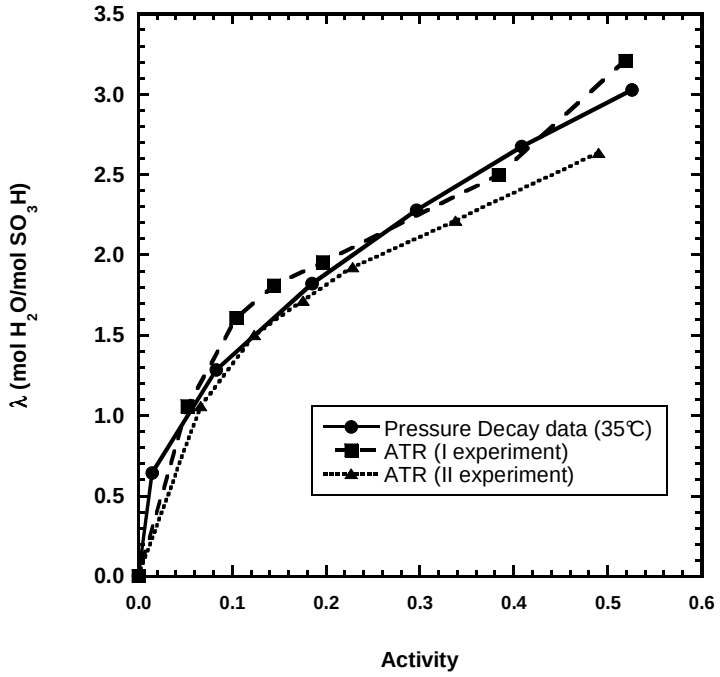

Fig. 4-14: Water sorption isotherms for an extruded Hyflon® Ion H membrane (EW=800 g_{pol}/mol -SO_3H) collected with an FTIR-ATR at 30°C and compared with data from pressure decay experiment.

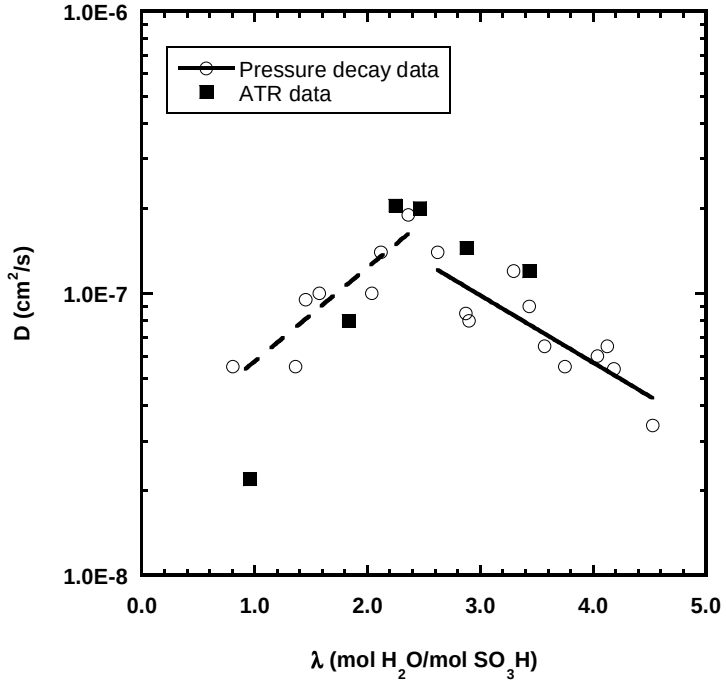

Fig. 4-15: Average diffusion coefficient of water in an extruded Hyflon® Ion H membrane (EW=800 g_{pol}/mol -SO_3H) collected with an FTIR-ATR at 30°C and compared with data from pressure decay experiment.

If the transient data for the same spectrum region are considered, the average apparent diffusion coefficient of water in the membrane for every step can be estimated as illustrated in Section 4.2.1. In Fig. 4-15, the result are compared to values obtained in experiments on similar membranes carried out with a pressure decay and the agreement is rather good, with a maximum in the diffusivity for an average concentration in the membrane of 2.5 mol H_2O/ mol SO_3H.

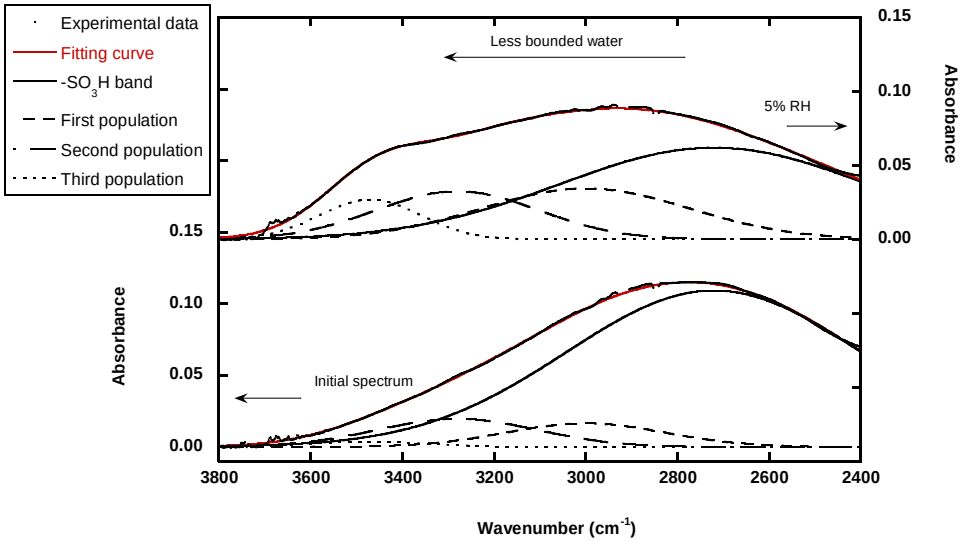

Fig. 4-16: Fitting of the spectra with 4 different peaks: 1 for $–SO_3H$ and 3 for water bonded with different strength. (a) initial spectrum of Hyflon® Ion H membrane evacuated at 30°C, (b) spectrum after hydration at 5% RH at 30°C.

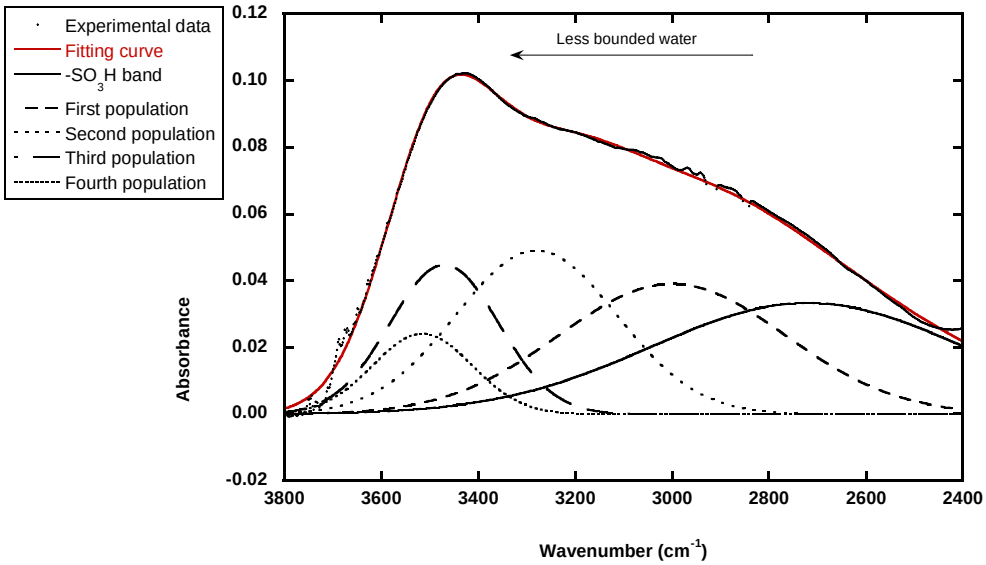

Fig. 4-17: Fitting of the spectra with 5 different peaks: 1 for $–SO_3H$ and 4 for water bonded with different strength; spectrum taken after hydration at 10% RH at 30°C.

In order to evidence the contributions of the different "populations" of water to the total water uptake, a specific analysis in the region of the stretching of the hydrogen bonds (2400-3800 cm^{-1}) was carried on. In particular, a fitting procedure can be performed using a software for the decomposition of complex spectra in their components (Fityk). The band shape were fixed to the Gaussian function while all the other parameters were allowed to vary. Four different bands can be identified in the initial spectra of the ionomer (Fig. 4-16): one at 2720 cm^{-1} that has no easy interpretation, and three related to water molecules that show a different degree of interaction with the sulphonic groups at 3000, 3280, 3470 cm^{-1}, with the strength of the bond decreasing with the increasing wavenumber. The peak at 2720 cm^{-1} could be related to the sulphonic groups and, inversely, to the fraction of water more strongly bonded to $–SO_3H$ groups, that can be only removed by increasing the temperature. The peak related to the sulphonic groups would decrease upon hydration not only for the rapid dissociation of these groups in presence of water but also due to the high swelling of the membrane that lowers the signal of the polymer bands in the spectrum. Another interpretation of this band [33] considers it related to an Evans window that is due to the increase of other bands attributed to water sorption which cause a local minimum in the spectra. Due to the not completely clear nature of the band, the swelling of the membrane was not determined from these data; in principle it can be calculated from the decrease in intensity of the bands at 1155 and 1220 cm^{-1} that are related to the CF bonds and thus are not affected by water sorption. However, the intensity of the CF signal was too high to obtain reliable data.

The other three bands (3000, 3280, 3470 cm^{-1}) can be associated to populations of water bonded to the sulphonic group with decreasing intensity. The less bonded water is at higher wavenumber as confirmed by the fact that, if the hydration is increased, a new population appears at 3515 cm^{-1} as it can be seen in Fig. 4-17.

If we use the same calibration constant between absorbance and mass uptake for all the water species, we can decompose the water sorption isotherm into the four contributions (Fig. 4-18). It can be noticed that the fourth population appears only in the second step (activity 0.1). In this plot the data were corrected to account for the presence of residual water using previous experimental results [36]; the values

determined with the spectrometer are thus comparable to sorption data obtained with a pressure decay on membrane cast from the hydroalcoholic solution and evacuated at 120°C (also reported in Fig. 4-18). The data are in good agreement confirming again that the formation process (i.e. casting or extrusion) does not affect the water sorption capacity of the membrane as already suggested by the spectra of the two materials (see Section 4.2.1).

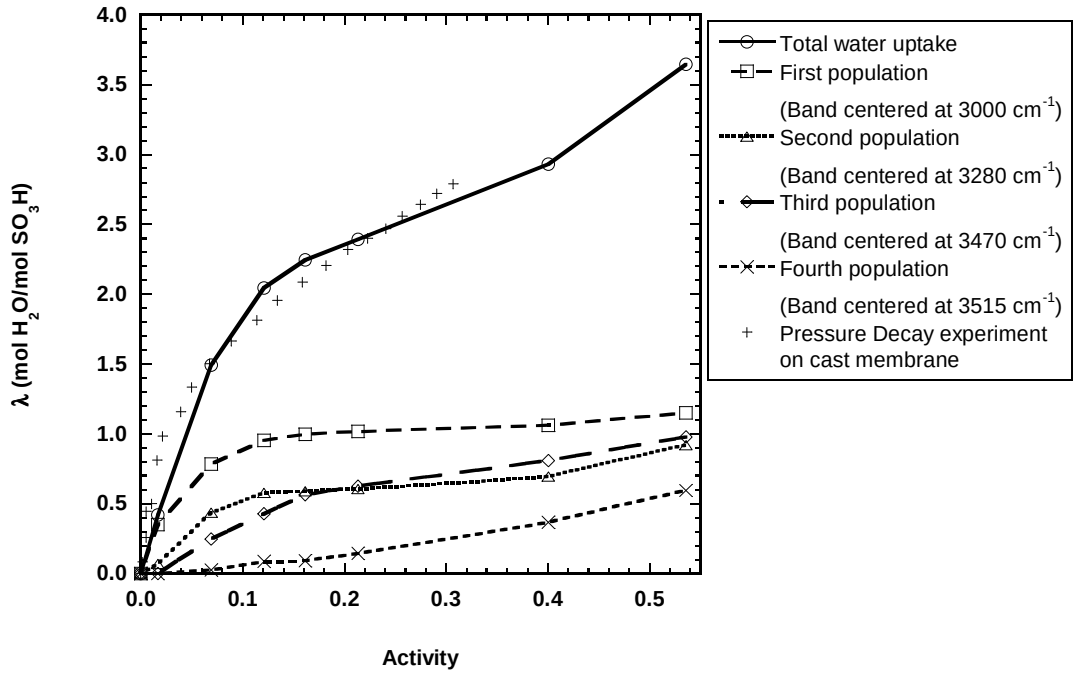

Fig. 4-18: Water sorption in Hyflon® Ion H membrane. Experimental total mass uptake and contribution of the different populations of water. Data for the cast membrane courtesy of Jacopo Catalano.

With the same method we can monitor the variation of the various species uptake along time. In Fig. 4-19, the kinetic behavior of the absorbance of the water populations together with the one for the $-SO_3H$ peak is reported for an increase in water vapor activity from 0.05 to 0.1. In this range of activity four water populations can be indentified and followed in their increase. The peak at 2720 cm^{-1}, on the contrary, decreases (Fig. 4-19 (a)).

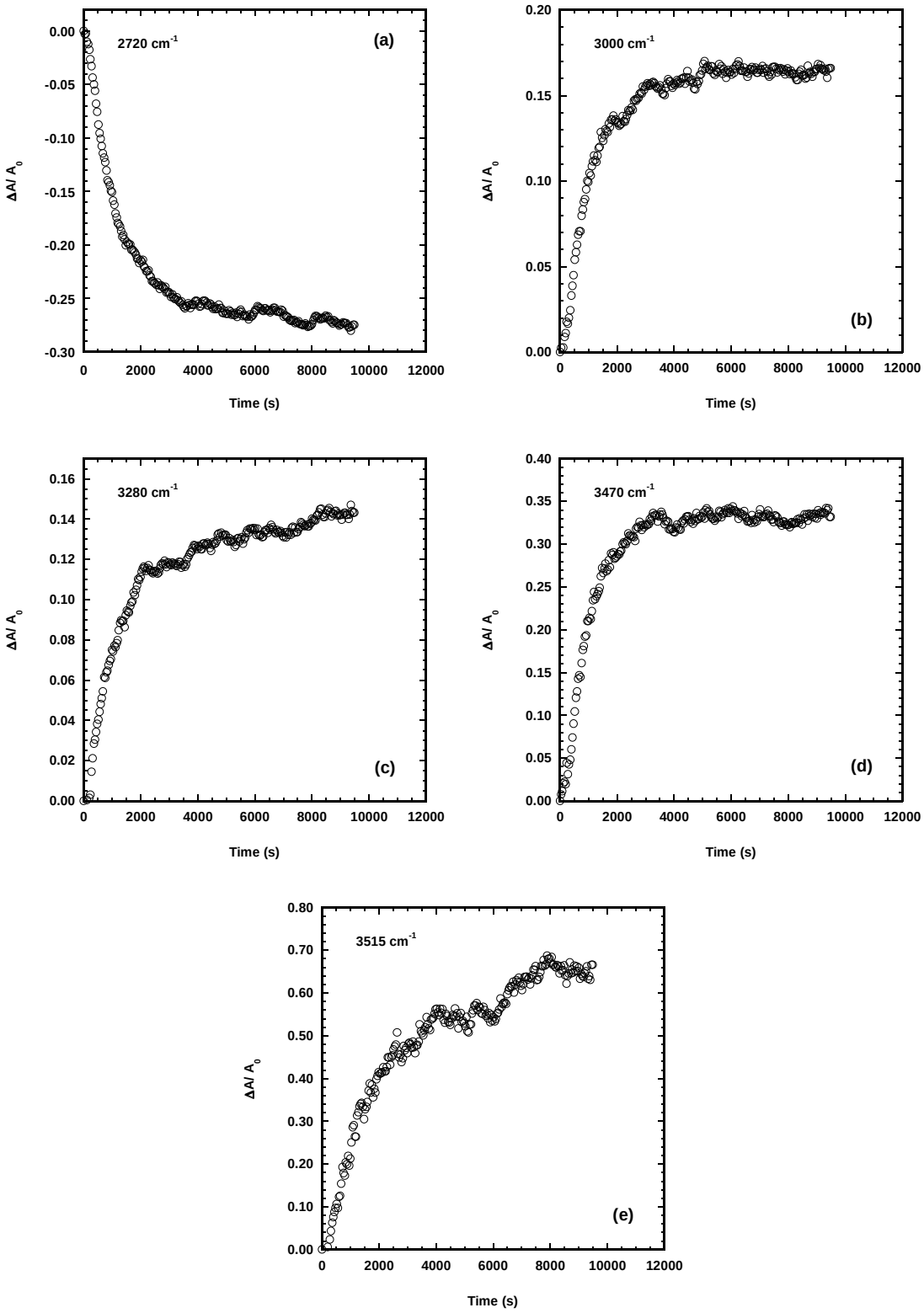

Fig. 4-1: Kinetic behavior of the different bands.

The equilibrium data for the different water populations can be described with a model that considers the equilibrium constants of the dissociation of hydrogen bonds. The underlying physical idea considers consecutive layers of water molecules that are bonded to the sulphonic group with decreasing strength. The first molecule is bonded irreversibly to the sulphonic group while the following reactions are supposed reversible. The reaction scheme considered is the following:

$$\begin{aligned}
&-SO_3H + H_2O \xrightarrow{K_1} -SO_3H\left[H_2O\right] \\
&-SO_3H\left[H_2O\right] + H_2O \underset{}{\overset{K_2}{\rightleftharpoons}} -SO_3H\left[H_2O\right]_2 \\
&-SO_3H\left[H_2O\right]_2 + H_2O \underset{}{\overset{K_3}{\rightleftharpoons}} -SO_3H\left[H_2O\right]_3 \\
&\text{.....} \\
&-SO_3H\left[H_2O\right]_{n-1} + H_2O \underset{}{\overset{K_n}{\rightleftharpoons}} -SO_3H\left[H_2O\right]_n
\end{aligned} \tag{4.20}$$

Each water population concentration at equilibrium is related to the preceding family and can be described through a Langmuir isotherm [40]:

$$\begin{aligned}
c_1 &= c_{-SO_3H[H_2O]} = K_1 \frac{a_w}{1+K_1 a_w} c_{siti} \\
c_2 &= c_{-SO_3H[H_2O]_2} = K_2 \frac{a_w}{1+K_2 a_w} c_1 \\
c_3 &= c_{-SO_3H[H_2O]_3} = K_3 \frac{a_w}{1+K_3 a_w} c_2 \\
&\text{.....} \\
c_n &= c_{-SO_3H[H_2O]_n} = K_n \frac{a_w}{1+K_n a_w} c_{n-1}
\end{aligned} \tag{4.21}$$

The dissociation constants are fitting parameters in this model and have to be adjusted on the experimental data for the different populations. In this case only the first three constant were fitted to the data while from the fourth the value of the constant was fixed at 1 as already reported for the case of polystyrene sulphonates studied by Glueckauf and Kitt [41]. The adjustable variables in the model are then four: the first three kinetic constants and the number of water molecules that can be bonded to each –SO_3H group.

The results obtained with the FTIR-ATR spectrometer are compared to the model with *n* Langmuir isotherms in Fig. 4-20. The fourth population observed in the spectra was considered the sum of all the (*n*-3) populations predicted by the model after the first

three. The agreement is pretty good considering that only four adjustable parameters are present (reported in Table 4-1) and at least in the low activity range here investigated the different group of water molecules can be identified and described with this model. The shape of the Langmuir isotherms can describe the data of water sorption at low water partial pressure but would not allow to predict the behavior of the material at higher activity since usually the isotherm for this kind of material change its concavity and the solubility increases dramatically at high activity.

K_1	69
K_2	19
K_3	19
n	20

Table 4-1: Parameters used in the model

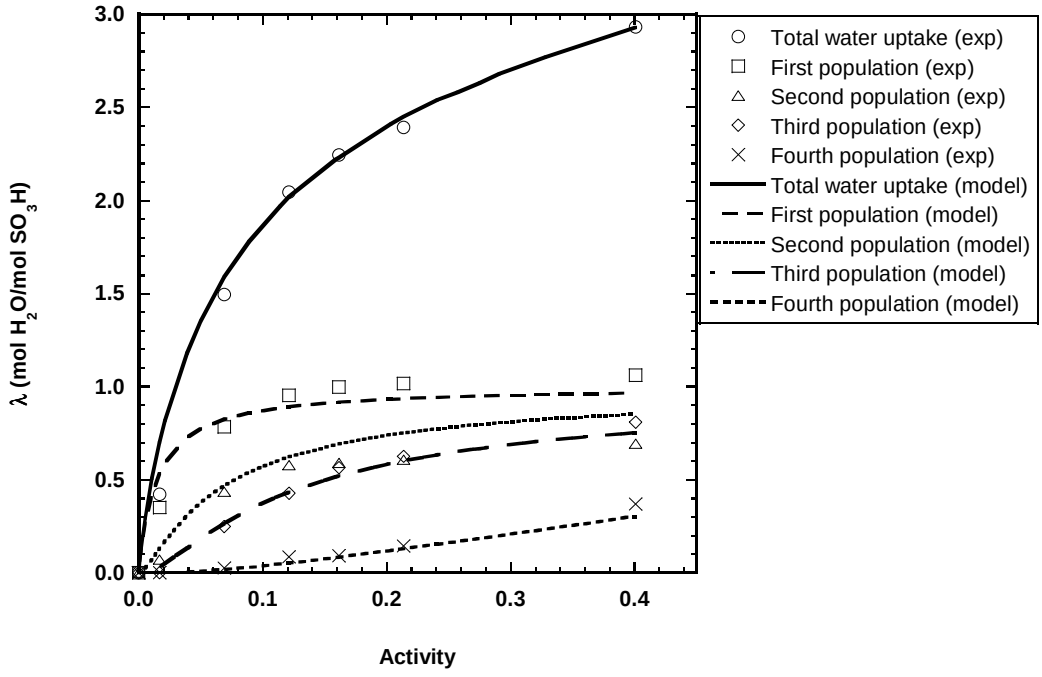

Fig. 4-20: Comparison of the contribution of each population to the mass uptake as measured with the spectrometer and as calculated through the model for solubility.

Conclusions

Hyflon® Ion H is a perfluorosulphonated material that can be employed as electrolyte in fuel cells. Therefore the behavior in presence of water is a really interesting and crucial topic that has already been largely investigated for similar material with a longer side chain (Nafion 117) since the water content of the membrane dramatically affects the characteristic of the membrane and therefore the performance of the fuel cell. In this work, the possible effect of different formation procedure has been studied, showing that the water sorption is significantly reduced by a high boiling solvent such as dimethylacetamide, while no difference has been found between extruded membranes and the ones cast from a hydroalcoholic solution. The excessive swelling of ionomers during fuel cell operation can cause problems due to excessive stress and has to be avoided. It is reported that this could be done lowering the equivalent weight of the membrane [3]; therefore the dilation behavior of extruded membranes of EW 800 gpol/mol-SO_3H has been studied up to temperature comparable to the operation temperature of DMFC. The swelling, even at low water vapor activity, that is low water content, is dramatically increased by heat and hence caution has to be paid in application. As a final issue, the water diffusion and sorption has been studied with a FTIR-ATR spectrometer that allows to distinguish among different populations of water bonded to the terminal sulphonic group of the side chain of the ionomer with decreasing strength. The isotherm can be decomposed in four contributions that can be model considering *n* Langmuir isotherms, with only four adjustable parameters.

References

1. Choi, P., *Investigation of Thermodynamic and Transport Properties of Proton-Exchange Membranes in Fuel Cell Applications,* Ph.D Thesis,2004,Worchester Polytechnic Institute.
2. Zawodzinski, T.A.J., Derouin, C., Radzinski, S., Sherman, R., J., Smith, V., T., Springer, T., E., et al., *Water Uptake by and Transport Through Nafion 117 Membranes.* Journal of The Electrochemical Society, 1993. **140**(4): p. 1041-1047.
3. Arcella, V., Troglia, C. and Ghielmi, A., *Hyflon® Ion Membranes for Fuel Cells.* Industrial & Engineering Chemistry Research, 2005. **44**(20): p. 7646-7651.
4. Kato, S., Nagahama, K. and Asai, H., *Permeation rates of aqueous alcohol solutions in pervaporation through Nafion membranes.* Journal of Membrane Science, 1992. **72**(1): p. 31.
5. Ghielmi, A., Vaccarono, P., Troglia, C. and Arcella, V., *Proton exchange membranes based on the short-side-chain perfluorinated ionomer.* Journal of Power Sources, 2005. **145**(2): p. 108.
6. Hallinan, D.T. and Elabd, Y.A., *Diffusion and Sorption of Methanol and Water in Nafion Using Time-Resolved Fourier Transform Infrared-Attenuated Total Reflectance Spectroscopy.* The Journal of Physical Chemistry B, 2007. **111**(46): p. 13221-13230.
7. Gebel, G., *Structural evolution of water swollen perfluorosulfonated ionomers from dry membrane to solution.* Polymer, 2000. **41**(15): p. 5829.
8. Hong, S.U., Barbari, T.A. and Sloan, J.M., *Multicomponent diffusion of methyl ethyl ketone and toluene in polyisobutylene from vapor sorption FTIR-ATR spectroscopy.* Journal of Polymer Science Part B: Polymer Physics, 1998. **36**(2): p. 337-344.
9. Sutandar, P., Ahn, D.J. and Franses, E.I., *FTIR ATR analysis for microstructure and water uptake in poly(methyl methacrylate) spin cast and Langmuir-Blodgett thin films.* Macromolecules, 1994. **27**(25 %R doi:10.1021/ma00103a013): p. 7316-7328.
10. Elabd, Y.A., Sloan, J.M. and Barbari, T.A., *Diffusion of acetonitrile in conformational isomers of an H12MDI polyurethane.* Polymer, 2000. **41**(6): p. 2203.

11. Rajagopalan, G., Immordino, K.M., Gillespie, J.W. and McKnight, S.H., *Diffusion and reaction of epoxy and amine in polysulfone studied using Fourier transform infrared spectroscopy: experimental results.* Polymer, 2000. **41**(7): p. 2591.
12. Sammon, C., Mura, C., Hajatdoost, S. and Yarwood, J., *ATR-FTIR study of the diffusion and interaction of water and electrolyte solutions in polymeric membranes.* Journal of Molecular Liquids, 2002. **96-97**: p. 305.
13. Sammon, C., Mura, C., Yarwood, J., Everall, N., Swart, R. and Hodge, D., *FTIR-ATR Studies of the Structure and Dynamics of Water Molecules in Polymeric Matrixes. A Comparison of PET and PVC.* The Journal of Physical Chemistry B, 1998. **102**(18): p. 3402-3411.
14. Sammon, C., Yarwood, J. and Everall, N., *A FTIR-ATR study of liquid diffusion processes in PET films: comparison of water with simple alcohols.* Polymer, 2000. **41**(7): p. 2521.
15. Yarwood, J., Sammon, C., Mura, C. and Pereira, M., *Vibrational spectroscopic studies of the diffusion and perturbation of water in polymeric membranes.* Journal of Molecular Liquids, 1999. **80**(2-3): p. 93.
16. Brugel, W., *An introduction to infrared spectroscopy*. 1962, New York: Wiley.
17. George, W.O. and Mcintyre, P.S., *Infrared spectroscopy*. 1987, New York: Wiley.
18. Howarth, O., *Theory of Spectroscopy*. 1973, London: Nelson.
19. Smith, B.C., *Fundamentals of Fourier Transform Infrared Spectroscopy*. 1996, New York: CRC Press.
20. Harrick, N.J., *Internal reflection spectroscopy*. 1987, NewYork: Harrick Scientific Corporation.
21. Cooley, J.W. and Tukey, J.W., *An Algorithm for the Machine Calculation of Complex Fourier Series.* Mathematics of Computation, 1965. **19**: p. 297-301.
22. Bracewell, R.N., *The Fourier Transform and Its Applications*. 1965, New York: McGraw-Hill Book Company.
23. Brigham, E.O., *The Fast Fourier Transform and Its Applications*. 1988, Englewood Cliffs, NJ: Prentice-Hall, Inc.
24. Harrick, N.J., *Internal reflection spectroscopy*. 1967, New York: Interscience Publications.
25. Mirabella, F.M., *Internal Reflection Spectroscopy: Theory and Applications*. 1993, New York: Dekker, M.
26. Giacinti Baschetti, M., *Development of experimental methods*

for the analysis of gas sorption in polymeric material, Ph.D Thesis, 2000, *DICMA*, Alma Mater Studiorum-Università di Bologna.

27. Fowles, G.R., *Introduction to Modern Optics*. 1975, New York: Dover Publ. Inc.
28. Jenkins, F.A. and White, H.E., *Fundamental of Optics*. 1957, New York: McGraw-Hill.
29. Gregory T. Fieldson, T.A.B., *Analysis of diffusion in polymers using evanescent field spectroscopy.* AIChE Journal, 1995. **41**(4): p. 795-804.
30. Balik, C.M. and Simendinger, W.H., *An attenuated total reflectance cell for analysis of small molecule diffusion in polymer thin films with Fourier-transform infrared spectroscopy.* Polymer, 1998. **39**(20): p. 4723.
31. Balik, C.M. and Xu, J.R., *Simultaneous measurement of water diffusion, swelling, and calcium carbonate removal in a latex paint using FTIR-ATR.* Journal of Applied Polymer Science, 1994. **52**(7): p. 975-983.
32. Hong, S.U., Barbari, T.A. and Sloan, J.M., *Diffusion of methyl ethyl ketone in polysiobutylene: Comparison of spectroscopic and gravimetric techniques.* Journal of Polymer Science Part B: Polymer Physics, 1997. **35**(8): p. 1261-1267.
33. Buzzoni, R., Bordiga, S., Ricchiardi, G., Spoto, G. and Zecchina, A., *Interaction of H_2O, CH_3OH, $(CH_3)_2O$, CH_3CN, and Pyridine with the Superacid Perfluorosulfonic Membrane Nafion: An IR and Raman Study.* The Journal of Physical Chemistry, 1995. **99**(31): p. 11937-11951.
34. Laporta, M., Pegoraro, M. and L., Z., *Perfluorosulfonated membrane (Nafion): FT-IR study of the state of water with increasing humidity.* Phys. Chem. Chem. Phys., 1999. **1**: p. 4619-4628.
35. Krtil, P., Trojanek, A. and Samec, Z., *Kinetics of Water Sorption in NafionThin Films; Quartz Crystal Microbalance Study.* The Journal of Physical Chemistry B, 2001. **105**(33): p. 7979-7983.
36. De Angelis, M.G., Lodge, S., Giacinti Baschetti, M., Sarti, G.C., Doghieri, F., Sanguineti, A., et al., *Water sorption and diffusion in a short-side-chain perfluorosulfonic acid ionomer membrane for PEMFCS: effect of temperature and pre-treatment.* Desalination, 2006. **193**(1-3): p. 398.
37. Zhang, C., Cappleman, B.P., Defibaugh-Chavez, M.D. and Weinkauf, H., *Glassy polymer-sorption phenomena measured with a quartz crystal microbalance technique.* Journal of Polymer Science Part B: Polymer Physics, 2003. **41**(18): p. 2109-2118.

38. Sauerbrey, G., *Verwendung von Schwingquarzen zur Wägung dünner Schichten und zur Mikrowägung.* Z. Phys., 1959. **155**: p. 206-222.
39. Yamamoto, Y., Ferrari, M.C., Giacinti Baschetti, M., De Angelis, M.G. and Sarti, G.C., *A quartz crystal microbalance study of water vapor sorption in a short side-chain PFSI membrane.* Desalination, 2006. **200**(1-3): p. 636.
40. Ruthven, D.M., *Principles of Adsorption and Adsorption Processes*. 1984, New York: Wiley.
41. Glueckauf, E. and Kitt, G.P., *A Theoretical Treatment of Cation Exchangers. III. The Hydration of Cations in Polystyrene Sulphonates.* Proceedings of the Royal Society of London. Series A, Mathematical and Physical Sciences, 1955. **228**(1174): p. 322.

Conclusions

The present work focused on the study of different systems where the diffusion of a low molecular species in a polymer is accompanied by other processes that modify the mass transport problem. The influence of dilation, insertion of particles and reactions was analyzed, first with an extensive experimental characterization of the various systems; then suitable models were developed to explain the particular circumstances and were used to process and understand the experimental results.

The bending beam technique was used to test the effects of the dilation and the stress induced in the polymer by penetrant diffusion. The experimental results for the bending of a cantilever coated with a test polymer were collected over time during the diffusion of a penetrant; at the same time also dilation data were collected. The measured data were processed considering the solution of a simulation model which accounts for the calculation of the deformation and stress profiles due to swelling. The model is based on a simple layer models for composite materials and can predict both the equilibrium value of the deflection of the coated cantilever and the kinetic of bending once the appropriate dilation relationship is taken into account. From the same model also the stresses that rise in the system due to the sorption process can be calculated.

Mixed matrix membranes based on fluorinated, high free volume matrices show attractive separation performances but there is a need for deeper investigation of the influence of inorganic filler on selectivity properties of polymeric materials. MMMs based on amorphous Teflon® and fumed silica were experimentally characterized to evaluate solubility, diffusivity and swelling due to two model penetrants. A new procedure that allows to predict solubility of every penetrant on the basis of data for one vapor was tested on the experimental data. The method has proved to be useful also for the determination of the diffusion coefficient and for an estimation of the permeability in the composite materials. The evaluation of the contributions of the permeability can hence be used to determine the ideal selective behavior of the composite membrane.

Oxygen scavenging systems can overcome lack of barrier properties in common polymers that, for other characteristics, are desirable materials for certain applications. The final goal of obtaining a membrane almost impermeable to oxygen leads to experimental times out of reach. Hence, all the variables affecting the process were first studied experimentally for SBS block copolymers. Then a simple model was developed in order to describe the transport of oxygen in the film, considering a single first order reaction that is fast compared to the diffusion process in the oxidized material. Furthermore, a model for predicting the oxygen barrier behavior of a film formed as a blend of OSP in a common packaging material was built, considering particles capable of reactions with oxygen embedded in a non-reactive matrix.

Hyflon® Ion H is a perfluorosulphonated material that can be employed as electrolyte in fuel cells and therefore the behavior in presence of water is crucial for the performances of the device. In this work, the possible effect of different formation procedure was studied, showing how solvents can compromise the structure of the material and therefore the water sorption capacity. Even the swelling due to the sorption process was measured since the excessive swelling of ionomers during operation can cause problems due to excessive stress and has to be avoided. As a finally issue, the water diffusion and sorption was studied with a FTIR-ATR spectrometer that can give deeper information on the bond between water molecules and the sulphonic termination of the side chain of the material and therefore on the structure of the hydrated polymer.

List of publications

Papers:

- Yamamoto, Y., Ferrari, M.C., Giacinti Baschetti, M., De Angelis, M.G. and Sarti, G.C.

A quartz crystal microbalance study of water vapor sorption in a short side-chain PFSI membrane. Desalination, 2006. **200**(1-3): p. 636.

- Ferrari, M.C., Piccinini, E., Giacinti Baschetti, M., Doghieri, F. and Sarti, G.C.

Solvent-Induced Stresses during Sorption in Glassy Polycarbonate: Experimental Analysis and Model Simulation for a Novel Bending Cantilever Apparatus. Industrial & Engineering Chemistry Research, 2008. **47**(4): p. 1071-1080.

- Ferrari, M.C., Carranza, S., Bonnecaze, R.T., Tung, K.K., Freeman, B.D. and Paul, D.R.

Modeling of oxygen scavenging for improved barrier behavior: Blend films. Journal of Membrane Science, 2009. **329**: p. 183-192.

Oral presentations:

- M. C. Ferrari, M. Galizia, M. G. De Angelis, G. C. Sarti

Mixed matrices based on amorphous Teflon® and fumed silica: experimental characterization and simulations with the NELF model
Gordon Research Conference: Membranes: Materials and Processes. , 9-15 August 2008, New London, NH.

- L.Basile, M.C. Ferrari, M.G. De Angelis, T.C. Merkel, G.C. Sarti

Sorption and Diffusion of Organic Vapors in Mixed Matrices Based on Teflon® AF2400 and Fumed Silica
2007 AIChE Annual Meeting, November 4-9, 2007, Salt Lake City, UT.

Conference proceedings:

- M.C. Ferrari, M. Giacinti Baschetti, F. Doghieri, G. C. Sarti

Analisi sperimentale della dilatazione e delle tensioni indotte dal solvente in film polimerici supportati
Atti del convegno Gr.I.C.U. 2008, Le Castella (KR), 14 -18 Settembre 2008.

- M.G. De Angelis, M. Galizia, M.C. Ferrari, G.C. Sarti,
Solubility and diffusivity of gases in nanocomposites formed by high free volume glassy polymers and fumed silica: experimental behaviour and simulation based on NELF model
ESAT 2008 proceedings, pp. 1005-1020, Cannes, 29 May-1 June 2008.

- M.C. Ferrari, M.G. De Angelis, M. Galizia, G.C. Sarti,
Sorption and swelling behavior of organic vapors in mixed matrix membranes based on Teflon® AF2400 and fumed silica
EWM 2008 proceedings, pp. 65-66, Algarve, May 2008.

- L.Basile, M.C. Ferrari, M.G. De Angelis, T.C. Merkel, G.C. Sarti
Sorption and Diffusion of Organic Vapors in Mixed Matrices Based on Teflon® AF2400 and Fumed Silica
2007 AIChE Annual Meeting Conference Proceedings November 4-9, 2007, Salt Lake City, UT.

- M. C. Ferrari, J. Catalano, M. Giacinti Baschetti, M. G. De Angelis, G. C. Sarti
Water transport in a short side chain PFSI membrane: Differences between cast and extruded membranes subject to different thermal treatments
PMSE Preprints, 232TH NATIONAL ACS MEETING, San Francisco, CA. September 10-14, 2006, (vol. 95).

- M. C. Ferrari, M. Giacinti Baschetti, F. Doghieri, G. C. Sarti.
Experimental and Model Description of Combined Effects between Stress and Diffusion in Glassy Polymers.
2006 AIChE Annual Meeting and Fall Showcase Conference Proceedings 12-17 November 2006, San Francisco, CA

- M. C. Ferrari, J. Catalano, M. Giacinti Baschetti, M. G. De Angelis, G. C. Sarti.
Water Transport in a Short Side Chain Pfsi Membrane: Differences between Cast and Extruded Membranes Subject to Different Thermal Treatments.
2006 AIChE Annual Meeting and Fall Showcase Conference Proceedings 12-17 November 2006, San Francisco, CA